EVALUATION OF ROCKY POINT VIADUCT CONCRETE BEAM

FINAL REPORT

SPR 381

Oregon Department of Transportation

EVALUATION OF ROCKY POINT VIADUCT CONCRETE BEAM

FINAL REPORT

SPR 381

by

Stephen D. Cramer, Bernard S. Covino, Jr., Gordon R. Holcomb,
Sophie J. Bullard, James H. Russell, Cheryl M. Dahlin, Cathy A. Summers
Albany Research Center, U. S. Department of Energy, Albany OR 97321

and

H. Martin Laylor and Steven M. Soltesz
Oregon Department of Transportation, Salem OR 97301-5192

for

Oregon Department of Transportation, Research Unit
200 Hawthorne Avenue S.E., Suite B-240, Salem OR 97301-5192

and

Federal Highway Administration
400 Seventh Street S.W., Washington, D.C. 20590

JUNE 2000

Technical Report Documentation Page

1. Report No. FHWA-OR-RD-00-18	2. Government Accession No.	3. Recipient's Catalog No.
4. Title and Subtitle EVALUATION OF ROCKY POINT VIADUCT CONCRETE BEAM		5. Report Date June 2000 6. Performing Organization Code
7. Author(s) Stephen D. Cramer, Bernard S. Covino, Jr., Gordon R. Holcomb, Sophie J. Bullard, James H. Russell, Cheryl M. Dahlin, Cathy A. Summers Albany Research Center, U. S. Department of Energy, Albany OR 97321 and H. Martin Laylor and Steven M. Soltesz Oregon Department of Transportation, Salem OR 97301		8. Performing Organization Report No.
9. Performing Organization Name and Address Oregon Department of Transportation Research Group 200 Hawthorne SE, Suite B-240 Salem, Oregon 97301-5192		10. Work Unit No. (TRAIS) 11. Contract or Grant No. SPR 381
12. Sponsoring Agency Name and Address Oregon Department of Transportation Research Group and Federal Highway Administration 200 Hawthorne SE, Suite B-240 400 Seventh Street S.W. Salem, Oregon 97301-5192 Washington, D.C. 20590		13. Type of Report and Period Covered Final Report 14. Sponsoring Agency Code

15. Supplementary Notes

16. Abstract

This study was intended to determine why it was necessary to replace the Rocky Point Viaduct (1954 - 1994), on the Oregon coast south of Port Orford, after a period of service that was much shorter than that of many other reinforced concrete bridges on the Oregon coast; to identify construction practices that may have contributed to its early failure; and to identify evaluation methods that are most effective for characterizing bridge condition. A 14.3 m (47 foot) section of concrete Beam A1 and bridge deck between the north abutment and pier 1 was removed from the seaward side of the Viaduct for evaluation of: (1) concrete properties; (2) reinforcing bar (rebar) corrosion; and (3) chloride migration in the concrete.

The harsh environment at the site was an important factor in the premature failure of the Viaduct. This led to substantial salt penetration of the concrete to the depth of the shear stirrups and square rebar. The severity of chloride penetration of the concrete was such that neither the original concrete cover nor subsequent efforts to repair the structure and prevent further corrosion could mitigate its effects on rebar corrosion. Shear stirrups had inadequate concrete cover for the severity of the environment. Early corrosion damage could be predicted from chloride depth profiles, concrete cover depths, and the rebar corrosion threshold. Application of the patch concrete merely delayed, but not for long, the occurrence of highly corrosive conditions around shear stirrups and the square rebar. Other efforts at preventing further corrosion damage (corrosion resistant coatings on the rebar, coal tar and linseed oil barrier coatings) were ineffective.

Chloride profiling, using concrete powder samples taken at small depth increments, was one of the most powerful techniques Oregon DOT has for assessing the condition of bridges on the Oregon coast. The other was half-cell potential mapping. Chloride profiles, when fit by Fick's second law of diffusion, yield an effective diffusion coefficient, D, for chloride in concrete and a surface chloride concentration, C_o, characteristic of the bridge-environment combination. Sampling to a depth of 15 cm (6 inches) in 1.3 cm (0.5 inch) increments would adequately define the chloride profile for bridges on the Oregon coast. The D and C_o obtained can be used to assess the severity of environmental conditions, to look back in time to understand performance problems related to corrosion damage, or to look forward in time to anticipate maintenance and repair needs. Once good values of D and C_o are obtained, chloride measurement using concrete powder sampling may not be necessary, except on a long-term basis (every 10 to 15 years) to check predictions.

Impressed Current Cathodic Protection (ICCP) over a period equivalent to 15 years service at Oregon coastal bridge conditions resulted in significant extraction of Cl from around the outer rebar. Chloride migration under the influence of the potential gradient dominated migration due to the concentration gradient. ICCP shifts the rebar to a state of diminished corrosion, i.e., a protected state, gradually reduces the aggressiveness of the concrete environment surrounding the rebar by reducing chloride ion concentrations, and increases alkalinity at the rebar surface so that the rebar may eventually return to a naturally passive state.

Bridge construction practices should consider, in addition to quality concrete and adequate cover, the aggressiveness of the site environment, including meteorological conditions and washing and sheltering that affect chloride deposition. Assessment of site environmental conditions would be a useful to bridge design to assure a structure would achieve the desired service life. Such an assessment recognizes that a wide range of microclimates exist on the Oregon coast. Site environments could be characterized by one of the following: measurement of atmospheric corrosion rates for mild steel, measurement of salt deposition rates, or determination of C_o from chloride profiling an existing or nearby structure. Chloride profiles for coastal bridges and a knowledge of corrosion initiation threshold chloride levels provide solid evidence supporting the selection by Oregon DOT of stainless steel rebar and microsilica (high-performance) concrete for use in new bridge construction on the Oregon coast.

17. Key Words bridge, cathodic protection, CP, corrosion, chloride, diffusion, environment, reinforced concrete, reinforcing bar, rebar	18. Distribution Statement Copies available from NTIS		
19. Security Classif. (this report) Unclassified	20. Security Classif. (of this page) Unclassified	20. No. of Pages 80 + appendices	22. Price

Technical Report Form DOT F 1700.7 (8-72) Reproduction of completed page authorized

SI* (MODERN METRIC) CONVERSION FACTORS

APPROXIMATE CONVERSIONS TO SI UNITS

Symbol	When You Know	Multiply By	To Find	Symbol
		LENGTH		
In	inches	25.4	millimeters	Mm
Ft	feet	0.305	meters	M
Yd	yards	0.914	meters	M
Mi	miles	1.61	kilometers	Km
		AREA		
In^2	square inches	645.2	millimeters squared	mm^2
Ft^2	square feet	0.093	meters squared	m^2
Yd^2	square yards	0.836	meters squared	m^2
Ac	acres	0.405	hectares	Ha
Mi^2	square miles	2.59	kilometers squared	km^2
		VOLUME		
Fl oz	fluid ounces	29.57	milliliters	mL
Gal	gallons	3.785	liters	L
Ft^3	cubic feet	0.028	meters cubed	m^3
Yd^3	cubic yards	0.765	meters cubed	m^3
NOTE: Volumes greater than 1000 L shall be shown in m^3.				
		MASS		
Oz	ounces	28.35	grams	g
Lb	pounds	0.454	kilograms	kg
T	short tons (2000 lb)	0.907	megagrams	Mg
		TEMPERATURE (exact)		
°F	Fahrenheit temperature	5(F-32)/9	Celsius temperature	°C

APPROXIMATE CONVERSIONS FROM SI UNITS

Symbol	When You Know	Multiply By	To Find	Symbol
		LENGTH		
mm	millimeters	0.039	inches	in
m	meters	3.28	feet	ft
m	meters	1.09	yards	yd
km	kilometers	0.621	miles	mi
		AREA		
mm^2	millimeters squared	0.0016	square inches	in^2
m^2	meters squared	10.764	square feet	ft^2
ha	hectares	2.47	acres	ac
km^2	kilometers squared	0.386	square miles	mi^2
		VOLUME		
mL	milliliters	0.034	fluid ounces	fl oz
L	liters	0.264	gallons	gal
m^3	meters cubed	35.315	cubic feet	ft^3
m^3	meters cubed	1.308	cubic yards	yd^3
		MASS		
g	grams	0.035	ounces	oz
kg	kilograms	2.205	pounds	lb
Mg	megagrams	1.102	short tons (2000 lb)	T
		TEMPERATURE (exact)		
°C	Celsius temperature	1.8 + 32	Fahrenheit	°F

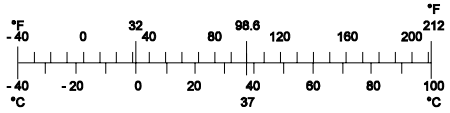

***** SI is the symbol for the International System of Measurement (4-7-94 jbp)

ACKNOWLEDGEMENTS

The authors thank Galen E. McGill, Oregon Department of Transportation, for his encouragement and support during the early stages of this project, and Curtis B. Cryer and Michelle L. Gallardo, Oregon Department of Transportation, for sharing their expertise in chloride profiling reinforced concrete bridges.

The authors thank Donald R. Jackson, Office of Technology Applications, Federal Highway Administration, U. S. Department of Transportation, and Ali Akbar Sohanghpurwala and Moavinul Islam, CONCORR Inc., for presenting the Federal Highway Administration Demonstration Project No. 84, "Corrosion Detection in Reinforced Concrete Structures," at the Albany Research Center. They thank David Whiting for presenting the Federal Highway Administration "FHWA-SHRP Showcase Workshop on Concrete Durability" at the Albany Research Center and for the loan of specialized equipment for evaluating concrete properties. The efforts of these folks are reflected in broad array of concrete and corrosion characterization techniques used in this study.

The authors also thank Melinda A. Hamilton, Idaho National Engineering Laboratory, U. S. Department of Energy, and Richard Veeh, Montana State University, for conducting the microbial survey of the Rocky Point beams and for the report "Evaluation of Microbially Influenced Degradation of Concrete Structures -- Rocky Point Viaduct Concrete Beam" by M. A. Hamilton, R. D. Rogers, and M. Zolynski, Biotechnology Group, Idaho National Engineering Laboratory (October 1996).

DISCLAIMER

EVALUATION OF ROCKY POINT VIADUCT CONCRETE BEAM

TABLE OF CONTENTS

LIST OF TABLES

LIST OF FIGURES

1.0 INTRODUCTION

Bridges located in coastal environments suffer many of the same corrosion problems as inland bridges exposed to applications of deicing salts. Salt contamination of concrete causes corrosion of the steel reinforcing bars (rebar). This leads to cracking of the concrete as the result of expansive forces produced by the corrosion product. Once this occurs, bridges must be either repaired or replaced.

A 1993 report to the federal government stated that 44 percent of the more than 500,000 bridges in the United States were either structurally deficient or should be posted for weight restrictions (*Burke, 1994*). Costs for bridge maintenance, rehabilitation and replacement, except for structural obsolescence, are a necessary but nonproductive use of Departments of Transportation resources. Safety concerns, disruptions in service, and economic impacts of catastrophic bridge failures are further liabilities for bridge owners and users. Better construction and rehabilitation practices that mitigate these costs and liabilities require understanding the causes of corrosion-related bridge failures, and the complex interplay between the physical, chemical and mechanical properties of concrete and steel rebar. Technology is needed to prevent further corrosion damage to existing bridges and to produce a 120+ year bridge life in new construction.

1.1 BACKGROUND

Much of the research that is responsible for extending the service life of new and existing bridges is less than 15 years old. Reinforced concrete bridges built 40 to 70 years ago were not built with the technological advantages for combating corrosion damage that are now increasingly being used in new bridge construction. Many of the older bridges along the Oregon coast are still in service and in sound condition. The purpose of this study was to determine reasons why it was necessary to replace the Rocky Point Viaduct (1954 -- 1994), on the Oregon coast south of Port Orford, after a period of service that was much shorter than that of many other bridges on the Oregon coast; to identify construction practices that may have contributed to its early failure; and to identify evaluation methods that are effective in assessing and characterizing the threat of corrosion to the bridge.

1.2 PROBLEM DEFINITION

The Rocky Point Viaduct, Figure 1.1, was replaced after just 40 years of service because of severe corrosion damage that resulted in loss of rebar cross-section and compromised the structural integrity of the viaduct. Sound older structures, such as McCullough bridges circa 1930, are present on the coast in seemingly similar environments. The early replacement of the Viaduct suggests corrosion damage effects that were not anticipated or understood at the time of construction. An understanding of those effects would provide a basis for improving construction practices for future bridges and renovation practices for existing bridges.

Figure 1.1: Original Rocky Point Viaduct (ca. 1975).

A 14.3 m (47 foot) section of concrete Beam A1 and bridge deck between the north abutment and pier 1 was removed from the seaward side of the Viaduct for evaluation, Figure 1.2. The beam measured approximately 1.2 m (48 inches) high, including the deck, and 0.38 m (15 inches) wide, and weighed approximately 19,000 kg (21 tons). The beam offered a unique opportunity to study a bridge structure after a long coastal exposure. The study provided basic data on the significant changes occurring in reinforced concrete structures in coastal and other high chloride environments. It allowed in-service verification of the factors contributing to bridge corrosion failures and created an opportunity for assessing current bridge evaluation and

renovation practices. This project was the initial effort by Oregon DOT to define measurements, sampling protocols, and results sufficient for predicting the remaining service life of other reinforced concrete structures.

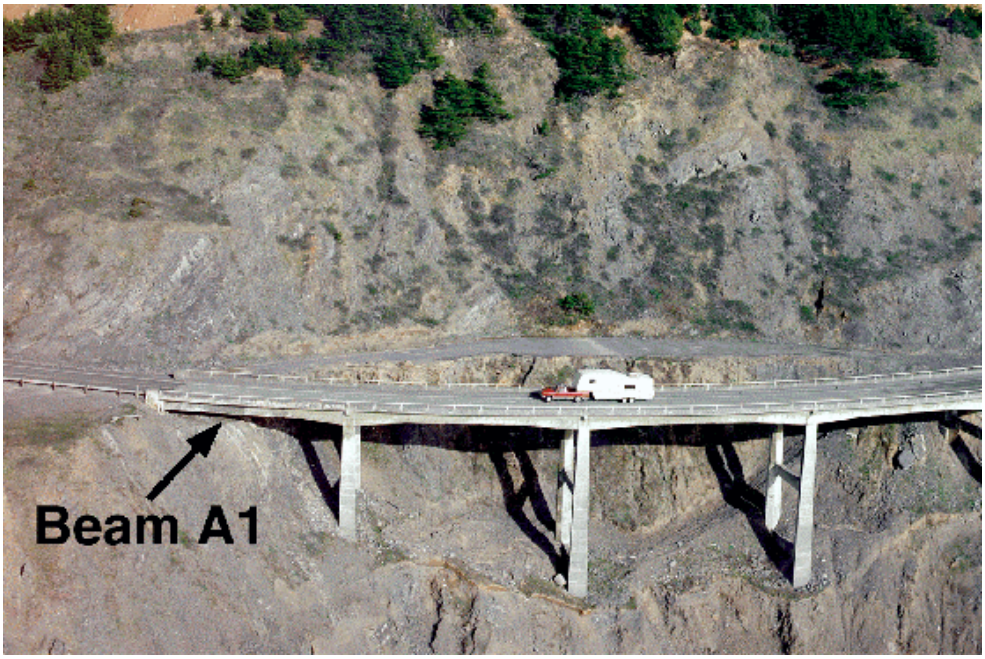

Figure 1.2: Original Rocky Point Viaduct (ca. 1975), showing location of Beam A1.

1.3 STUDY OBJECTIVES

The objective of the study was to identify the significant physical, mechanical and chemical factors that contributed to failure of the Viaduct. This objective was met by a four part evaluation of Beam A1 which addressed: (1) concrete properties; (2) rebar corrosion; (3) chloride penetration of concrete; and (4) chloride migration in concrete during impressed current cathodic protection (ICCP). Specific work in each of these areas included the following:

Part 1: Physical, mechanical, and chemical properties of concrete – The beam was nondestructively mapped to show the location of patches, concrete delamination and spalling, corrosion damage, and rebar. Physical, chemical and mechanical properties of sound original and patch concrete were determined and compared to each other, to the original design specifications, and to the beam maintenance history.

Part 2: Rebar corrosion damage survey – Surveys of corrosion potentials, corrosion rates, and microbial species were related to the Viaduct maintenance history, including efforts to correct significant early corrosion damage to the concrete, and to the structure condition at the time of replacement.

Part 3: Chloride distribution in concrete – Chloride ion distribution profiles were measured in both patch and original concrete and related to concrete cover depth and the onset of rebar corrosion and structural damage to the concrete.

Part 4: Chloride migration in concrete during ICCP – Sections of the beam were protected for one year using ICCP and thermal-sprayed zinc anodes. Changes in the chloride ion distribution profile were measured to quantify the effect of potential gradient on chloride migration.

1.4 WORK PLAN SYNOPSIS

A post-mortem analysis of the Rocky Point Viaduct was conducted to determine what construction practices may have contributed to the early failure of the Viaduct and to identify "lessons learned" that would extend the lives of new bridges constructed on the Oregon coast and improve the rehabilitation of existing bridges (*Covino, Cramer, Holcomb, Bullard, and Laylor, 1999*). The post-mortem analysis consisted of identifying significant physical, chemical, and mechanical factors that contributed to the Viaduct failure. It involved correlating the maintenance and repair history of the Viaduct with an evaluation of the Viaduct condition using present bridge evaluation practices.

2.0 CONSTRUCTION AND REPAIR HISTORY

2.1 CONSTRUCTION HISTORY

The Rocky Point Viaduct, located near Port Orford, Oregon, was replaced after 40 years of service. Located on U. S. Route 101 southeast of Port Orford, the Rocky Point Viaduct was constructed in 1955 at a coastal site 25 m (80 ft) east of the Pacific Ocean at an elevation of 35 m (115 ft). The Viaduct was a T-beam structure with 5 spans, Figure 1.1. Its total length was 114 m (374 ft) and it had a deck width of 10.6 m (34.8 ft).

Concrete in the deck and beams was prepared according to the following mix design:

Table 2.1: Rocky Point Viaduct concrete mix design

Concrete component	Amount in concrete
Type I Portland cement	269 kg/m^3 (593 lb/yd^3)
19 to 38 mm (0.75 to 1.5 inch) aggregate	341 kg/m^3 (752 lb/yd^3)
4.75 to 19 mm (0.19 to 0.75 inch) aggregate	633 kg/m^3 (1396 lb/yd^3)
<4.75 mm (<0.19 inch), fine aggregate and sand	488 kg/m^3 (1076 lb/yd^3)
Water	142 kg/m^3 (313 lb/yd^3)

The coarse aggregate came from the north bank of the Rogue River 9.7 km (6 mi) upstream from the ocean. The sand most likely came from the mouth of Brush Creek; there was no record of washing the sand. The water-cement ratio was 0.53. Three to six percent entrained air was specified for the concrete. Compressive strength after 60 days of curing was 42.7 MPa (6.2 ksi). Because significant patching occurred later, the concrete used at the time of construction is described in this report as “original” concrete.

The environment at the Viaduct location is one of the more severely corrosive on the Oregon coast. Atmospheric corrosion data for mild steel panels placed on the Oregon coast during the period 1994 through 1997 in a separate study conducted by the Albany Research Center, U. S. Department of Energy (*Cramer, 2000*) are given in Tables 2.2 and 2.3. The panels were exposed as one-sided panels, with the bare side facing up, boldly exposed, inclined at an angle of 30 degrees with the horizon and facing due west. The panels were exposed for a period of 2 to 3 years. Table 2.2 illustrates the wide range of microclimates existent on the Oregon coast by showing mild steel corrosion rates for a series of sites from the Oregon/California border to the Oregon/Washington border. Corrosivity of a specific site is dependent on a variety of factors ranging from local climate, adjacent land forms and vegetation (valleys and mountains, forests), to prevailing winds in relation to bridge orientation and, most importantly, to distance from the ocean. Corrosion rates in the coastal microclimates varied by a factor of more than 35. Sites that

were nominally similar had very different corrosion rates, e.g., Manzanita and Lincoln City. The corrosivity of the Viaduct site was the highest observed for bridge sites along the Oregon coast.

Table 2.2: Mild steel corrosion rate as a function of location along the Oregon coast. One-sided skyward samples were boldly-exposed on bridges and utility poles at 30 degrees to the horizon for 2 to 3 years. [1]

Site	Straight-line distance from OR/CA border km	Straight-line distance to ocean m	Mild steel corrosion rate µm/y
Astoria	477	50	291
Youngs Bay Bridge	477	6437	15
Manzanita	419	100	358
Lincoln City	331	100	90
Spencer Creek Bridge	305	91	449
Newport	294	50	363
Yaquina Bay Bridge	293	457	64
Cape Creek Bridge	241	91	57
Umpqua River Bridge	191	792	12
Reedsport	190	250	45
Cape Blanco	94	200	392
Rocky Point Viaduct	76	25	850 [2]
Brush Creek Bridge	67	244	142
Rogue River Bridge	48	1524	17
Gold Beach	47	250	25
Brookings	7	50	376

[1] Source: Coastal atmospheric corrosion study, Stephen D. Cramer, Albany Research Center, U.S. Department of Energy, Albany OR, April 2000.
[2] by extrapolation in Figure 2.1.

Table 2.3 shows the dramatic effect distance from the ocean has on the corrosion rate of mild steel. Corrosion rates rose dramatically within several hundred meters of the ocean. The increase was over 100-fold comparing the rate at the Newport 50-meter site and the Albany site. With the Viaduct site closer to the ocean than any of the atmospheric corrosion sites, deposition rates for salt and moisture were higher, leading to a much higher corrosivity.

Table 2.3: Mild steel corrosion rate as a function of the distance from ocean and location along the Oregon coast. One-sided skyward samples were boldly-exposed on utility poles at 30 degrees to the horizon for 2 to 3 years. [1]

Site		Straight-line distance from OR/CA border km	Straight-line distance to ocean m	Mass loss rate µm/y
Astoria --	site 1	477	50	291
	site 2		250	53
	site 3		1600	16
	site 4		4000	15
Portland --	site 5	376	104000	11
Newport –	site 1	294	50	363
	site 2		200	152
	site 3		1300	18
	site 4		6250	13
Albany –	site 5	294	83000	3
Reedsport –	site 1	191	250	45
	site 2		2300	16
	site 3		6250	8
Cape Blanco –	site 1	94	200	392
	site 2		1800	49
	site 3		2150	13
	site 4		4500	13
Rocky Point Viaduct		76	25	850 [2]
Gold Beach –	site 1	48	250	25
	site 2		1750	11
	site 3		7150	8
Grants Pass –	site 4	51	99200	3
Brookings –	site 1	7	50	376
	site 2		550	15
	site 3		1700	14
	site 4		3050	12

[1] Source: Coastal atmospheric corrosion study, Stephen D. Cramer, Albany Research Center, U. S. Department of Energy, Albany OR, April 2000.
[2] by extrapolation in Figure 2.1.

The corrosion data from Tables 2.2 and 2.3 are plotted in Figure 2.1 as a function of distance from the ocean. Extrapolation of the fitted curve yields an estimate of the mild steel corrosion rate at the Viaduct site of 850 µm/y. This value can be considered a measure of the corrosivity of the site, i.e. of the environment, not of the black iron rebar corrosion rate in concrete, and it is dependent upon a complex array of environmental factors. Another measure of the site corrosivity could be the salt deposition rate at the site measured by a chloride candle. Another measure could be the surface chloride concentration on the structure as determined from a fit of the chloride ion distribution profile in the concrete. Each of these methods provides a way for DOT's to characterize the corrosivity of a site.

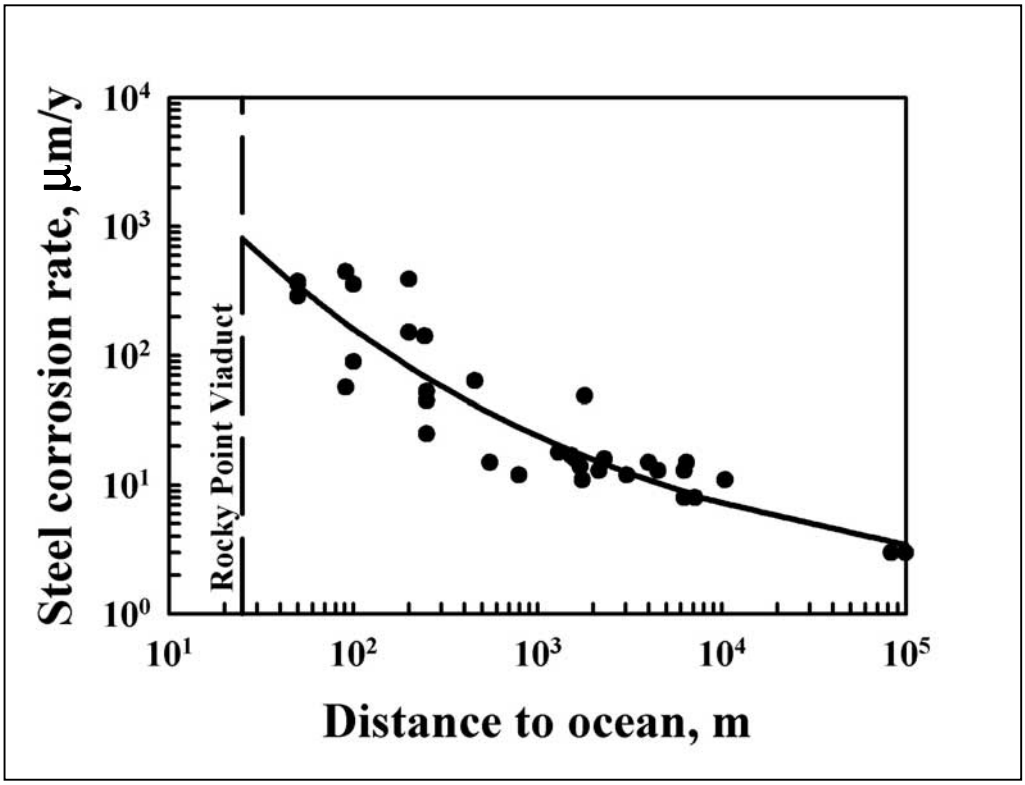

Figure 2.1: Mild steel atmospheric corrosion rates along the Oregon coast as a function of distance from the ocean, with Rocky Point Viaduct site shown as vertical dashed line. The data are from Tables 2.3 and 2.4. Solid line is least squares fit of data.

The selection of a bridge such as the Rocky Point Viaduct in the early 1990s for repair, rehabilitation, or replacement required inspectors to rate the Viaduct substructure and superstructure condition according to Federal Highway Administration guidelines. The current Oregon DOT procedure for selecting bridge repair, rehabilitation or replacement projects involves identifying a structure with specific problems, determining the severity of the problems, ranking it with other bridges, and determining the cost of possible solutions *(Johnson and Nelson, 1999*). The general steps in the current process are as follows:

- The structure is ranked according to the twelve deficiency categories identified by the Oregon DOT to describe the condition of a bridge. The deficiency categories are listed in Table 2.4.

- A team consisting of a structural design manager, a bridge inspector, and the district maintenance supervisors review the structure condition as defined by the Deficiency Categories. Conflicts within the data are resolved and missing data are obtained.

- The review team assigns a priority to the structure for each deficiency category. A "9" is assigned if the work needs to be done within two years; an "8" if the work needs to be done in three to four years; a "7" if the work should be done within four years but could be delayed two more years, incurring a higher maintenance cost. The priorities "6" through "0" are used

to rate work that needs to be done in the foreseeable future. The result is a rating for the structure in each category that allows Oregon DOT to prioritize needed repair, rehabilitation, or replacement.

- A second review team consisting of the structural design managers, the preservation manager, and the Bridge Management System staff use the category ratings to prioritize work statewide.

- Finally, the ratings by category are combined into a single list of structures ranked from highest to lowest statewide priority. For each project, the cost to resolve specific problems and the cost to replace the structure are calculated. Critical in the final ranking and cost calculations is field perspective as to how projects fit in conjunction with overall plans.

- Once a project has been selected, the decision to repair, rehabilitate, or replace is based on a life cycle cost comparison for the various options.

In 1991, the Viaduct was estimated to have a remaining service life of 2 years, equivalent to having been rated high in selected Deficiency Categories and ranked high for statewide project selection.

Table 2.4: Bridge deficiency categories *(Johnson and Nelson, 1999*).

Category	Description
Seismic	Susceptibility to collapse in moderate earthquake
Scour	Susceptibility to undermining of bridge foundations in stream beds
Load Capacity	Deficiency in carrying capacity for legal loads due to deterioration
Substructure	Spalling, cracking, etc. in piers, columns and footings
Superstructure	Spalling, cracking, etc. in girders and truss members
Deck	Rutting, cracking, delamination, etc. in bridge decks
Rails	Rail safety hazards (vehicle snagging) or inadequate crash resistance
Underclearance	Inadequate vertical clearance due to obsolete design or asphalt overlays on the roadway below
Movable Bridge	Obsolete or deteriorated mechanical or electrical systems
Corrosion	Coastal bridges subject to corrosion from salt intrusion
Major Paint	Major steel structures in need of protective coating and lead abatement
Deck Width	Insufficient width to handle traffic demand based on bridge width standards only (bottleneck bridges)

2.2 MAINTENANCE AND REPAIR HISTORY

The inspection and maintenance records of the Rocky Point Viaduct are summarized below:

- **1954** – Viaduct was constructed.
- **July 1967** – The first report of maintenance problems for the Viaduct was made. The steel rocker assemblies were badly rusted.

- **May 1968** – The steel rocker assemblies were badly rusted. The concrete beams were cracking and needed chipping and patching.
- **January 1969** – Concrete was spalling along the outside of the west facing beam between Bent No. 1 and Bent No. 2. Concrete was spalling back to the rebar, and the rebar was badly rusted. A request was made that loose concrete around the rebar be removed and patched, and steel rocker assemblies be sandblasted and painted.
- **June 1969** – Concrete beams were cracked due to rebar corrosion and needed chipping and repair. Rebar was exposed on the columns. Rust scale on the rebar was up to 4 mm (0.16 inch) thick; this was equivalent to 0.8 mm (0.03 inch) loss of steel cross-section. Steel rocker assemblies were badly rusted.
- **September 1969** – The first repairs were made to the Viaduct. Damaged original concrete was removed from around the rebar; rebar was sandblasted to remove rust; some rebar was primed with coal-tar epoxy, other rebar was primed with an inorganic zinc coating. Coal-tar epoxy was coated on the original concrete surface exposed by removal of damaged concrete to improve bond with the subsequent patches. Patches were cast around the rebar to replace original concrete removed from damaged areas. The surface of concrete beams was sealed with linseed oil to prevent further chloride penetration of the original concrete and chloride penetration of the patch concrete. Steel rocker assemblies were sandblasted and painted. No details on the patch concrete mix design were in the maintenance or construction records.
- **July 1970** – Rebar was exposed on some of the columns and column concrete was streaked with rust. Small cracks were found on the surface of all beams. Cracks transverse to the Viaduct axis were observed in the deck. Concrete was spalling from deck overhangs. A suggestion was made to patch concrete damage in columns and deck overhangs.
- **May 1976** – Concrete was cracking and spalling from the deck and columns. There was substantial section loss from exposed rebar due to corrosion. Joint material was falling out of the deck.
- **June 1981** – The deck concrete was full of salt and concrete on the bottom of the deck was falling off. Attempts to patch the deck bottom were unsatisfactory.
- **February 1991** – Inspectors gave the Viaduct substructure and superstructure a condition rating 4 (Federal Highway Administration Bridge Inspection Handbook – poor condition, advanced section loss, deterioration, spalling). The estimated remaining service life of the Viaduct was 2 years. Considering the state of bridge deterioration and the cost of repair, the decision was made to replace the structure.
- **1994** – Traffic was routed onto a temporary structure and the original Rocky Point Viaduct was removed.
- **1995** – The replacement Rocky Point Viaduct was opened for use and the temporary structure removed.

The replacement Viaduct, placed in service in 1995, is shown in Figure 2.2.

Figure 2.2: New Rocky Point Viaduct (ca. 1997).

2.3 DEMOLITION AND STUDY BEAM INSTALLATION

The Rocky Point Viaduct was demolished in 1994, Figure 2.3. One beam from the original structure, Beam A1 in Figures 1.2 and 2.3, was preserved with the deck intact for study. The north end of Beam A1 rested on Abutment No. 1 while the south end rested on Bent No. 1. Beam A1 was at the extreme west edge of the viaduct and thus was exposed to the full impact of the environment.

Figure 2.3: Rocky Point Viaduct demolition (1994).

Beam A1 was structurally typical of all beams in the Viaduct. It had a 0.38 x 1.1 m (15 x 44 inch) cross section (not including the deck). The bottom of the beam contained up to eight lengths of 38 mm (1.5 inch) square rebar. Shear stirrups 13 mm (0.5 inch) diameter were spaced along the length of the beam and extended up into the deck. The square rebar and shear stirrup steel had a tensile strength of approximately 556 MPa (81 ksi).

Approximately 14.4 m (47 ft) of the 20 m (66 ft) beam was delivered in one piece to the U. S. Department of Energy, Albany Research Center (ARC) in Albany OR, Figure 2.4. For convenience in transportation, the beam was cut 5.6 m (18.4 ft) short of abutment No. 1. At ARC, the beam was cut in half at its midpoint using a diamond saw. The two resulting sections so formed are referred to in this report as Section 1 (Figure 2.5) and Section 2 (Figure 2.6). In addition, three 0.3 m (1 ft) thick vertical slices were cut from the beam for studying chloride migration during cathodic polarization using planar thermal-sprayed zinc anodes, Figure 2.7. These slices were taken at the midpoint of the beam where structural damage from corrosion appeared least severe.

Figure 2.4: Unloading of Beam A1 from lowboy at Albany Research Center using two cranes to support the beam.

Figure 2.5: Section 1 of the Rocky Point Viaduct beam (east face), grid elements A1 to G47 (right to left).

Figure 2.6: Section 2 of the Rocky Point Viaduct beam (west face), grid elements A54 to G94 (left to right).

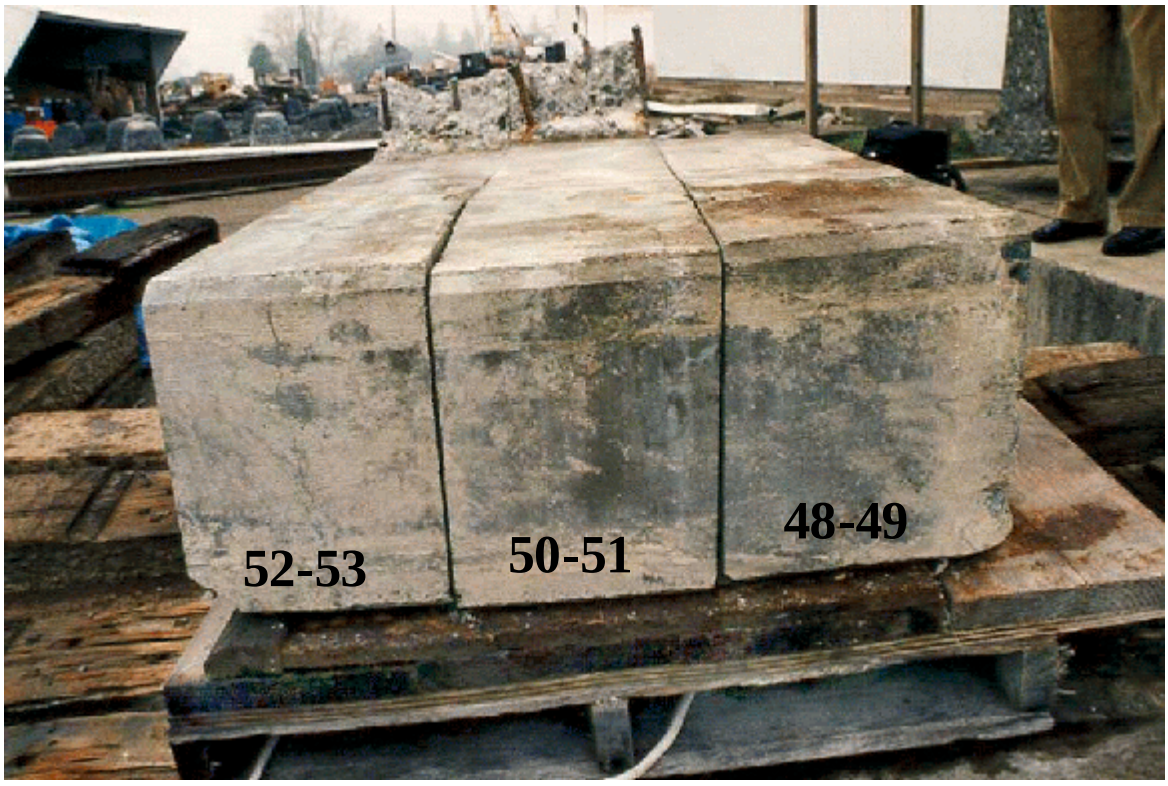

Figure 2.7: Beam slices for chloride migration studies, grid elements A48-G49, A50-G51, and A52-G53.

Steel H-girders were bolted to the deck portion of the beam for support after the beam sections were inverted (deck side down) for study, Figures 2.5 and 2.6. **All figures and drawings of the beam are shown with the beam in this inverted position with the deck side down.** A roofed shelter was built over the beam to prevent rain from wetting the beam and leaching salt from the concrete.

A thin layer of cementitious material was found on the surface of the beam. This layer contained a linseed oil coating that was applied in 1969. It was removed by sandblasting with a nickel-based slag to prevent interference with electrochemical corrosion tests.

After sandblasting, a grid with elements measuring 152 x 152 mm (6 x 6 inch) was painted onto the east and west faces of the beam sections. A grid with elements measuring 152 x 127 mm (6 x 5 inch) was applied to the bottom of the beam. **All observations and measurements are referenced to these grids.** The grid is illustrated in Figure 2.8 and runs continuously the length of the two sections. Longitudinal grid locations on Section 1 ran from 1 to 47; on Section 2 from 54 to 94. The three 0.3 m (1 ft) thick slices included the remaining longitudinal grid locations, i.e., 48-49, 50-51, and 52-53, Figure 2.7. The vertical grid on the sections ran from A to G, with A being the bottom of the beam (top of Figure 2.8) and G being the deck. With the beam inverted, the vertical grid starts with A at the top and descends to G at the deck.

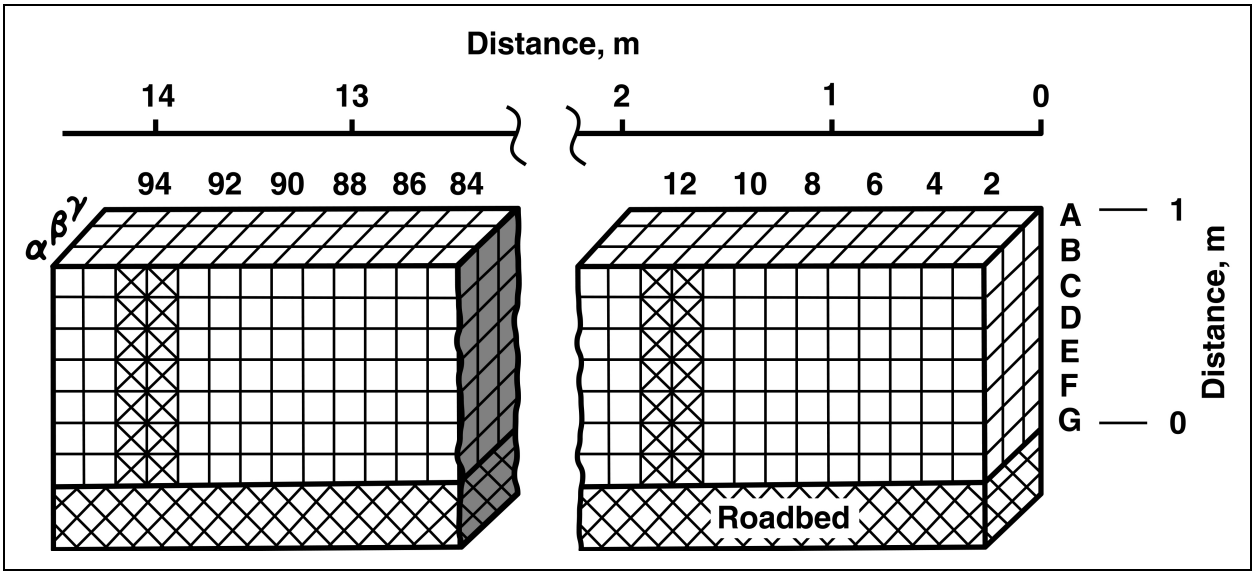

Figure 2.8: Grid placement on beam, Sections 1 and 2.

Reinforcing steel and shear stirrups were located and marked on the beam. Rebar and shear stirrups were tested for continuity in each section of the beam using an AC bridge null procedure. Isolated rebar and shear stirrups were made electrically continuous with all other rebar though copper wire connections.

3.0 BEAM EVALUATION TECHNIQUES

The condition of Beam A1 was characterized by:

- a visual and delamination survey;
- a half-cell potential survey;
- identification and enumeration of microbes on the surface and within cracks;
- chemical and petrographic analysis of the concrete;
- compressive strength and void fraction measurements on the concrete;
- surface air permeability measurements;
- determination of acid and water soluble chloride ion concentrations in the concrete as a function of depth, i.e., chloride ion distribution profile;
- *in situ* rebar corrosion rate measurements; and
- changes in the chloride ion distribution profile resulting from chloride ion migration during ICCP using planar, thermal-sprayed zinc anodes.

3.1 VISUAL AND DELAMINATION

3.1.1 Visual Inspection

The visual survey identified the location of cracks, visible delaminations, exposed rebar, patch and original concrete, and cuts where diaphragms between beams were removed.

3.1.2 Delamination Survey

A delamination survey was conducted using ASTM D 4580-86, "Practice for Measuring Delaminations in Concrete Bridge by Sounding"(*ASTM, 1994a*), as a guide. Delaminations were detected by noting a dull or hollow sound upon striking the beam with a hammer. The location and extent of delaminations were determined and recorded.

3.2 HALF-CELL POTENTIAL SURVEY

The beam was wetted 30 minutes before potential mapping. Rebar half-cell corrosion potential measurements were taken using ASTM C 876-91, "Standard Test Method for Half-Cell Potentials of Uncoated Reinforcing Steel in Concrete"(*ASTM, 1994b*), as a guide. A high impedance voltmeter was connected between the rebar and a reference electrode. A $Cu/CuSO_4$ reference electrode, an electrical junction device (wetted sponge), and an electrical contact solution for wetting the sponge were used to measure the potential of the rebar at the center of each element in the grid. Half-cell potential data were collected and input into contour plotting software. Results were recorded as rebar corrosion potential (in millivolts) versus the $Cu/CuSO_4$ reference electrode and mapped as a function of position on the beam.

3.3 MICROBIAL SURVEY

Three groups of bacteria are known to create conditions that are conducive to degrading concrete, i.e., microbially-influenced degradation (MID). These are: sulfur-oxidizing bacteria, nitrifying bacteria, and some heterotrophic bacteria. All have been isolated from concrete surfaces. The first step in determining whether MID affects concrete is to determine if these bacteria are present at the site of concrete degradation. If they are present, it would then be necessary to determine how actively they promoted MID and the source of energy for metabolic activity. The survey reported here was limited to identifying and counting (enumerating) cells that occurred at selected sampling sites on the beam.

Microbial specimens were obtained by swabbing and scraping the sampling sites. Swabbing consisted of rubbing a sterile cotton swab moistened with sterile deionized water repeatedly over a 200 mm^2 (0.3 $inch^2$) area of the concrete surface. The absorbent tip of the sampling swab was then placed into a 1.5 mL (0.05 oz) snap-top centrifuge tube containing 1 mL (0.034 oz) of sterile deionized water. Scraping was accomplished with a sterilized spatula. Scraped material was caught in a sterilized 50 mL centrifuge tube containing 5 mL of sterile, deionized water.

Small chunks and flakes of rebar corrosion product and concrete from the beam were retrieved using a hammer and chisel. This material was caught in a sterilized Whirl Pak bag and then aseptically transferred to a 50 mL screw-capped tube. Half of the volume of the tube had previously been filled with a foam plug. Sterile, deionized water was used to saturate the pore volume of the plug. The samples were placed on top of the wetted plug and a second foam plug was placed over the sample. In this way the sample was secured in a moist, protective environment for transportation to the Idaho National Engineering Laboratory for analysis.

Samples were collected from both the east and west faces of Sections 1 and 2 at locations given in Chapter 4. A total of 39 samples were obtained from 17 locations. Of these, 31 samples were used to determine the presence of bacteria. Enumeration of microbes was done by the most probable number (MPN) method (*Tratnall and Pope, 1993*).

3.4 CONCRETE PETROGRAPHY

Fourteen 50 and 75 mm (2 and 3 inch) diameter cores were taken from the beam section using a gas-powered core drill, diamond core bits, and water as a coolant. They were used for petrographic analysis, and for void fraction and compressive strength measurements. The 75 mm diameter cores penetrated the full thickness of the beam (0.38 m or 15 inches). They were split into cores approximately 190 mm (7.5 inch) long and tagged according to the beam face (east or west) they represented. The 50 mm diameter cores were shorter, from 75 to 150 mm (3 to 6 inches) in length and tagged according to the face they represented. Mineralogy and lithology of the concrete aggregate was determined by petrographic analysis of the cores, Table 3.1. Coring locations are given in Table 3.1 by the Core Number, which is equivalent to the grid element from which the core was taken. Cores used for compressive strength and void fraction measurements are also listed in Table 3.1.

Aggregate constituents smaller than 4.75 mm in largest dimension were treated as fine aggregate and sand. These constituents were identified and quantified by statistical grain counts, made of all aggregate grains in thin-section fields of view, or of all grains that passed under the cross-hairs of the microscope as parallel, equally-spaced passes were made over thin-sections.

Aggregate constituents greater than 4.75 mm in largest dimension were treated as coarse aggregate, and include the 4.75 to 19 mm and 19 to 38 mm fractions in the concrete mix. Coarse aggregate constituents were identified by examination of polished sections from four split cores and of aggregate exposed at the surface of the 75 mm diameter cores. All coarse aggregate visible on the polished sections were identified and counted. All coarse aggregate within a grid laid out on the exterior surface of the 75 mm diameter cores were identified and counted. In some cases, fragments were removed from aggregate and the minerals present were identified using refractive index oils and a petrographic polarized-light microscope.

A preliminary macroscopic scan of deteriorated areas of concrete, including areas under loosened aggregate, was done using ultra-violet light to determine if significant alkali-silica reaction (ASR) products were present. Seventeen thin sections, prepared for the aggregate study, were examined for reaction products by polarized-light microscopy. Two thin sections were examined by scanning-electron microscopy (SEM) with energy-dispersive x-ray analysis (EDX) and wavelength-dispersive x-ray analysis (WDX). Each thin section was inspected for features that would indicate the presence of reaction products characteristic of: alkali-silica reactions (ASR), alkali-carbonate reactions (ACR), ettringite formation, gypsum formation, carbonation, and chlorination.

Reactions between the concrete and mounting media, such as epoxy, balsam, index oils, water, and alcohol, produced distinctive new reaction products which were observed after only a few days; **these reaction products were disregarded**. Sample preparation also resulted in the formation of cracks; **these cracks were identifiable and disregarded**.

Table 3.1: Cores taken from the Beam A1 sections.

Core No.	ARC lab No.	No. of thin sections	Coarse aggregate identification	Notes
		75 mm (3 inch) Diameter Cores – original concrete		
3D	ME3658		**X**	Boiling water porosity test; compressive strength test.
7D	ME3641	2	**X**	Split, polished core
9E	ME3649	1	**X**	Boiling water porosity test; compressive strength core
14G	ME3642	1		
21E	ME3639	1		
25G	ME3645	1	**X**	Split, polished core.
27F	ME3648	1	**X**	Boiling water porosity test; compressive strength test.
32F	ME3635	1		
41E			**X**	
56F	ME3637/3638	2		
63F	ME3660		**X**.	Compressive strength test
69A/B	ME3646	2		
69E	ME3636	1		
79C	ME3647	1	**X**	Split, polished core
82G	ME3661		**X**	Compressive strength test
85F	ME3640	2	**X**	Split, polished core.
93E	ME3662		**X**	Boiling water porosity test; compressive strength test.
		50 mm (2 inch) Diameter Cores – patch concrete		
15G	ME3673		**X**	
30B	ME3643	1		
36A	ME3644	1		
57C	ME3674		**X**	
77G	ME3675		**X**	

3.5 CONCRETE PROPERTIES

3.5.1 Compressive Strength

Compressive strength of the original concrete was measured using the 75 mm diameter cores. AASHTO T 22-92, "Compressive Strength of Cylindrical Concrete Specimens," was used as a guide in making these measurements (*AASHTO, 1995a*). Since the cores were taken through the full 0.38 m thickness of the beam, they were cut in half at the midpoint to yield a set of cores approximately 178 mm long characterizing the west (or ocean) facing side of the beam and the east (or landward) facing side of the beam.

3.5.2 Void Fraction

Permeable voids within the concrete were determined as a percentage of concrete volume using the boiling water test from ASTM C 642-90, "Standard Test Method for Specific Gravity, Absorption, and Voids in Hardened Concrete"(*ASTM, 1995c*), and from AASHTO T 209-94, "Maximum Specific Gravity of Bituminous Paving Mixtures"(*AASHTO, 1995b*), also known as the Rice specific gravity method.

3.5.3 Surface Air Permeability

Another measure of the permeability of the concrete to the ingress of atmospheric constituents is surface air permeability. Surface air permeability of the concrete on the east face of Section 1 was measured using a concrete air permeability tester (also described as a surface air flow permeability indicator). This instrument is based on the principle that flow of air through a concrete surface will be higher for concrete with a higher permeability. Operation of the instrument required a vacuum of about 640 mm (25 inch) Hg. Air flow was measured by a mass flowmeter. The instrumentation is available as a self-contained portable unit, Figures 3.1 (a) and 3.1(b). Its operation is described in the "Showcase Workshop on Concrete Durability" (*FHWA-SHRP, 1995*) and in SHRP-S-329, "Condition Evaluation of Concrete Bridges Relative to Reinforcement Corrosion – Volume 7: Method for Field Measurement of Concrete Permeability" (*Whiting and Cady, 1993*).

Figure 3.1a: Measuring permeability of concrete with portable Surface Air Flow Permeability Indicator (SHRP Product 2031).

Figure 3.1b: Surface Air Flow Permeability Indicator showing measuring head with foam rubber gasket that makes an airtight seal with the concrete surface.

3.5.4 Chloride Content and Distribution

Chloride ion concentration in the concrete was determined using the Oregon DOT sampling technique and equipment, Figure 3.2. Pulverized concrete powder samples are removed through the hollow center of a drill bit from the hole created by a hammer drill. The concrete powder is collected on a filter for later analysis of calcium and chloride ion concentration. The concrete powder samples are collected over equally spaced depth increments into the concrete so that the chloride ion distribution profile can be reconstructed. The sampling equipment included an impact hammer drill, a hollow drill bit, a powder collector, and a vacuum source. Concrete powder samples were collected at 12.7 mm (0.5 inch) depth increments through the entire 0.38 m thickness of Beam A1. Care was taken to avoid cross-contamination of samples with powder from earlier samples. This was done by vacuuming out the drill hole(s) in the concrete between each sample collection, and by removing powder from the hollow drill and the collection line after each sample collection. Full descriptions of the equipment and procedures followed in powder sampling the concrete to produce samples for chemical analysis are given in APPENDIX D – Sections D.1.1 and D.1.2.

Figure 3.2: Chloride profiling beam with Oregon DOT powder sampling apparatus. Worker is holding the rotary hammer with the left hand and the polypropylene pipe spacer surrounding the air bit with the right hand. The powder collection filter is hanging from the air system adapter below the air bit.

All of the square rebar lay in the patch concrete in grid locations A through C, Figure 3.3. Original concrete contained only shear stirrups and represented most of the beam cross-section, grid locations D through G. Patch concrete chloride ion samples were taken from grid locations A and B, with the axis of the sampling hole running between the square rebar. Original concrete samples were taken from grid locations E and F. The first set of powder samples was taken from the "as-received" beam. Two additional sets were taken after 0.5 and 1.0 years of ICCP, and were labeled 0.5 and 1.0 year samples.

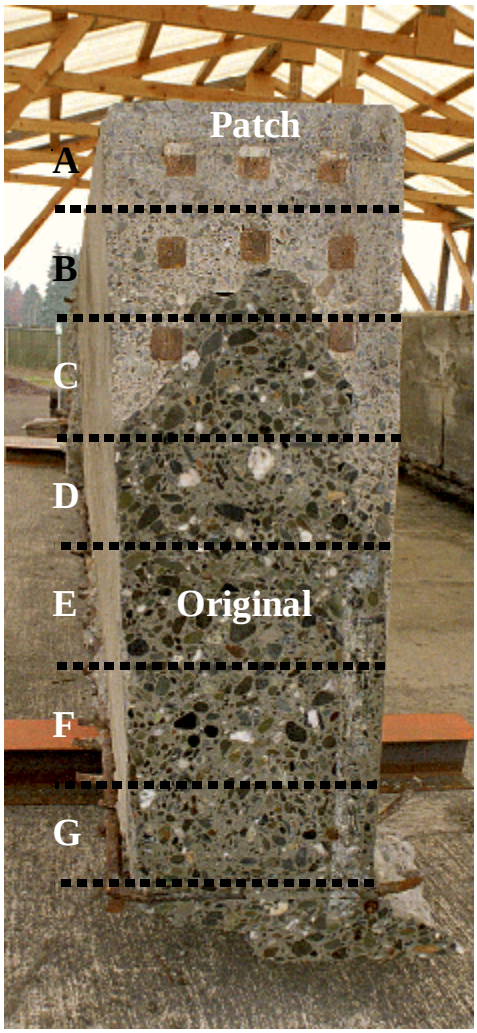

Figure 3.3: Cut end of Section 2 showing square rebar, the original and patch concrete, and the grid locations used in taking Cl powder samples for determining chloride profiles and chloride migration under ICCP.

All powdered concrete samples were analyzed for both acid (total) and water soluble chloride ions, with the results expressed as weight fraction of the powder sample. Analysis techniques given in AASHTO T 260-94, "Sampling and Testing for Chloride Ion in Concrete and Concrete Raw Materials," were used as a guide (*AASHTO, 1995c*). Calcium concentration was also determined for each powder sample and used to correct the chloride concentration values for the amount of aggregate contained in the powder sample. The procedures followed in analyzing the powdered concrete samples are described in APPENDIX D – Section D.1.2.

3.6 CORROSION RATE AND CONCRETE RESISTIVITY

A direct measure of corrosion state of the reinforcing bar is the instantaneous corrosion rate expressed as the corrosion current, I_{corr}. The corrosion rate was measured using the GECOR6 apparatus from James Instruments and used in Federal Highway Administration Demonstration

Project No. 84, "Corrosion Detection in Reinforced Concrete Structures" (*FHWA, 1992*). The GECOR6 is based on linear polarization theory and involves perturbing the rebar corrosion potential, E_{corr}, with small dc potentials (±10 to ±20 mV) and measuring the resulting current. The measurements are used to calculate the corrosion current, I_{corr}.

An electrical connection was made to the reinforcing bar, and a multi-sensor disk was placed on the concrete surface over the reinforcing bar. The multi-sensor disk has three $Cu/CuSO_4$ reference electrodes and two guard rings that limit the area beneath the sensor disk where the corrosion rate is measured. A wet sponge facilitates electrical contact between the multi-sensor disk and the concrete. After the GECOR6 indicates the corrosion potential of the rebar is stable enough for a measurement, the linear polarization procedure is begun. The unit then reports the corrosion potential in mV vs. $Cu/CuSO_4$ and the corrosion rate in $\mu A/cm^2$.

Corrosion rates were measured at locations on the east face of Section 1 from grid location A1 to G14. The grid elements were divided in half for the corrosion rate measurements, thereby doubling the number of grid elements in both directions. Using this half-element grid, it was easier to position the multi-sensor disk directly over a length of rebar to make the corrosion rate measurement. All the measurements were made in grid elements that were not delaminated nor contained cracks. Duplicate measurements were made at many of the locations and the mean value was reported. The measurements were made on a mild (18-24° C or 65-70° F) and dry day in August.

It is claimed the GECOR6 can also be used to measure concrete resistivity. Concrete resistivity, when computed from resistance measurements, is proportional to the cross-sectional area of the concrete volume contained between the measuring surfaces and inversely proportional to the distance from the surface of the concrete to the rebar. However, GECOR6 does not use cover depth in calculations (it is not an input to the computational algorithm), and the manual shows an equation with the resistivity proportional to the diameter of the cross-sectional area (instead of the square of the diameter, as it should be) and to a factor "2" that may be an approximation for the reciprocal of the thickness of the concrete cover. For these reasons, the authors failed to see the value in measuring concrete resistivity with the GECOR6, and measurements were terminated.

3.7 CHLORIDE MIGRATION

Cathodic protection is the most effective and widely used method for controlling rebar corrosion in concrete in high chloride environments (*Mudd, Mussinelli, Tettamanti, and Pediferri, 1988*). Thermal-sprayed anodes are increasingly being used in CP installations for coastal bridges (*Appostolos, Parks and Carello, 1987; Bullard, Cramer, Covino, Holcomb, McGill and Reis, 1998; Covino, Cramer, Bullard, Holcomb, McGill and Cryer, 1996*). The three beam slices (i.e., sections 48-49, 50-51, and 52-53 taken from the Beam A1 mid-section, Figure 2.7) contained the salt accumulated in the concrete over 40 years exposure on the Oregon coast. They presented a unique opportunity to examine the effect of ICCP on chloride migration and any benefits that may accrue.

To accomplish this, the three slices were prepared for ICCP using thermal sprayed zinc anodes in the same manner as used by Oregon DOT for coastal bridge installations (*Bullard, Cramer, Covino, Holcomb, McGill and Reis, 1998; Covino, Cramer, Bullard, Holcomb, McGill and Cryer, 1996*). The twin-wire arc-spray parameters for applying zinc anodes on coastal bridges are given in Table 3.2.

Table 3.2: Twin-wire arc-spray parameters for zinc used as an anodes in reinforced concrete bridge cathodic protection systems in coastal environments (*Rogers, 2000*). [1]

Wire diameter mm (inch)	Current A	Voltage V_{dc}	Spray rate kg/hr	Deposition efficiency %
3.2 (1/8)	350	27	37.6	58.0
3.2 (1/8)	450	27	46.2	53.6
4.8 (3/16)	350	27	51.2	64.8
4.8 (3/16)	450	27	61.2	67.4

[1] atomizing gas, air; atomizing gas pressure, 0.62-0.79 MPa (90-110 psi); spray orientation, normal to surface at 15-23 cm (6-9 inches) distance; multiple spray passes to build up anode thickness.

Impressed current cathodic protection was applied to the beam slices for a total of 1.0 years at the accelerated rate of 30 mA/m^2 (compared to the rate of 2.2 mA/m^2 used by Oregon DOT in coastal ICCP installations). The one year test period was equivalent to the charge passed at Oregon DOT coastal ICCP installations over 15 years operation. The anode reaction is:

$$\mathbf{Zn + 2H_2O \rightarrow Zn(OH)_2 + 2H^+ + 2e^-} \qquad \mathbf{(3\text{-}1)}$$

Under drying conditions, and bridges undergo repeated wetting and drying cycles, the zinc hydroxide can be converted to zinc oxide:

$$\mathbf{Zn(OH)_2 \rightarrow ZnO + H_2O} \qquad \mathbf{(3\text{-}2)}$$

The dominant cathode reaction is:

$$\mathbf{2H_2O + O_2 + 4e\text{-} \rightarrow 4OH^-} \qquad \mathbf{(3\text{-}3)}$$

with the rebar cathodically protected by:

$$\mathbf{Fe^{2+} + 2e^- \rightarrow Fe} \qquad \mathbf{(3\text{-}4)}$$

Reaction 3-3 shows that the pH of the rebar-concrete interface increases as a consequence of cathodic protection. This may lead to conditions where the rebar can again become passive and protected by the naturally formed iron oxide film. Acidification of the anode-concrete interface, Reaction 3.1, is another consequence of cathodic protection.

Preparatory to thermal spraying the beam slices, the deck section was removed from each slice. The cut faces were masked off to prevent coating with zinc. The exposed surfaces were then sandblasted with green nickel slag to produce a medium sandpaper finish without overexposing the aggregate. The sandblasted surface was then thermal sprayed with Zn to form a Zn anode

with a thickness of about 20 mil (*Covino, Bullard, Holcomb, Russell, Cramer, Bennett, and Laylor, 1999; Covino, Bullard, Holcomb, Russell, Cramer, McGill, and Cryer, 1997*). The cut faces were then coated with epoxy paint to prevent moisture entry or loss along the beam axis (since this would not have occurred in the uncut beam) and to electrically insulate exposed rebar.

The beam slices, with Zn anode in place, were then placed inside a tented enclosure constructed in the laboratory for controlling humidity and temperature, Figure 3.4. The enclosure conditions were 70 pct relative humidity (RH) and 21° C (70° F). The slices were kept in this enclosure for one month to equilibrate with tent conditions before ICCP was begun.

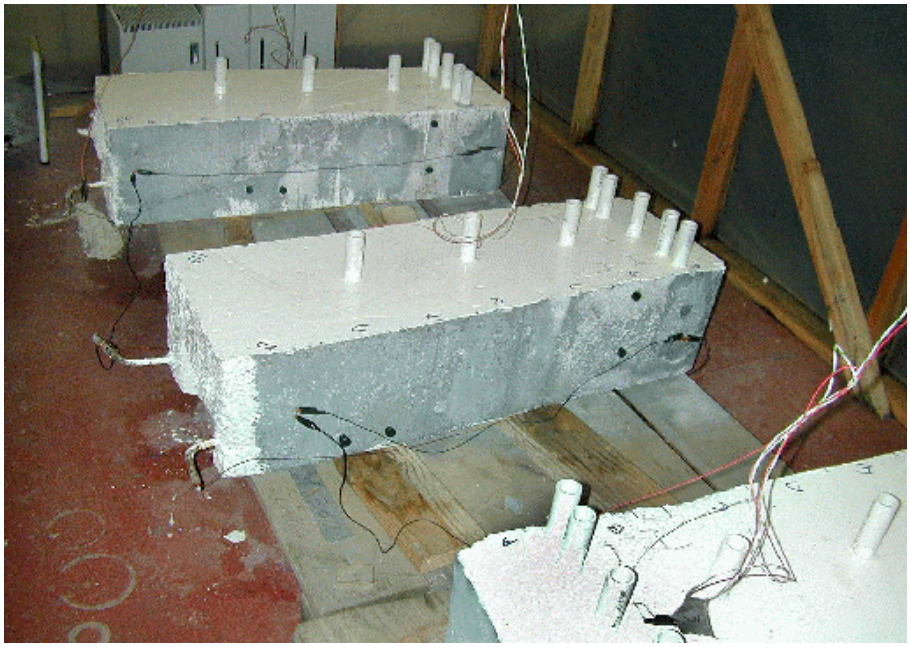

Figure 3.4: Beam slices in temperature and humidity controlled tent. The white polypropylene pipes are locations for measuring rebar potential with $Cu/CuSO_4$ reference electrode.

3.7.1 Accelerated ICCP

The rebar and shear stirrups in each beam slice were made electrically continuous. Electrical connection was made to the thermal-sprayed Zn anode using a metal washer pressed into the Zn coating surface with a metal screw electrically isolated from the rebar and shear stirrups. Multiple connections were made to provide redundancy in case a connection failed. The square rebar and shear stirrup cathode elements of each beam slice were connected to the thermal-sprayed Zn anode to form a typical constant current ICCP system. The anode-to-cathode voltage floated according to the instantaneous resistance of the beam slices.

The beam slices were connected in series so that only one constant current source was needed. The current and the operating voltage for each slice, and the enclosure temperature and relative humidity were monitored on an hourly basis over the one-year duration of the experiment. The

zinc anode on each slice was wetted by spraying with deionized water once a day to simulate coastal wetting from rain and fog. Current was maintained at about 3 mA/ft^2 of anode area, an acceleration by a factor of 15 times greater than the value 2.2 mA/m^2 (0.2 mA/ft^2) used by the Oregon DOT on coastal bridges. Average values of the anode and cathode areas and current densities are given in Table 3.2.

Table 3.3: Chloride migration constant current ICCP test parameters.

Test parameters	Slice grid sections		
	48-49	**50-51**	**52-53**
cathode area[1], m^2 (ft^2)	0.453 (4.88)	0.460 (4.95)	0.372 (4.00)
cathode current density, mA/m^2 (mA/ft^2)	32.9 (3.06)	32.5 (3.02)	38.5 (3.74)
anode area[2], m^2 (ft^2)	0.692 (7.45)	0.758 (8.16)	0.734 (7.90)
anode current density, mA/m^2 (mA/ft^2)	21.6 (2.01)	19.7 (1.83)	20.3 (1.89)

[1] Cathode area is the total surface area of the square rebar and any shear stirrups in the slice.
[2] Anode area is the total slice area thermal sprayed with zinc.

3.7.2 Chloride Content and Distribution

Patch concrete and original concrete Cl profiles in the beam slices were determined using the same powder sampling technique described in Section 3.5.4 after 0.5 and 1.0 years of ICCP. The patch concrete samples were taken from grid elements A and B and the original concrete samples were taken from grid elements E and F, Figure 3.3.

3.8 CONTOUR MAPS

The results of potential, corrosion rate, and air permeability surveys are presented as contour maps generated by TRANSFORM software (Version 3.3).[1] The half-cell potential and surface air permeability contour maps were produced on a 152 mm (6 inch) grid; the corrosion rate contour map was produced on a 75 mm (3 inch) grid.

The surveys did not include every grid location. A number of locations were in damaged concrete or on rough surfaces. Missing data points were calculated in TRANSFORM by using the Kriging technique, a weighted fill method to estimate missing data points while preserving known data values. Estimates of missing data points are weighted using a variance matrix to produce the contour surface that best represent the data. The contour maps were generated by interpolating within the data sets and adding contours: every 50 mV for the potential maps, every 1 µm/y for the corrosion rate map, and every 10 ml/min for the air permeability map.

[1] Fortner Research LLC, Sterling VA (phone 703-478-0181)

4.0 RESULTS AND DISCUSSION

4.1 VISUAL AND DELAMINATION

4.1.1 Visual Inspection

The beam cross section at grid location 54 is shown in Figure 3.3. The patch concrete is at the top of the photo surrounding the large square rebar and extends down the cross-section into grid element D. The original concrete was differentiated from the patch concrete by wetting the original concrete. The figure also shows the configuration and cover over the square rebar and the shear stirrups. Cover depth in Beam A1 is not known for the original concrete since it was removed from the bottom of the beam in 1969. Cover depth for the square rebar and shear stirrups in the patch concrete are given in Table 4.1 for a limited number of direct measurements with a ruler. Average concrete cover over the square rebar was 4.96 cm (1.84 inches) at the bottom of the beam and 6.75 cm (2.65 inches) on the sides of the beam. Average cover over the shear stirrups, located outside of the square rebar, was much shallower: 2.80 cm (1.10 inches) on the bottom and 3.22 cm (1.27 inches) on the sides. A more conservative estimate of the shear stirrup cover on the sides, based on the square rebar cover depth, is 4.97 cm (1.96 inches). This estimate was used later in estimating time to cracking based on chloride ion distribution profiles. The cover depths in Table 4.1 suggest the time to cracking will be even less than computed in these analyses (see Section 4.5.4).

Table 4.1: Concrete cover over square rebar and shear stirrups in patch concrete.

Beam location	Concrete cover, depth in cm (inches)		
	minimum	**average**	**maximum**
sides:			
square rebar	5.20 (2.05)	6.75 (2.65)	8.20 (3.23)
shear stirrups	2.50 (0.98)	3.22 (1.27)	4.00 (1.57)
Bottom:			
square rebar	4.30 (1.69)	4.96 (1.84)	6.00 (2.36)
shear stirrups	not measured	2.80 (1.10) [1]	not measured

[1] Most of concrete spalled from beam and could note be measured. Estimated from shear stirrup dimensions and typical separation of shear stirrup from square rebar.

A coal-tar epoxy joint was found at the interface between the patch and original concrete. This joint is the continuous black line between the patch and original concrete seen in Figure 4.1. It was installed during the 1969 repair to prevent salt from diffusing into the patch concrete from the original concrete.

Figure 4.1: Coal-tar epoxy joint between patch and original concrete.

Inspection of the exposed rebar showed: a coal-tar epoxy coating on some of the square rebar, evidently to act as a barrier to further corrosion, Figure 4.2; and an inorganic zinc paint on some of the remaining rebar, evidently to serve as a sacrificial coating and prevent further corrosion damage to the rebar, Figure 4.3. In addition, a linseed oil coating was applied to the exterior of the beam, covering both exposed original concrete and patch concrete, Figure 4.4. Clearly, given the premature failure of the Viaduct, the coal-tar epoxy joint, the coal-tar and inorganic zinc coatings on the square rebar, and the linseed oil coating were ineffective in preventing further corrosion damage.

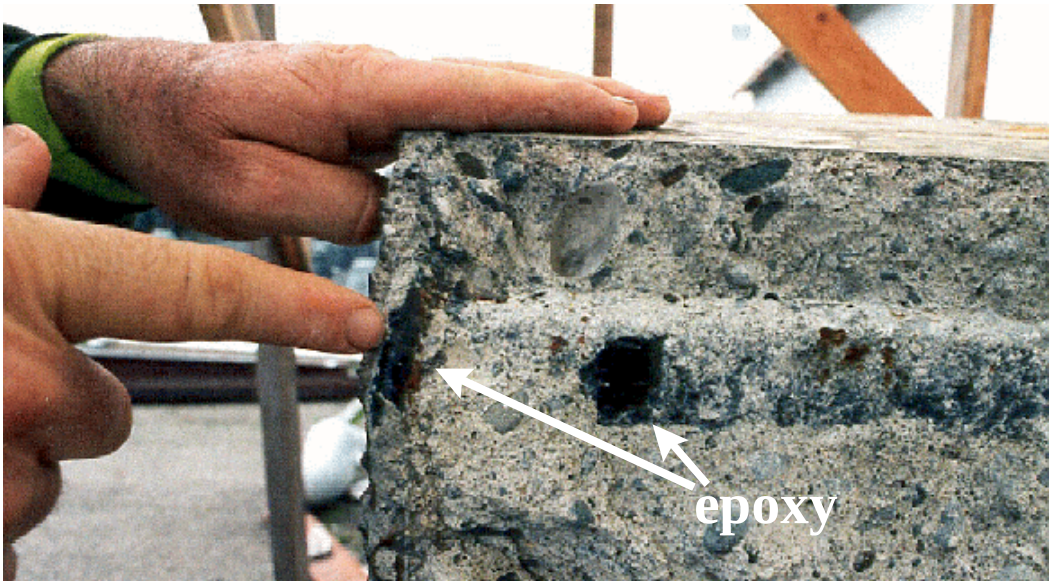

Figure 4.2: Coal-tar epoxy coating on square rebar.

Figure 4.3: Inorganic zinc coating on square rebar.

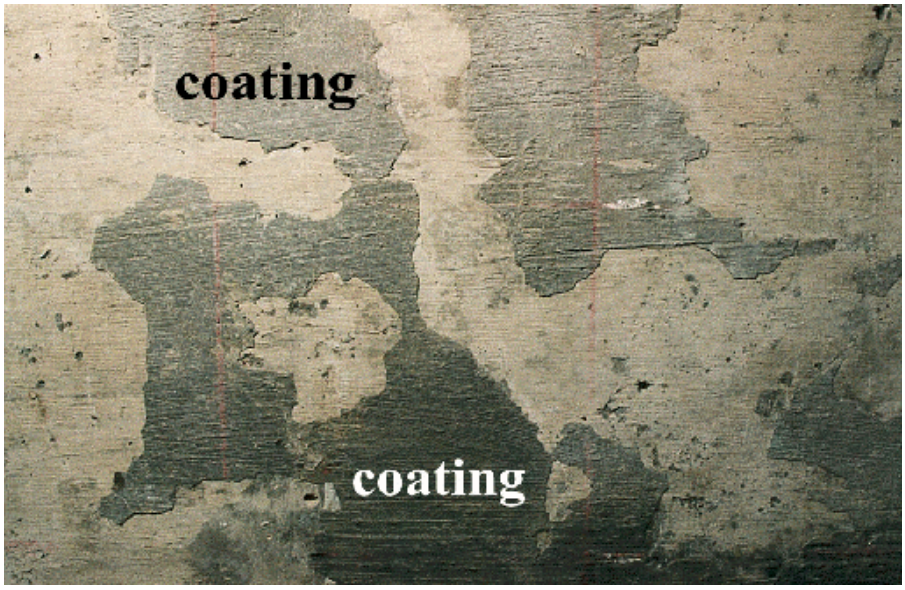

Figure 4.4: Remnants of linseed oil coating on concrete.

The cuts through the beam mid-section to make the beam slices used in chloride migration studies revealed massive cracking within the deck radiating from the round deck rebar, Figure 4.5. In this figure the top of the deck is at the bottom of the image. A close-up of the rebar shows the extent of damage resulting from rebar corrosion, Figure 4.6. Only 0.025 mm (1/1000 inch or 1 mil) of rebar corrosion is sufficient to cause concrete to crack (*McDonald, Pfeifer and Sherman, 1998*). The cracking occurs because the corrosion products (rust) are more voluminous than the steel that is removed by corrosion (*Kubaschewski and Hopkins, 1962*). The

more voluminous corrosion products generate stresses within the concrete that exceed the tensile strength of the concrete (*Allan, 1995*). The resultant cracking of the concrete exposes rebar to additional paths for chloride penetration of the structure that further accelerate corrosion. These processes can lead to massive spalling of cover concrete and further exposure of the underlying rebar to the environment. Concrete damaged in this way has been seen on a number of reinforced concrete bridges on the Oregon coast. The cracking seen in Figures 4.5 and 4.6 is a manifestation of these processes.

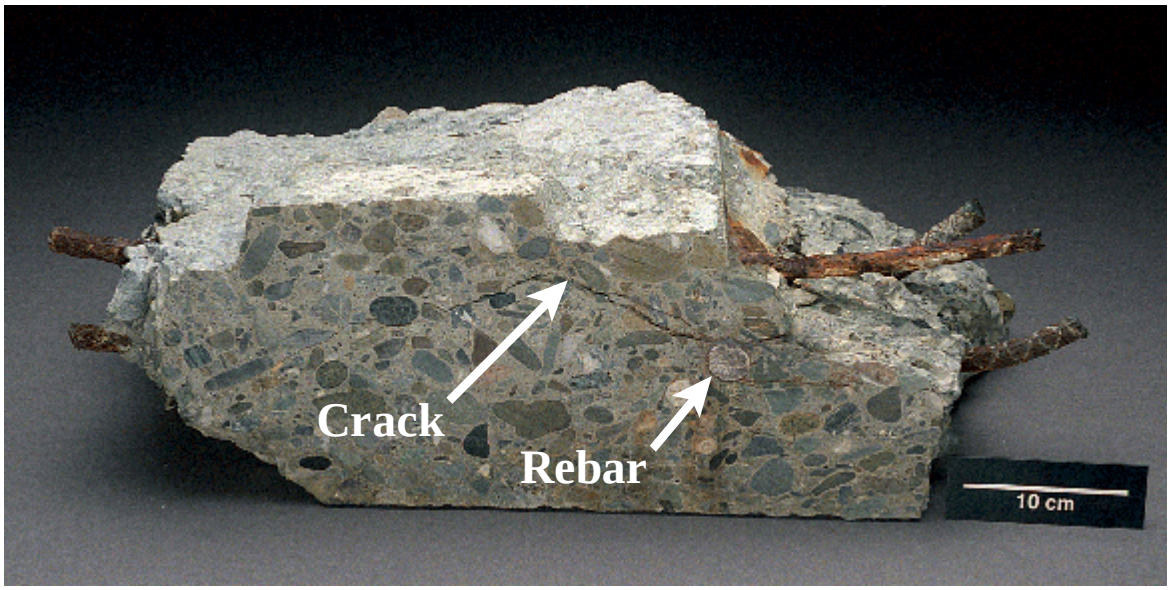

Figure 4.5: Deck cross-section showing cracks radiating from rebar.

Figure 4.6: Close-up of deck cross-section showing cracks radiating from rebar.

4.1.2 Delamination Survey

Cracks, delaminations, and spalls in the beam are schematically shown in Figures 4.7 through 4.10. These are the features that ultimately led to the replacement of the Rocky Point Viaduct. Once they began to develop, the rebar was increasingly exposed to the corrosive coastal environment and experienced loss of section at an accelerating rate, weakening the structure.

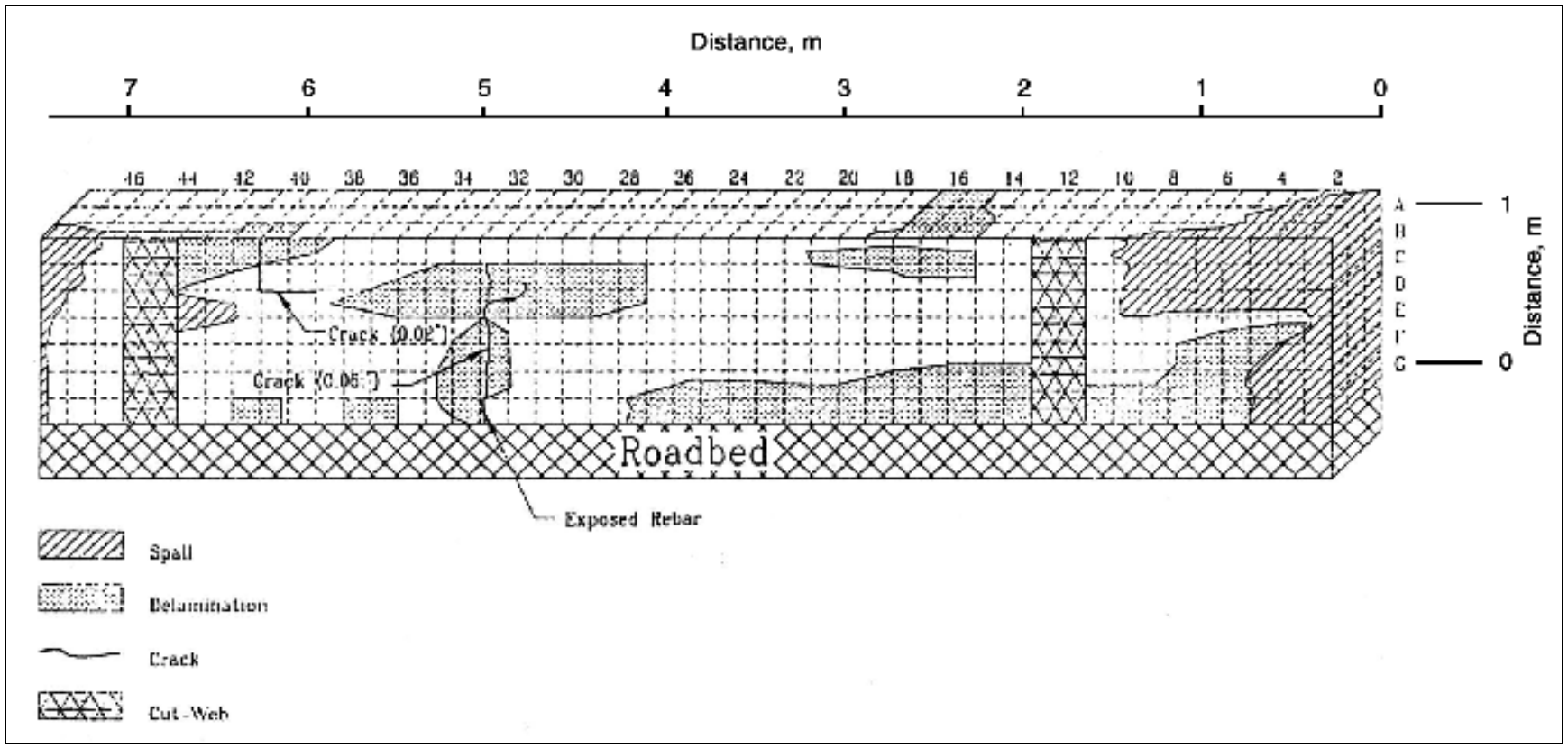

Figure 4.7: Schematic of section 1, east face, showing visual inspection and delamination survey results.

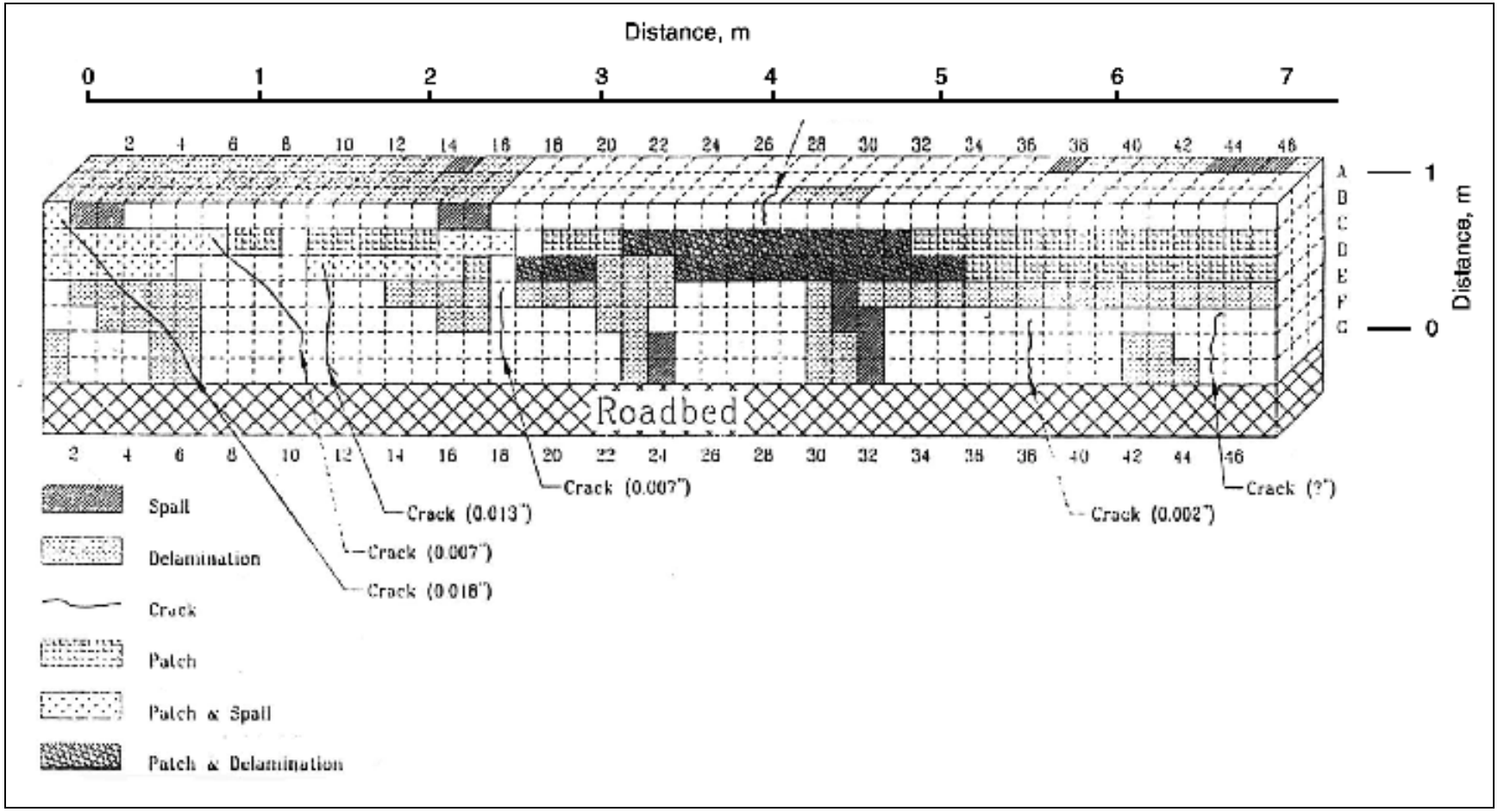

Figure 4.8: Schematic of section 1, west face, showing visual inspection and delamination survey results.

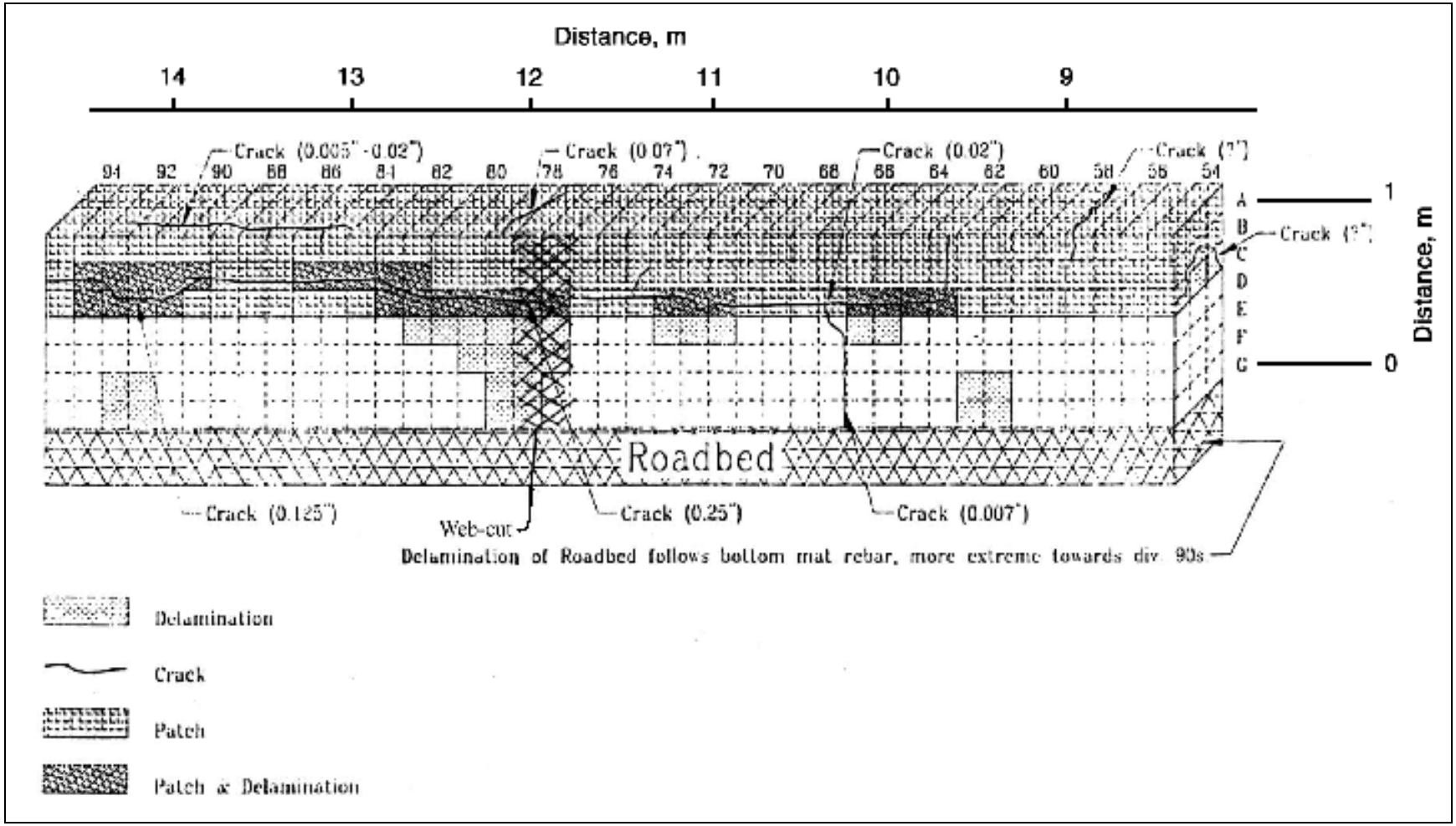

Figure 4.9: Schematic of section 2, east face, showing visual inspection and delamination survey results.

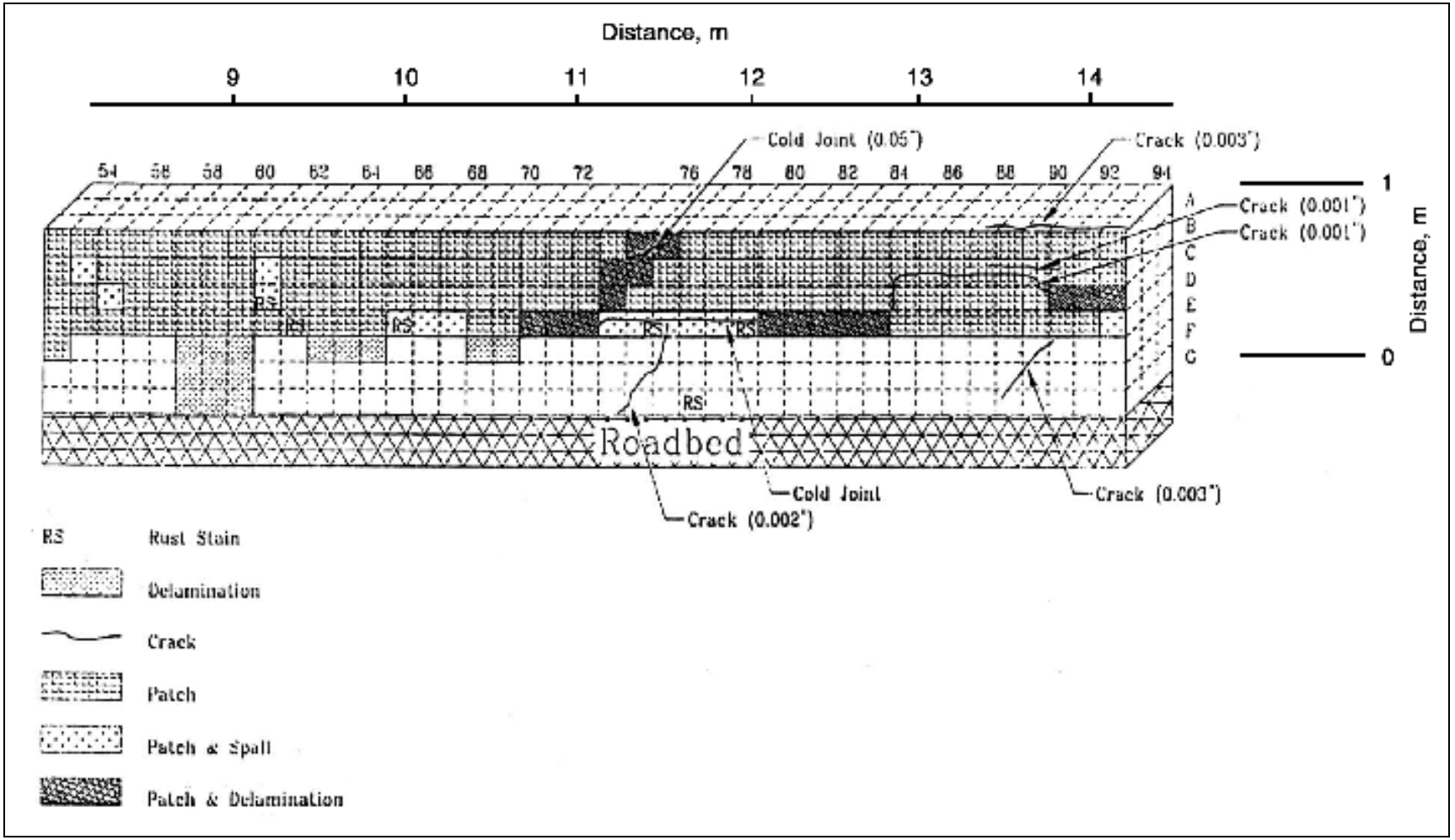

Figure 4.10: Schematic of section 2, west face, showing visual inspection and delamination survey results.

4.2 HALF-CELL POTENTIAL SURVEY

Rebar corrosion potentials are mapped in Figures 4.11 through 4.14 for Beam A1. The potential survey data are contained in APPENDIX A. If potentials are more positive than -200 mV vs. $Cu/CuSO_4$, then there is a greater then 90 percent probability that no rebar corrosion is occurring in the area at the time of the measurement. If potentials are in the range -350 to -200 mV, corrosion activity is uncertain. If potentials are more negative than -350 mV, there is a greater than 90 percent probability that corrosion is occurring at the time of the measurement (*ASTM, 1994b*). There are substantial areas of the beam that had potentials more negative than -350 mV.

Shear stirrups were the location of high corrosion activity at the contact with the deck and near the bottom of the beam. While areas of high probability for corrosion activity are not completely correlated with the location of the shear stirrups, many of the shear stirrup locations had very negative (i.e. high) corrosion potentials. These areas extended along the line of the shear stirrup from the deck upwards to the square rebar. The shear stirrups had the least concrete cover of the steel in the beam. Chloride ions diffusing into the concrete would reach the shear stirrups before the square rebar, and corrosion would initiate on the shear stirrups first.

Comparing the potential surveys, Figures 4.11 through 4.14, with the visual and delamination surveys, Figures 4.7 through 4.10, there was obvious correlation between the areas of severe damage around the square rebar and areas of high corrosion potential. However, the potential surveys also showed areas of high corrosion potential over the shear stirrups that was not necessarily evident from the visual and delamination surveys. Furthermore, the damage to the concrete in the lower part of the beam where the square rebar was located could more likely be attributed initially to the presence of the shear stirrups and their associated shallow cover concrete. Thus the shear stirrups appear to be the primary cause of early damage to the beam.

The probability that corrosion damage initiated with the shear stirrups is also suggested by Figure 2.5. Here the portion of the beam that rested on Bent No.1 has an inclined lower edge (top of the figure) that is severely spalled, and all of the shear stirrups are exposed. The inclined lower edge would have been a collector for precipitation draining from the beam, particularly dew and fog containing high concentrations of chloride ion. This would lead to longer periods of wetness and higher rates of chloride diffusion into the concrete. As a consequence, corrosion of the shear stirrups would initiate earlier along this edge, the concrete would crack and spall, and more aggressive conditions would exist for continued corrosion of the shear stirrups and square rebar.

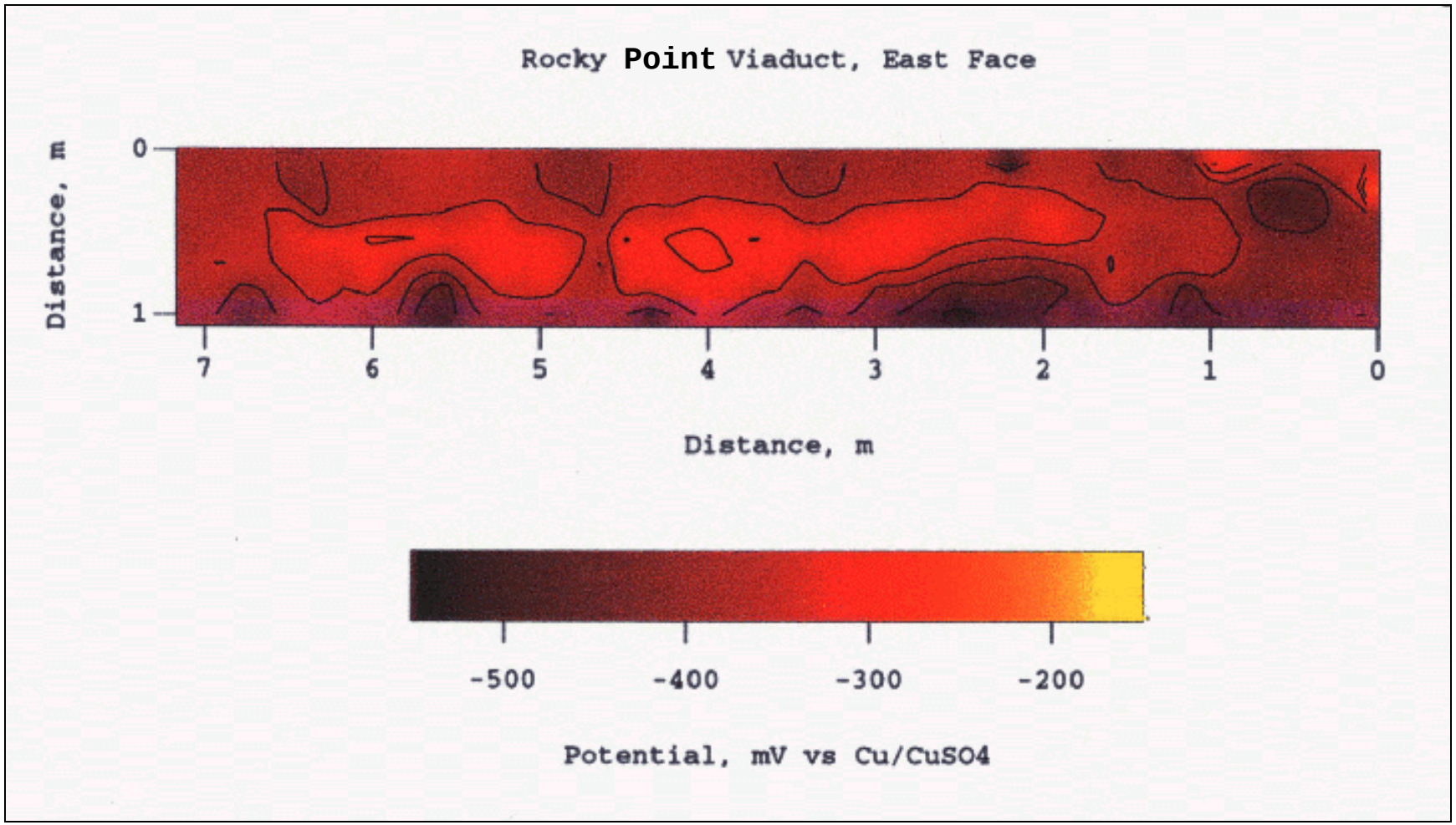

Figure 4.11: Contour map of rebar potential for Section 1 (east face).

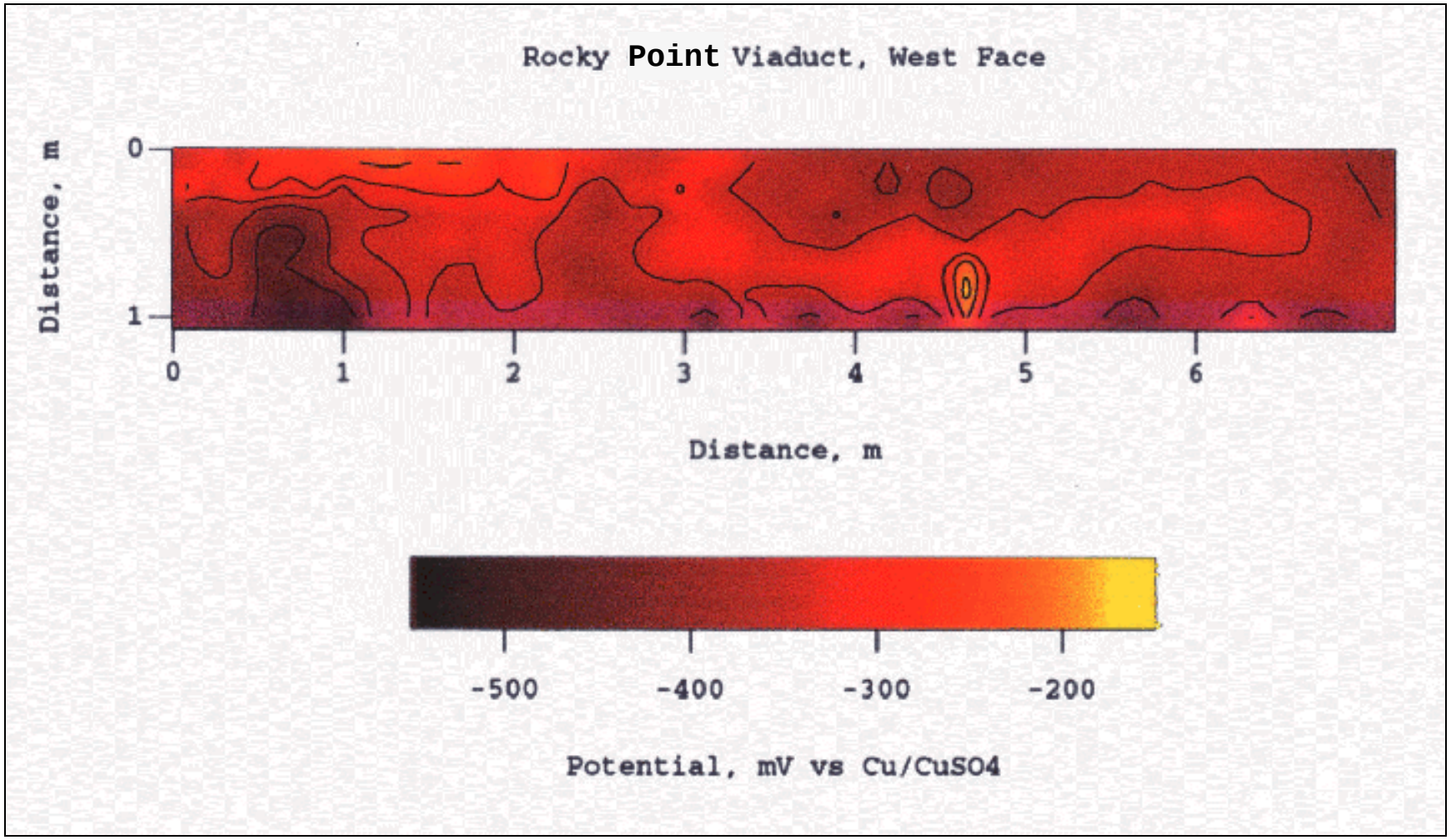

Figure 4.12: Contour map of rebar potential for Section 1 (west face).

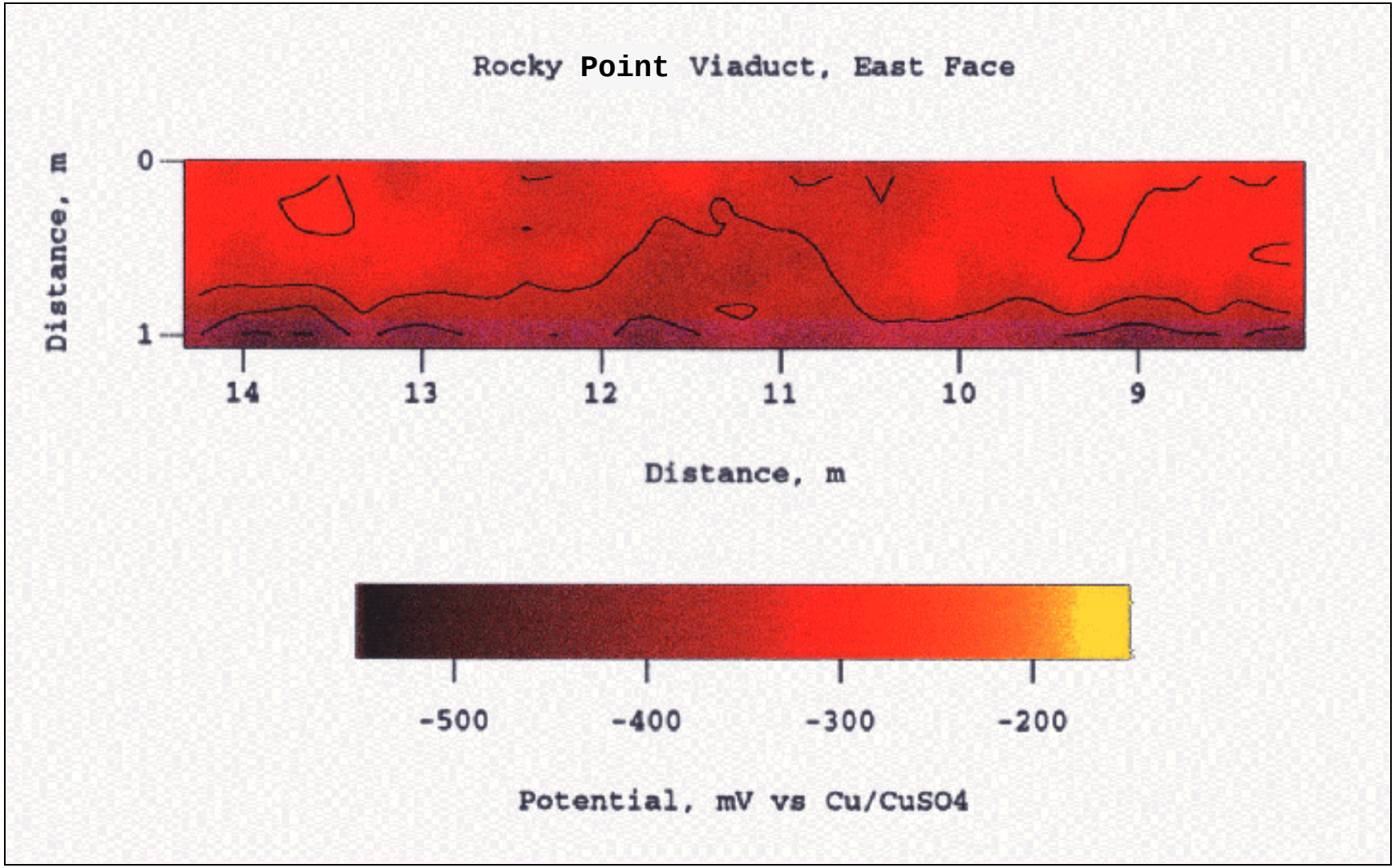

Figure 4.13: Contour map of rebar potential for Section 2 (east face).

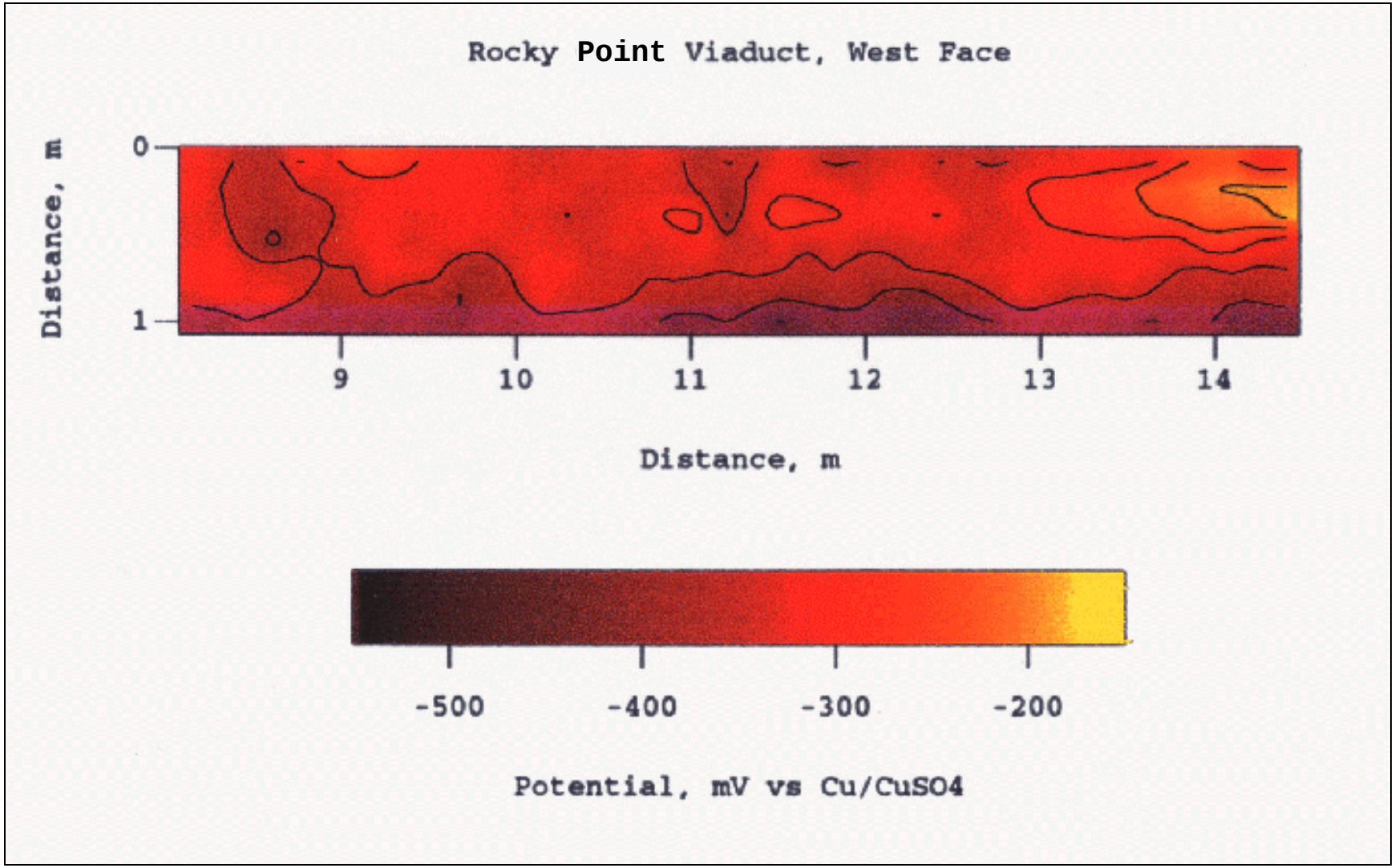

Figure 4.14: Contour map of rebar potential for Section 2 (west face).

4.3 MICROBIAL SURVEY

Only the *T. thiooxidans* bacteria were found on Beam A1. These microbes were found on spalled original concrete, on patch concrete, and on spalled patched areas. Bacteria enumeration results from the Rocky Point cultures are given in Table 4.2. The numbers of bacteria ranged from 7.8×10^2 to 4.9×10^7 cells/cm^2 (50×10^2 to 32×10^7 cells/in^2). An average of 10^7 *T. thiooxidans* cells per cm^2 were recovered from samples 13, 15, and 17 of section 1 and sample 24 of section 2, with an average of 10^3 cells/cm^2 at three additional locations on section 2 (Samples 20, 22, and 26).

T. thiooxidans was found only on the west (ocean) facing side of the beam. This finding leads to the suggestion that nutrients from the ocean were the source of the sulfur oxidized by the microbes. One of the microbe metabolic products is sulfuric acid. Later results will show the original concrete on the west side of the beam had a lower compressive strength than original concrete on the east side, although not so much lower as to affect structural performance of the beam. It is not known at this time whether there is a correlation between the presence of the bacteria on the west side of the beam and the lower compressive strength of the concrete on this side.

Sulfur oxidizing bacteria grow in an ecosystem that is generally hostile to most other organisms. Sulfides are the energy source for these bacteria. When *T. thiooxidans* are present in large numbers, the pH in their vicinity can reach 0.5 to 1.0. Such acid environments will attack the cementitious material in the concrete and destroy its structural integrity. This type of attack normally leaves a white precipitate of gypsum ($CaSO_4$) behind. However, no evidence of gypsum was found, probably due to repeated washing of the beam surface by rain and removal of gypsum in precipitation runoff.

While nowhere in the literature has it been suggested that bacterial action contributes to the deterioration of reinforced concrete bridges, this is a subject that should not be categorically dismissed.

Table 4.2: Numbers of *thiobacilli* recovered from Rocky Point Viaduct microbial cultures.

Sample number	Numbers of recovered thiobacilli, cells/cm^2 [1]			Beam section, exposure
	T. neapolitanus	***T. intermedians***	***T. thiooxidans***	
1	nd	Nd	nd	Section 1 east
2	nd	Nd	nd	"
6	nd	Nd	nd	"
8	nd	Nd	nd	"
10	nd	Nd	nd	"
11	nd	Nd	nd	Section 1 west
13	nd	Nd	4.9×10^7	"
15	nd	Nd	1.1×10^7	"
17	nd	Nd	7.8×10^6	"
20	nd	Nd	3.9×10^3	Section 2 west
22	nd	Nd	3.1×10^2	"
24	nd	Nd	1.3×10^7	"
26	nd	Nd	7.8×10^2	"
30	nd	Nd	nd	"
33	nd	Nd	nd	Section 2 east
36	nd	Nd	nd	"
38	nd	Nd	nd	"

[1] nd means not detected.

4.4 CONCRETE PETROGRAPHY

APPENDIX B contains definitions for the components making up the coarse and the fine aggregate, and the key to identification of coarse aggregate minerals in color and black-and-white photographs of the 75 mm (3-inch) diameter cores, Figures 4.15 through 4.20. APPENDIX B also includes detailed results of the petrographic analyses.

4.4.1 Fine aggregate

A statistically significant number of aggregate particles was counted for original concrete and patch concrete. The patch concrete shown in Figure 3.3 was called Patch 1. The patch material in 75 mm diameter core 69A/B was substantially different from Patch 1 and was called Patch 2. The mean abundance and standard deviation for the fine aggregate components derived from grain counts are shown in Table 4.3. An immediately obvious difference between the original and Patch 1 concrete was the presence of devitrified slag particles in Patch 1. Compared to the original concrete, Patch 1 concrete contained more grains in the following categories: serpentinite, quartz, and feldspar. It contained fewer grains in the following categories: chert and quartzite (silica); granite, diorite, and andesite; and fewer holes.

The fine aggregate in Patch 2 was significantly different from that of the original concrete or of Patch 1. There were no slag fragments in Patch 2. In addition, schist and gneiss were much more abundant in Patch 2 and quartz much less common than in Patch 1 concrete. These differences suggest Patch 2 was a different concrete mix, either used in a repair at a different time or in a repair at the same time but from a different batch of concrete.

The average grain size of the Patch 1 concrete fine aggregate was somewhat coarser than the original concrete fine aggregate, although no quantitative size measurements were made. The aggregate-to-cement ratio was higher in Patch 1 concrete than original concrete, and much of the aggregate was iron-stained. Patch 1 concrete had relatively few holes in the cementitious matrix, and large areas of anisotropic matrix, i.e., the matrix had different optical properties in each coordinate direction.

Table 4.3: Percent abundance of mineral and rock fragments in fine aggregate.

Constituent	Original concrete (n = 14)[1]	Patch 1 concrete (n = 2)[1]	Patch 2 concrete (n = 1)[1]
Rock fragments			
Chert/quartzite	36.4±11.3	22.6	20.1
Schist/gneiss	11.9 ± 7.7	11.0	25.0
Mafic igneous/metamorphic	3.2 ± 3.2	5.9	7.6
Serpentinite	0.8 ± 0.9	2.9	0.7
Granite/diorite/andesite	4.8 ± 3.1	0.4	2.8
Sandstone/graywacke	2.4 ± 1.9	2.4	9.7
Shale/slate	0.1 ± 0.1	0.0	0.0
Undifferentiated rock	6.1 ± 3.9	9.4	6.3
Mineral constituents			
Opaque	1.7 ± 2.3	1.3	2.8
Carbonate	0.7 ± 0.8	0.4	1.4
Quartz	18.9 ± 6.5	29.2	8.3
Ferromagnesian silicates	2.1 ± 2.1	1.1	2.8
Feldspar	4.1 ± 2.7	8.8	3.5
Other constituents			
Slag	0.0 ± 0.0	2.6	0.0
Wood	0.1 ± 0.2	0.0	0.0
Holes	6.5 ± 4.0	2.0	9.0
TOTAL, pct.	100.0	100.0	100.0

[1] n = number of thin sections.

4.4.2 Coarse aggregate

A statistically significant number of aggregate particles was counted for the original concrete. Many constituents of the coarse aggregate fraction in original concrete are the same as those in the fine aggregate. Results of grain counts are shown in Table 4.4. Photographs of the three-inch cores are given in Figures 4.15 through 4.20. The coarse aggregate grains are identified in the black-and-white photographs using the key given in Appendix B.2.3. In a qualitative visual comparison of patch and original concrete cores, the coarse aggregate of the patch concrete had a smaller maximum size than that of the original concrete, probably to facilitate flow of concrete around the square rebar during the 1969 patching project.

Table 4.4: Percent abundance of rock fragments in coarse aggregate.

Constituent	Original concrete (n = 10)[1]	Patch 1 concrete (n = 3)[1]
Chert/quartzite	21.2 ± 6.0	10.0
Schist/gneiss	25.2 ±10.4	28.3
Mafic igneous	2.9 ± 2.9	0.0
Serpentinite	4.4 ± 3.6	3.3
Granite/diorite	22.7 ± 9.1	41.8
Andesite	2.6 ± 3.1	3.3
Sandstone/graywacke	13.2 ± 4.7	8.3
Shale/slate	6.9 ± 9.3	3.3
Clay ball	0.9 ± 1.8	0.0
Wood	0.0 ± 0.0	1.7
TOTAL, pct.	100.0	100.0

[1] n = number of cores.

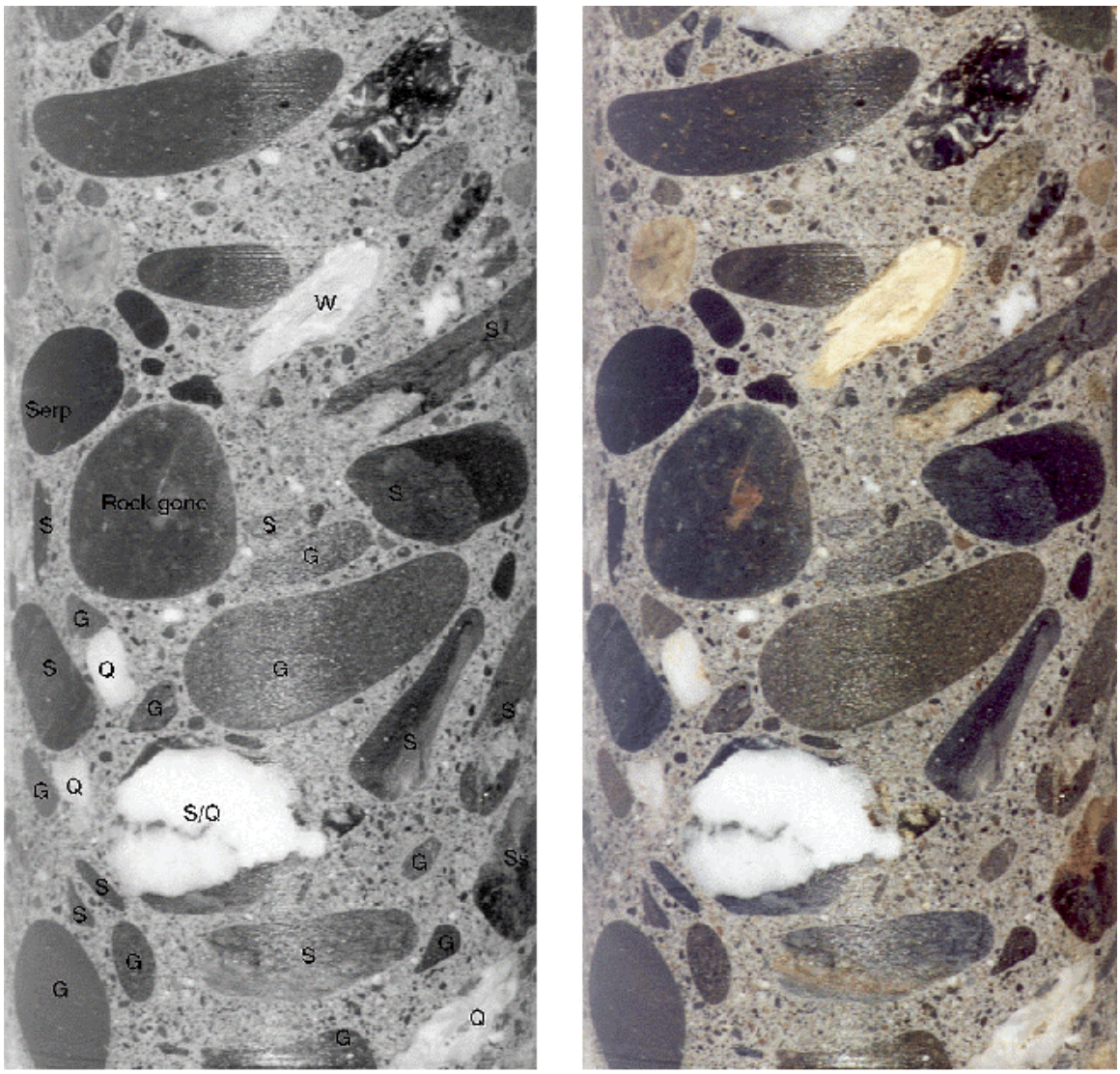

Figure 4.15: Coarse aggregate minerals in 3-inch diameter core 27F-E. See Appendix B.2.3 for key to coarse aggregate mineral identification.

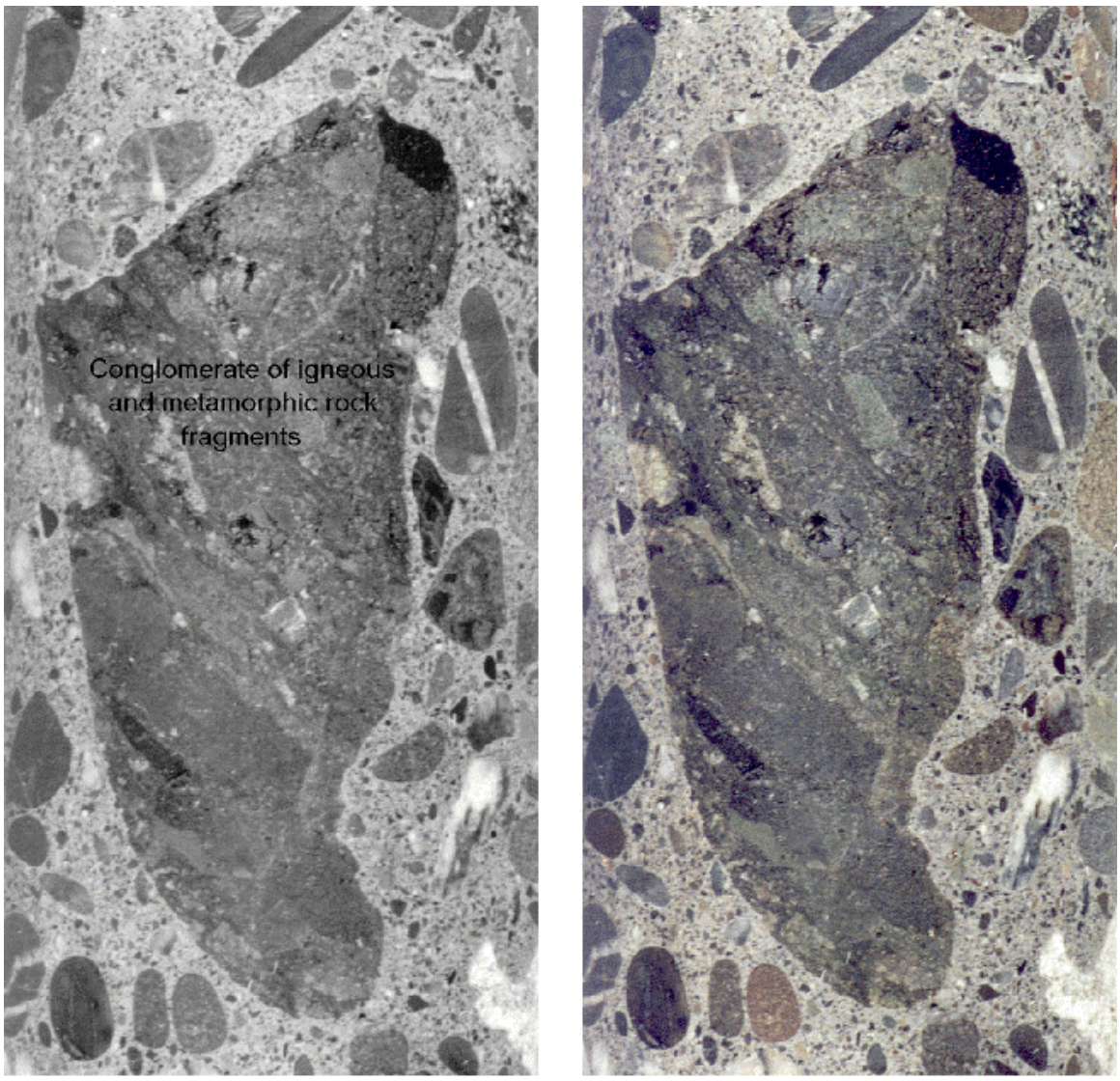

Figure 4.16: Coarse aggregate minerals in 75 mm (3-inch) diameter core 41E-E. See Appendix B.2.3 for key to coarse aggregate mineral identification.

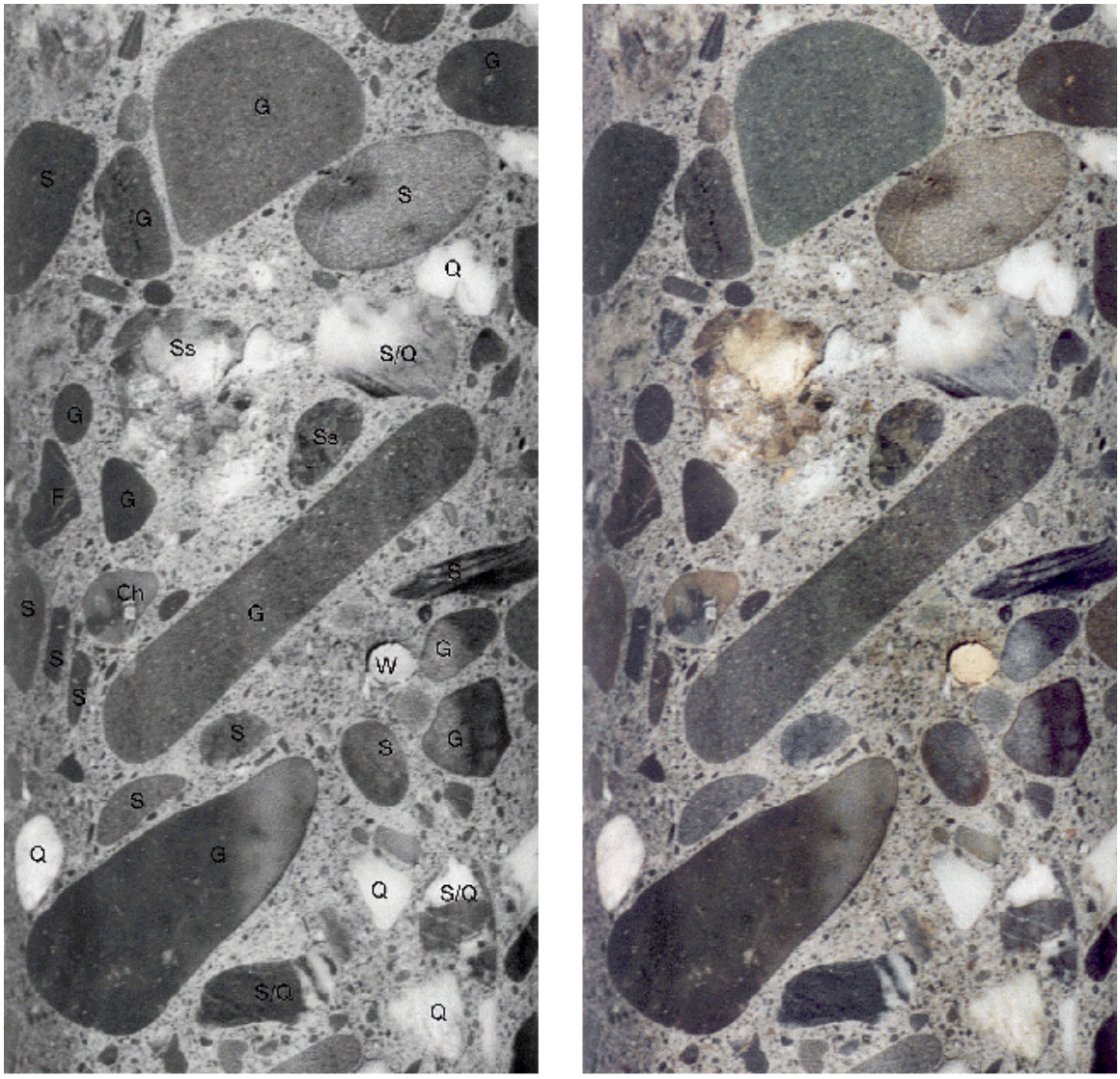

Figure 4.17: Coarse aggregate minerals in 75 mm (3-inch) diameter core 41E-W. See Appendix B.2.3 for key to coarse aggregate mineral identification.

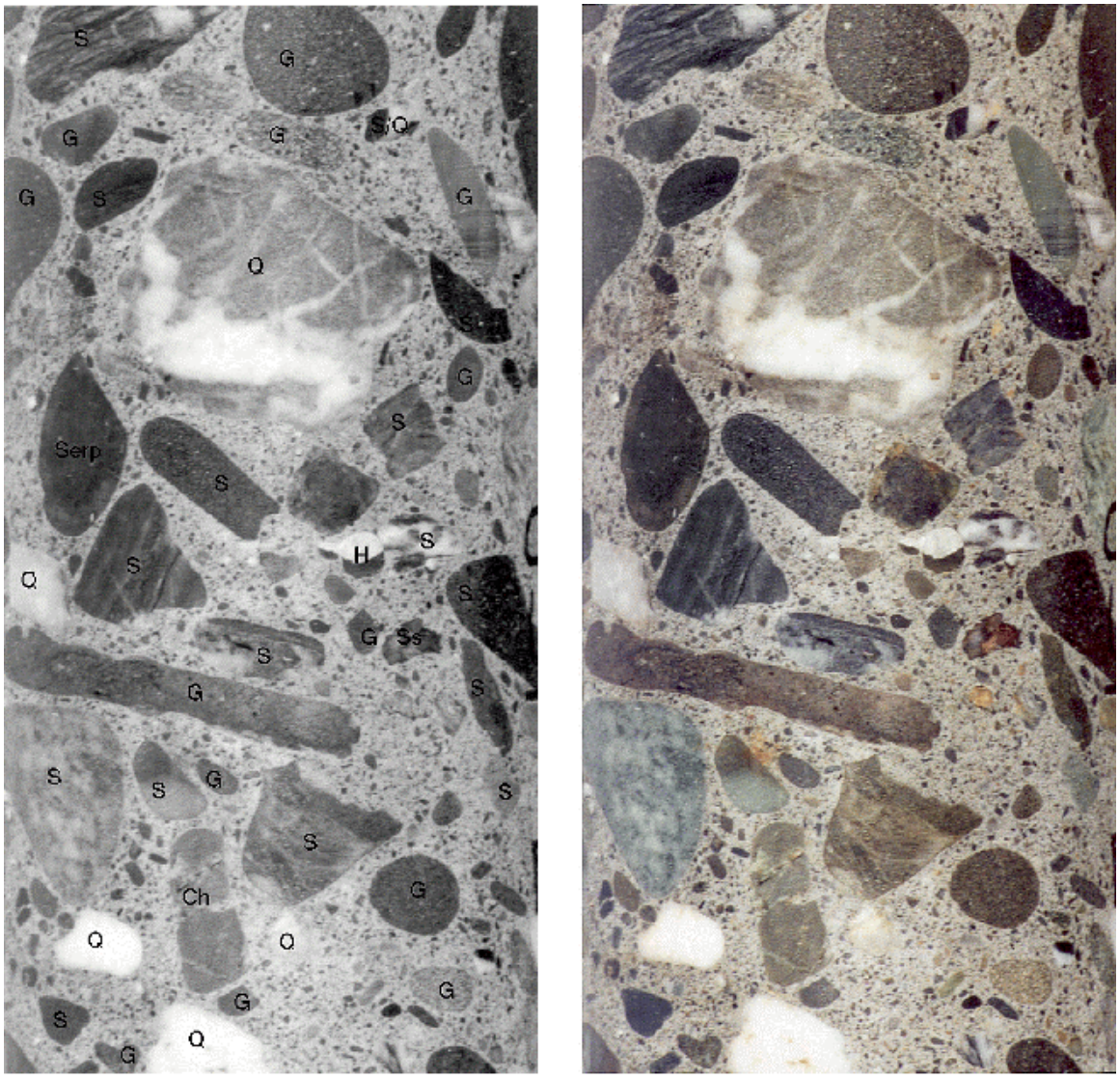

Figure 4.18: Coarse aggregate minerals in 75 mm (3-inch) diameter core 63F-E. See Appendix B.2.3 for key to coarse aggregate mineral identification.

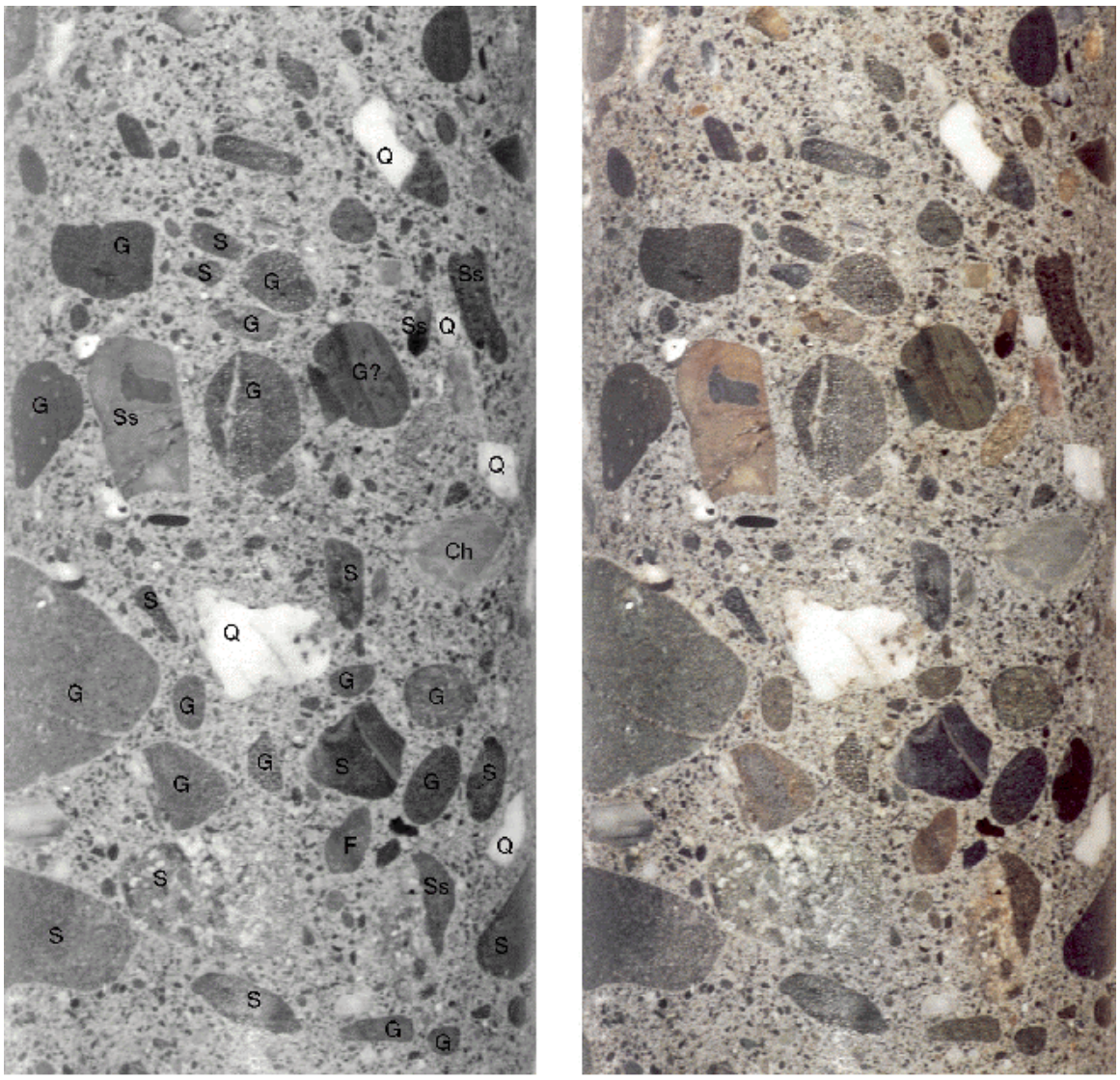

Figure 4.19: Coarse aggregate minerals in 75 mm (3-inch) diameter core 82G-E. See Appendix B.2.3 for key to coarse aggregate mineral identification.

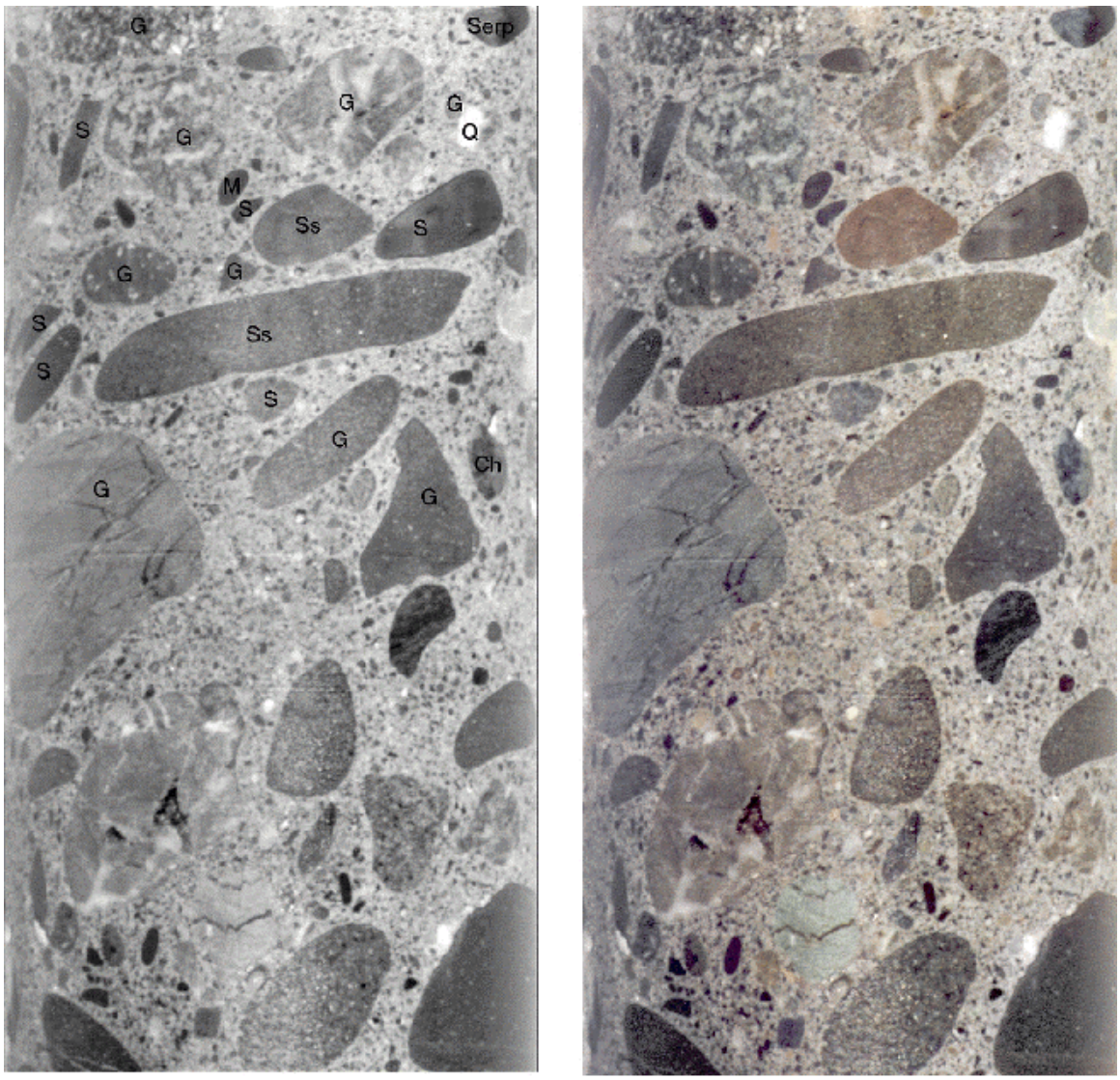

Figure 4.20: Coarse aggregate minerals in 75 mm (3-inch) diameter core 82G-W. See Appendix B.2.3 for key to coarse aggregate mineral identification.

4.4.3 Reaction Products

Very few areas of the thin sections produced evidence of significant reaction products; but traces of reaction products were observed in both the original and the patch concrete cores. No sodium-rich gel products or reaction rims were found that would indicate either ASR or ACR reactions had occurred to any significant extent in either the original concrete or in the patch concrete. However, in all of the samples, fine aggregate materials in the cement included abundant quantities of cryptocrystalline quartz (some of which is of metamorphic origin), quartz-rich rocks, and plagioclase feldspar, materials considered important reactants in ASR occurrences. No sulfate minerals indicative of gypsum or ettringite formation were detected in the original concrete samples, although small pyrite crystals, a ready source of sulfur, were observed in some of the larger aggregate rock.

Sparse areas in original concrete and patch concrete had cross-cutting veins of calcium carbonate that indicate some reaction with carbonic, hydrochloric, or other acid. These areas also contained fragments of shell material that were in the process of being solubilized and recrystallized into the carbonate veins. The carbonate veins were mixed with residual calcium oxide and calcium silicate hydrate cement material. The presence of shells indicates beach sand was the source for some of the fine aggregate. This fact would suggest the opportunity existed for contamination of the concrete by sea salt from the use of unwashed beach sand in the concrete mix.

Reactions within the aggregate materials that occurred prior to use in the concrete mix were confined to individual grains. Vein and fracture fillings of such materials as quartz, opal, calcite, clays, and iron oxide minerals are common in aggregate materials, as are reaction rims, and they are not part of the concrete deterioration process.

In summary, the composition of the original concrete included a high amount of cryptocrystalline silica, sources of sodium in plagioclase feldspar and sea salt, and a source of sulfur in pyrite. These constituents are known to contribute to the formation of ASR, gypsum and ettringite in hardened concrete. However, the petrographic results suggest that premature deterioration of the Rocky Point Viaduct was not due to their presence.

4.5 CONCRETE PROPERTIES

4.5.1 Compressive Strength

Compressive strength measurements were made on original concrete core samples taken from the east and west faces of the beam. Mean values were 54.7 MPa (7.94 ksi) for the east face and 50.9 MPa (7.39 ksi) for the west face with a pooled standard deviation for the mean compressive strength of 2.10 MPa (0.305 ksi), Table 4.5. The mean values are 27 and 19 pct higher, respectively, than the compressive strength of the original concrete reported after 60 days aging when the Viaduct was constructed, 42.7 MPa (6.20 ksi).

Table 4.5: Compressive strength of original concrete on east (landward) and west (ocean) faces of Beam A1.

75 mm (3 inch) dia. Core number	Original concrete compressive strength, MPa (ksi)	
	East face	West face
3D	70.3 (10.20)	49.5 (7.18)
9E	62.1 (9.01)	56.5 (8.20)
21E	52.5 (7.62)	53.5 (7.76)
27F	48.6 (7.06)	48.6 (7.05)
32F	54.1 (7.84)	56.4 (8.18)
41E	58.8 (8.53)	64.4 (9.35)
56F	46.4 (6.73)	44.4 (6.44)
63F	55.5 (8.06)	43.9 (6.37)
69E	45.3 (6.58)	46.6 (6.76)
82G	48.4 (7.03)	50.8 (7.38)
93E	60.0 (8.71)	45.9 (6.67)
average	**54.7 (7.94)**	**50.9 (7.39)**
Standard dev., S_x	**7.65 (1.11)**	**6.27 (0.91)**
Pooled std. dev., $S_{p,x}$	**6.96 (1.01)**	
std. Dev. of avg., $S_{p,}$	**2.10 (0.305)**	
H_0: $_E$ = $_W$; t-value	**1.80**	
Degrees of freedom	**9**	

The null hypothesis that the west and east face compressive strengths were equal had a t-value of 1.80. Thus, the difference between the compressive strength for the west and east faces of the beam after 40 years of weathering was significant at the 10 pct level.

While this difference does not explain the rapid deterioration of the Viaduct, it does suggest that chemical and/or microbial reactions within the concrete may affect in a small way the mechanical strength of the concrete over time. These reactions are related to the delivery to and retention by the beam surface of chemicals and nutrients from the highly corrosive Viaduct environment.

4.5.2 Void Fraction

Permeable voids in original concrete had an average value of 10.6 percent; permeable voids in the patch concrete had an average value of 15.6 percent, Table 4.6. In other words, the patch concrete installed in 1969 was about 50 percent more porous than the original concrete. The higher porosity would suggest sea salt could more readily be retained and concentrated on the patch concrete surface than the original concrete. Furthermore, the higher porosity of the patch concrete should permit chloride ions to be more readily transported by diffusion, capillarity, and convection into the concrete to initiate corrosion of the rebar and shear stirrups.

Porosity values obtained for the original concrete by the boiling water and the Rice specific gravity methods differed by about 10 percent.

Table 4.6: Void fraction of original and patch concrete.

Three-inch dia. core number	Void fraction, volume pct.	
	Boiling water method	Rice specific gravity method
Original concrete		
3D	9.9	9.3
9E	10.9	10.7
27F	9.4	7.1
41E	9.8	9.8
63F	10.4	9.8
82G	11.6	11.6
93E	11.9	7.4
average	10.6	9.4
Patch concrete		
37A	16.0	---
55A	15.0	---
69A (patch 2)	15.8	---
average	15.6	

4.5.3 Surface Air Permeability

Surface air permeability of the concrete was measured on the east side of Section 1. The results are shown as a contour plot in Fig. 4.21. The survey data are tabulated in APPENDIX C. On average the patch concrete had higher permeabilities than the original concrete. This result is similar to that from the void fraction measurements and has the same consequences, i.e., the patch concrete was more likely to retain and concentrate chloride ions on the beam surface and facilitate chloride ion transport into the concrete.

Surface air permeabilities for several other structures on the Oregon Coast were measured in an effort to provide additional meaning to the measurements presented in Fig. 4.21. Bare concrete on Bent 8 and Pier 9 of the Yaquina Bay Bridge (Newport OR) gave values ranging from 14.5 to 17.2 mL/min (0.9 to 1.1 in^3 /min). Measurements on a 2-year old thermal-sprayed zinc anode installed as part of an ICCP system on the Yaquina Bay Bridge south approach gave values ranging from 42.8 to 50.0 mL/min (2.6 to 3.1 in^3 /min). Measurements on the Cape Creek Bridge (south of Yachats OR) gave measurements ranging from 51.5 to 57.6 mL/min (3.1 to 3.5 in^3 /min) for bare concrete on a cross brace, and from 55.5 to 56.3 mL/min (about 3.4 in^3 /min) for a thermal spray zinc anode in use for the past 5 years in an ICCP system. The variability of these field measurements did not allow further refinement of the air permeability data.

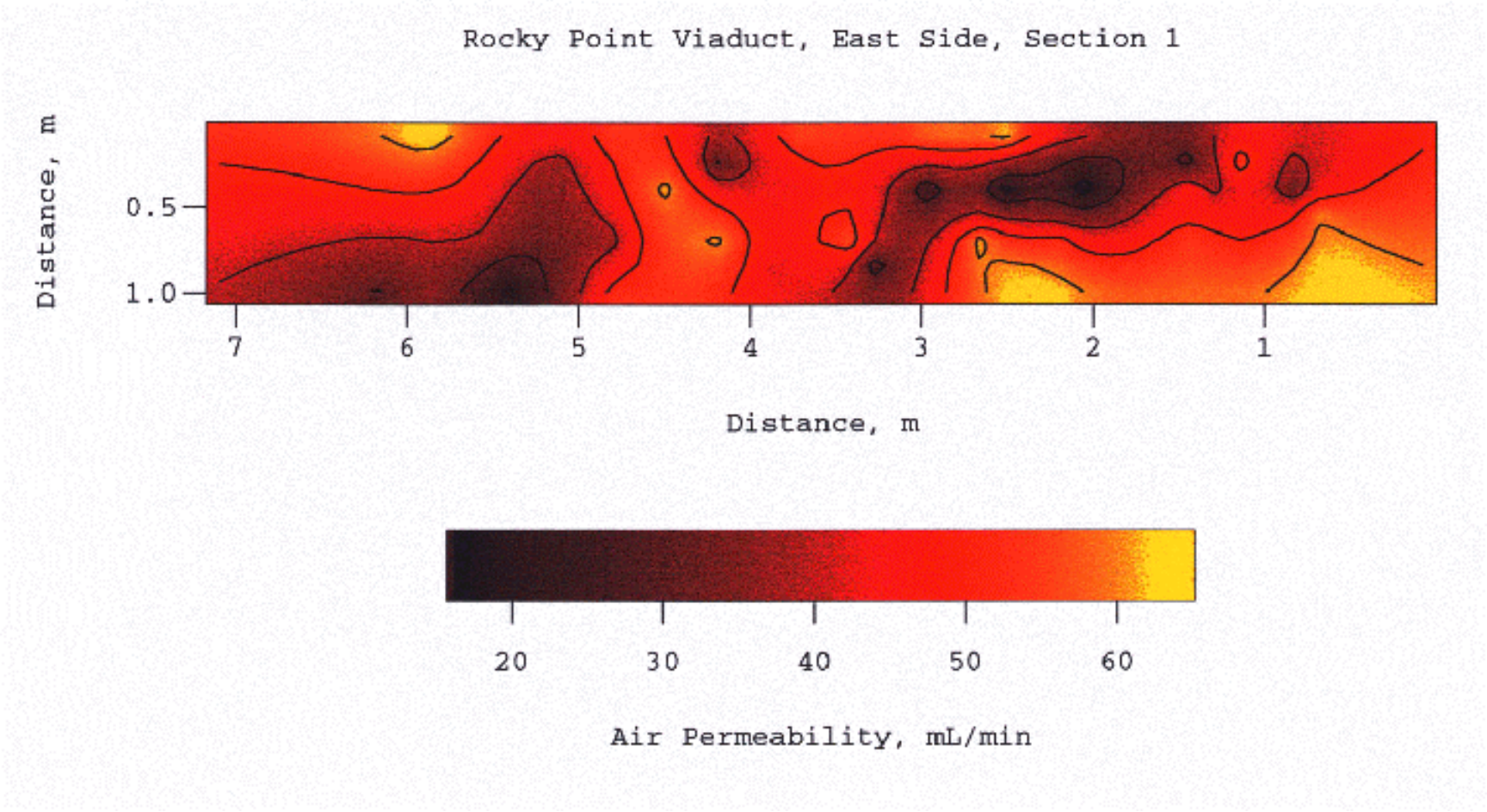

Figure 4.21: Contour map of surface air permeability for Section 1 (east face).

4.5.4 Chloride Content and Distribution

Chloride ion distribution profiles were established using concrete powder samples taken from 380 mm (15 in) deep holes through the beam at 12.7 mm (0.5 inch) increments. The samples were taken for parts of the beam experiencing high corrosion activity, i.e., half-cell potential values more negative then -350 mV vs. $Cu/CuSO_4$ (*ASTM, 1994b*). Detailed results are given in APPENDIX D, Section D.2, for acid and water soluble chloride ions and soluble calcium in the patch and original concrete. Also included in APPENDIX D are the analytical procedures and data reduction methods used in producing and analyzing the profiles.

The chloride ion profile results are plotted in Figures 4.22 and 4.23 for original and patch concrete, respectively. The positions of the square rebar (R) and the shear stirrups (S) are included in the figures. Shear stirrups had substantially less concrete cover than the outer course of square rebar. The chloride ion corrosion threshold for black iron bar, 0.74 kg Cl/m^3 (1.25 lb Cl/yd^3) *(McDonald, Pfeifer, and Sherman, 1998*), has been drawn on the figures to provide a reference for the initiation of corrosion on the shear stirrups and square rebar. Literature values of the chloride ion corrosion threshold for black iron rebar range from 0.47 to 0.83 kg Cl/m^3 (0.8 to 1.4 lb Cl/yd^3) of concrete *(McDonald, Pfeifer, and Sherman, 1998; Thomas, 1996; West and Hime, 1985*).

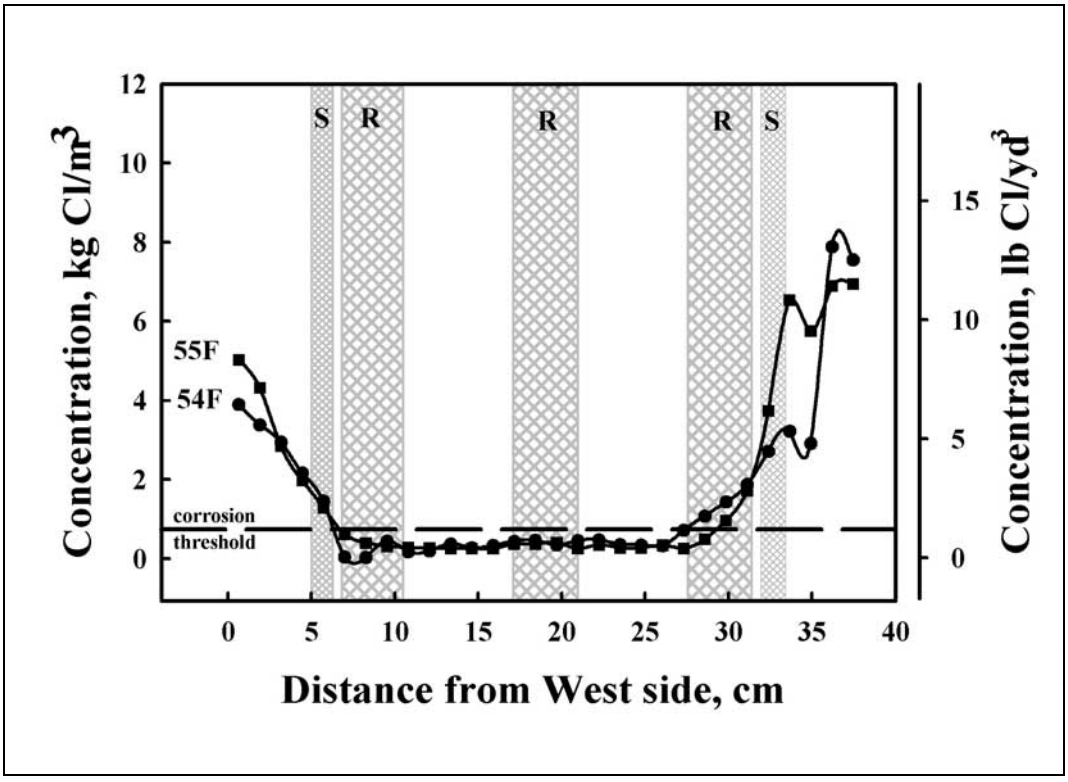

Figure 4.22: Chloride distribution profiles for original concrete in the "as-received" beam. The average of the profiles is the heavy solid line. West is the ocean facing side of the beam.

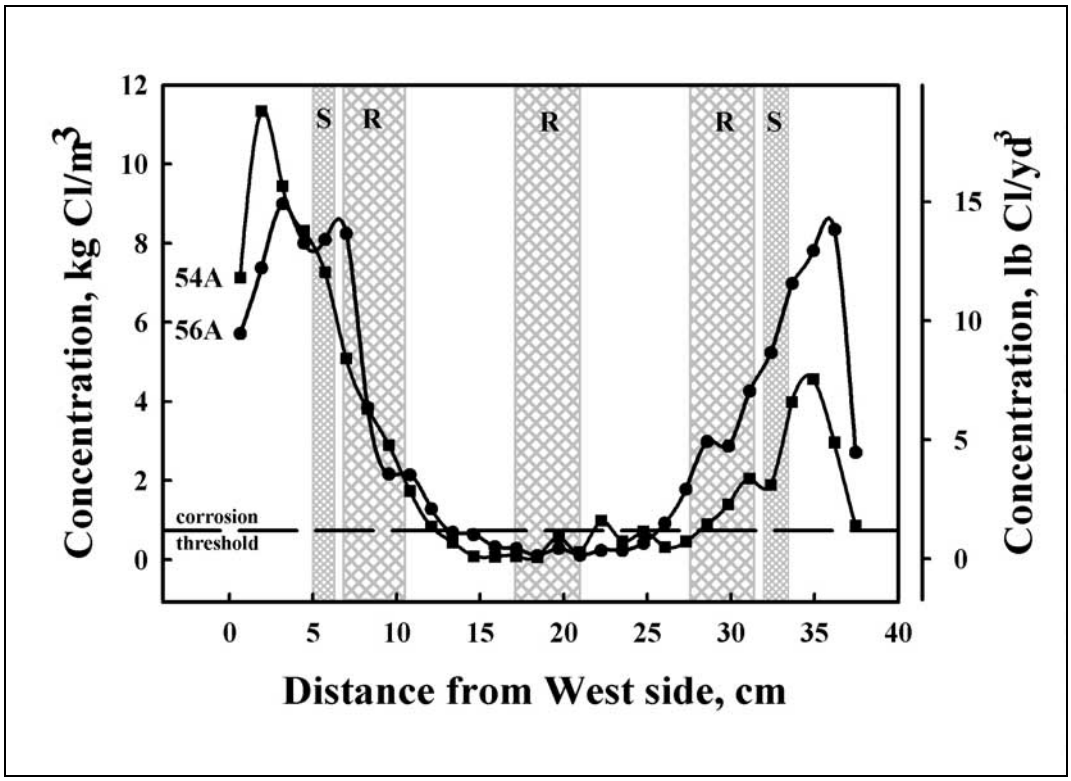

Figure 4.23: Chloride distribution profiles for patch concrete in the "as-received" beam. The average of the profiles is the heavy solid line. West is the ocean facing side of the beam.

The chloride profiles are not symmetrical, indicating that chloride deposition was different on the two vertical faces of the beam. Profiles were different for the original and the patch concrete, indicating that properties of the concrete affected chloride deposition and migration. The shear stirrups and outer reinforcing bar are embedded in concrete containing chloride at levels well above the corrosion threshold for black iron bar. The chloride gradient between the interior and outer reinforcing bar provides the opportunity for macro-cell corrosion if the inner and outer layer of bar were electrically continuous. The higher surface concentration of Cl on the west face of the patch concrete suggests the porous patch concrete can more readily retain and concentrate chlorides deposited on its surface in salt fogs, dew, and salt spray than can the original concrete despite identical rates of salt deposition. On the sheltered east face where salt deposition was probably very different from the exposed the surface concentration of Cl was roughly the same for the patch and original concrete.

The data shown in Figures 4.22 and 4.23 are for acid soluble chlorides. Data were also taken for water soluble chlorides. For the patch concrete, these values were nearly identical to the total chloride values. This would indicate that all of the chloride in the patch concrete was water soluble and originated as chloride ion deposited on the beam and diffused into the concrete. In the beam interior, chloride concentrations went to zero for the patch concrete indicating that there was no chloride in the concrete mix at the time the patch was applied, Figure 4.23.

The results are different for the original concrete. Original concrete analyses showed a consistent difference of up to 0.47 kg Cl/m^3 (0.8 lb Cl/yd^3) chloride between the total chloride and the water soluble values, with the total chloride values being higher. This would indicate that chloride ions had reacted with the cement paste at the time of curing to form water insoluble minerals. Furthermore, the acid and water soluble values were non-zero in the beam interior where diffusion had not yet altered the concrete composition. These facts suggest that chloride was present in the concrete at the time of curing. A background level of total chloride exists in the original concrete of 0.35-0.47 kg Cl/m^3 (0.6-0.8 lb Cl/yd^3), Figure 4.22.

Calculations were made to identify the source of the background chloride in the original concrete interior. These calculations equated the Cl present in the concrete to the amount of $CaCl_2$ accelerator, sea water, or unwashed beach sand required to produce the Cl. They showed that the Cl level present in the original concrete was too low to have been introduced either by a $CaCl_2$ accelerator or from the use of seawater in preparing the concrete mix. However, the level is consistent with the use of salt-contaminated beach sand in the concrete mix. For example, the use of beach sand with 0.1 percent NaCl contamination would result in approximately 0.41 kg Cl/m^3 (0.7 lb Cl/yd^3) chloride in the concrete mix, roughly the Cl concentration present as a background level, Figure 4.22.

To test this idea, surface samples of sand were removed from the beach north of the Yaquina Bay inlet (at Newport OR) at regular distances from the waterline up to the bluff overlooking the beach. These sand samples were analyzed for total chloride using the same analytical procedure for the concrete powder samples. The results are given in Figure 4.24. They show that 0.1 weight percent sodium chloride is not an unreasonable level to find in unwashed beach sand, and unwashed beach sand could very well have been the source of the background level of chloride in the original concrete.

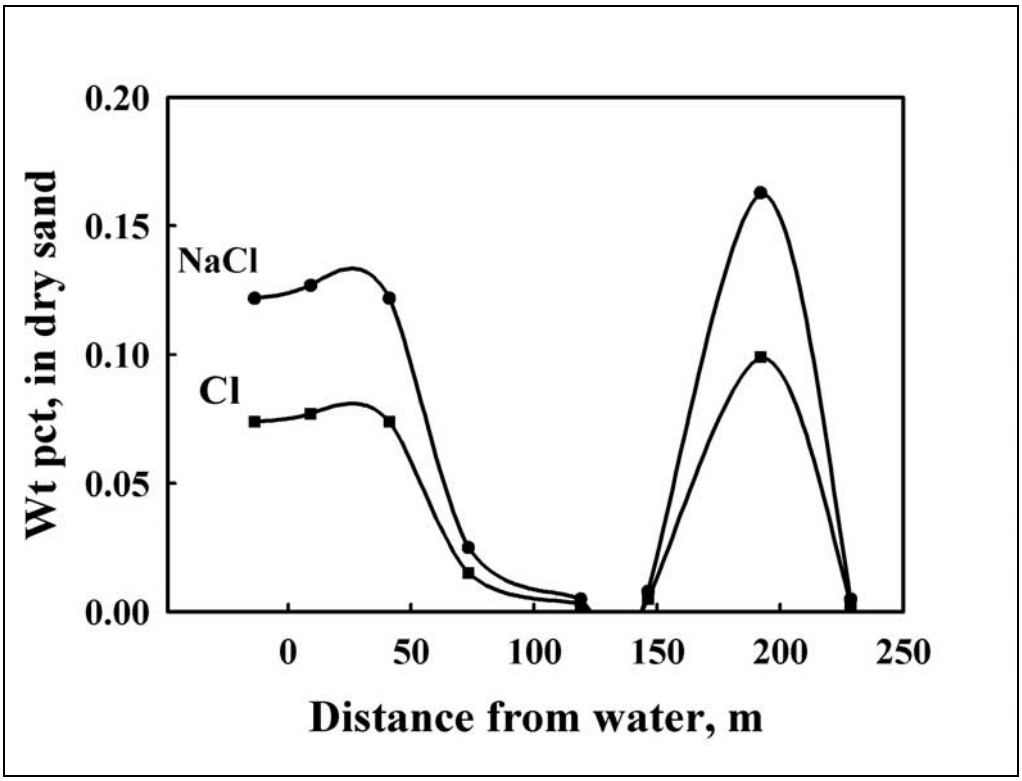

Figure 4.24: Cl and NaCl concentration profiles for surface samples of beach sand from Newport OR.

The Cl profiles in Figures 4.22 and 4.23 were modeled using Fick's second law of diffusion to determine effective chloride diffusivities (D) and surface concentrations (C_o). While the near-surface concentration of chloride ion is affected by salt deposition and by precipitation washing, the chloride concentration at greater depths changes more slowly in accordance with the laws of diffusion (*Bentz, 2000; McDonald, Pfeifer and Sherman, 1998*; *Shewmon, 1963*; *West and Hime, 1985*). Fick's law of diffusion is given by the following equation:

$$\frac{\partial^2 c(x,t)}{\partial x^2} = \frac{1}{D}\frac{\partial c(x,t)}{\partial t} \qquad \textbf{(4-1)}$$

where:
$c\ (x,t)$ (mass per unit volume) = the chloride concentration at a depth x in the concrete;
t is the age of the structure; and
D (area per unit time) = the apparent diffusion coefficient for chloride ion in concrete.

A one-dimensional solution to Equation 4-1 is given by Equation 4-2 for a system initially free of solute and exposed to a constant surface concentration of chloride ion C_o at time zero is:

$$c(x,t) = C_o \left(1 - erf\ \frac{x}{2\sqrt{Dt}}\right) \qquad \textbf{(4-2)}$$

where:
C_o (mass per unit volume) = the apparent concentration of chlorides at the structure surface, i.e., roughly the average surface chloride concentration;
erf(z) = the error function (also known as the probability integral) with argument $z = \{x/2\ D\ t\}$; and z is dimensionless.

A more general form of Equation 4-2 for the case where a background level of chloride, C_b, is present in the concrete at the time of construction substitutes $\{c(x,t) - C_b\}$ for $c(x,t)$ and $\{C_o - C_b\}$ for C_o . Least-squares procedures for fitting the chloride ion profile data to obtain the Fick's law parameters D and C_o are given in APPENDIX D, Sections D.3 and D.4, using a program in BASIC, and Section D.5 using a spreadsheet and its equation solver.

At the surface of the patch concrete on both the east and west faces of the beam, the chloride ion profiles show a decrease in concentration; no such decrease is evident for the original concrete, Figures 4.22 and 4.23. This decrease is related to the ability of precipitation and dew draining from the beam face to leach chloride ions from the near surface region. Since the chloride ion profiles are diffusion controlled, the surface concentration should be C_o on average. Thus, it is inferred that there should be periods when the near surface region of the beam has chloride concentrations well above those shown in Figure 4.23. The more porous nature of the patch concrete compared to the original concrete influences these variations. It facilitates convective leaching by precipitation washing, and concentration of chloride by dry deposition, so that the surface chloride concentration varies in a cyclic manner related to short term variations in the beam environment.

The Fick's law parameters obtained from fitting the chloride profile data are given in Table 4.7. The effective diffusivity values are higher for the patch concrete than the original concrete by a factor of two. Surface Cl concentrations for the patch concrete on the west face are much higher than for the original concrete. Surface Cl concentrations on the east face are the same for the patch and original concrete. These results would suggest the higher porosity of the patch concrete manifests itself in greater chloride ion mobility in the concrete. Furthermore, where interactions of the concrete surface with the environment are favorable, e.g., the west face, the porosity of the patch concrete allows chloride ions to be concentrated on the surface to a high level. Similarly, washing effects are more pronounced on the patch concrete where chloride ions are more readily leached from the porous patch concrete. On the east face, where salt delivery is the determining factor and the beam is sheltered from washing effects, the porosity of the patch concrete has the same surface chloride ion concentration as the original concrete. The diffusion coefficient values in Table 4.7 are within the range of values reported in the literature, 0.9 to 52 x 10-8 cm2/s (9.6 to 550 x 10-12 ft2/s) (*Bentz, 2000*).

Table 4.7: Surface chloride concentration, C_o, and effective diffusion coefficient, D, based on least-squares fit of "as-received" chloride profiles to Fick's second law for diffusion.

Concrete, orientation	C_o [1] kg Cl/m^3 (lb Cl/yd^3)	D Cm^2/s
Original concrete, west face	5.26 (8.87)	0.948×10^{-8}
Patch concrete, west face	15.0 (25.3)	3.25×10^{-8}
Original concrete, east face	9.58 (16.2)	1.24×10^{-8}
Patch concrete, east face	9.62 (16.2)	3.14×10^{-8}

[1] lb/yd3 = 0.592 kg/m3

Inspection of Figure 4.22 shows the square rebar on the west face of the beam was just reaching the corrosion threshold for Cl in the original concrete at the time the Viaduct was replaced. On the east face, the corrosion threshold was exceeded well before this time. The shear stirrups were at a shallower cover depth on both the sides and the bottom than the square rebar, Table 4.1. Thus the shear stirrups would be in a corrosive environment earlier than the square rebar. Concrete cover was shallower on the bottom than the sides, 2.80 cm (1.10 inch) for the shear stirrups on the bottom compared to 3.22 cm (1.27 inches) on the sides. This led to even shorter times for corrosion to initiate. Furthermore, salts would accumulate on the bottom and corners of the beam as salt-laden water drained from the beam face and evaporated. Thus, the shear stirrups were highly vulnerable to early corrosion, particularly on the beam bottom and at the corners.

Inspection of Figure 4.23 shows the square rebar adjacent to the beam sides to be in a corrosive environment in the patch concrete well before the Viaduct was replaced. This would also be true for the square rebar at the bottom of the beam and for the shear stirrups everywhere in the patch concrete. Thus, the replacement of the Cl contaminated concrete surrounding the rebar in 1969 by patch concrete did not mitigate potential corrosion problems due to Cl penetration of the concrete. In fact, the patch concrete was substantially less of a barrier to Cl transport to the rebar and shear stirrups than the original concrete. Corrosion damage was only delayed by the patch concrete installed in 1969, and not by a significant amount.

The values for C_o and D given in Table 4.7 were used to compute chloride profiles in original and patch concrete for selected times, Figures 4.25 and 4.26, respectively. The positions of the shear stirrups and square rebar are shown in these figures. Figure 4.25 shows that the shear stirrups were at the corrosion threshold in original concrete after about 14 years on the west side of the beam and about 8 years on the east side. These times clearly could lead to the observed concrete cracking and corrosion damage observed in the 15-year period preceding the 1969 repair and patching. The presence of the background level of chloride in the original concrete may have shortened the time to corrosion initiation, but not by very much. Figure 4.26 shows that the shear stirrups were at the corrosion threshold in patch concrete after about 4 years on the west side of the beam and after about 2 years on the east side. The installation of patch concrete clearly did not significantly extend the service life of the Viaduct by protecting the rebar from exposure to corrosion-inducing chloride ion.

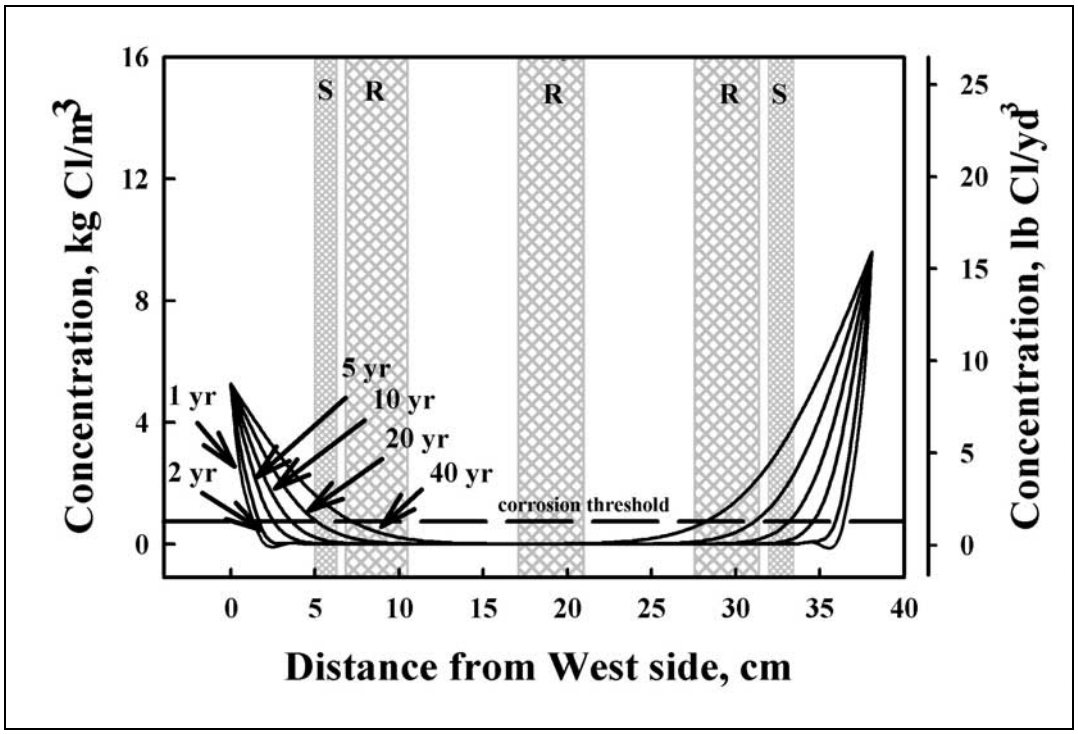

Figure 4.25: Chloride distribution profiles for original concrete as a function of time exposed to the environment. Basis: least-squares fitted parameters in Table 4.6; time zero is 1954. West is the ocean facing side of the beam.

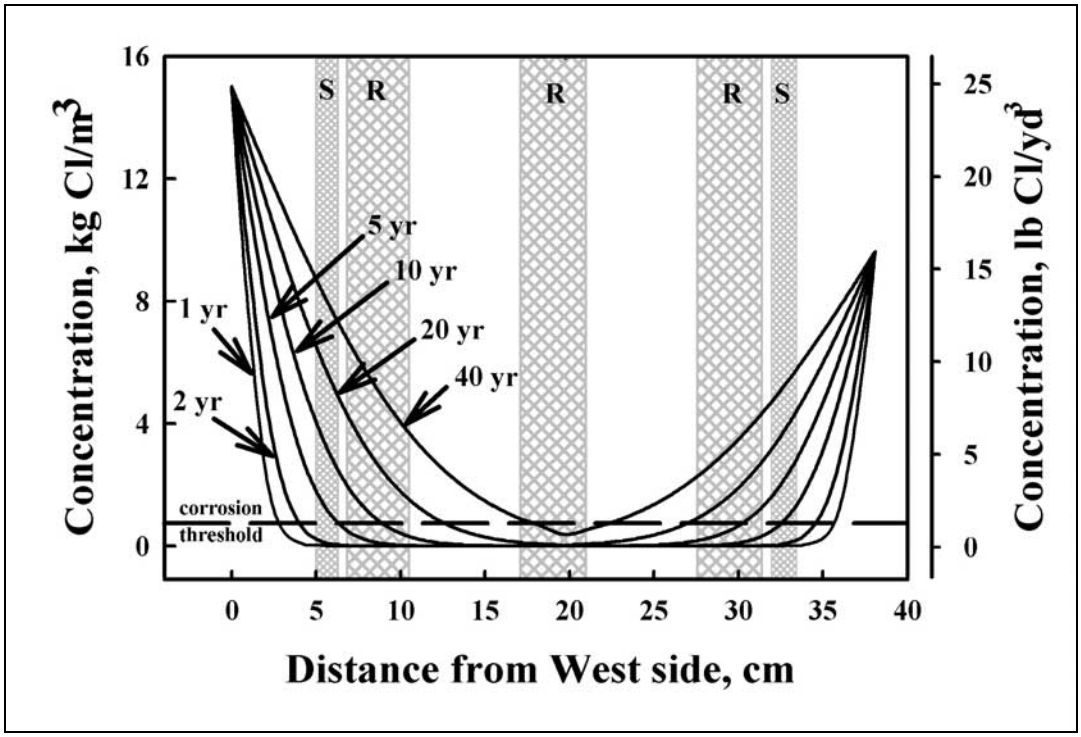

Figure 4.26: Chloride distribution profiles for patch concrete as a function of time exposed to the environment. Basis: least-squares fitted parameters in Table 4.6; time zero is 1969. West is the ocean facing side of the beam.

From the view of corrosion damage, the cover depth of the shear stirrups was the weak link in the beam. Using the parameter values in Table 4.7, a 4.97 cm as a conservative estimate for shear stirrup cover depth (see Section 4.1.1), and a corrosion threshold of 0.74 kg Cl/m3 for black iron rebar, the time to corrosion initiation can be estimated from Fick's law. The corrosion threshold would have been reached and corrosion initiated in original concrete in 19.0 years on the west side and 10.1 years on the east side. For patch concrete the calculations give 3.1 years for the west side and 4.0 years for the east side. The time between corrosion initiation and concrete cracking (time to cracking) is dependent on the corrosion rate, cover depth, concrete properties, properties of the steel/concrete interface, and the size of the reinforcing steel. It has been estimated that 25.4 μm (0.001 inch) of corrosion will result in the initiation of cracking in concrete (*McDonald, Pfeifer, and Sherman, 1998*). For black iron rebar in typical construction, the time to cracking has been observed to occur within five years (*Liu and Weyers, 1998*). Sagues (1994) suggests that cracking will occur within 3 to 4 years.

Table 4.8: Estimation of time-to-corrosion initiation and time-to-corrosion cracking in chloride-contaminated reinforced concrete.

Concrete, orientation	Estimated time to corrosion initiation, years [1]	Estimated time to concrete cracking, years	
		Sagues (1994)	Liu and Weyers (1998)
Original concrete, west face	19.0	22.5	24.0
Patch concrete, west face	3.1	6.6	8.1
Original concrete, east face	10.1	13.6	15.1
Patch concrete, east face	4.0	7.5	9.0

[1] based on corrosion threshold for black iron bar of 0.74 kg Cl/m3 (1.25 lb Cl/ft3) and shear stirrups with 4.97 cm concrete cover.

The time to cracking value for the east face of the original concrete in Table 4.8 was within the time, 15 years, during which corrosion-related damage of the concrete was first observed on the Viaduct, and when major repair of the structure was required. With substantially less cover for the shear stirrups on the bottom of the beam, cracking would have been observed in these areas at times considerably less than 15 years. The calculations show that the threat of corrosion damage can be estimated well from measured chloride ion distribution profile and a knowledge of cover depth and corrosion threshold for the rebar. They also demonstrate that corrosive conditions vary everywhere on the structure and that cracking will not appear uniformly over the structure but appear first in predictable areas of high risk. These areas are determined by the corrosivity of the environment and the complex interaction of the structure with the environment. Summing the effects of chloride ion corrosion damage in original concrete, and then the effects on patch concrete, the 1969 Rocky Point repair delayed further damage to the structure by only 8 to 9 years.

The effect of diffusion coefficient on the chloride ion profile for 40-year-old concrete is shown in Figures 4.27. The two-fold difference in diffusion coefficient observed between patch and original concrete greatly increases chloride penetration of the patch concrete, Figure 4.27. Newer concretes, such as microsilica (silica-fume, high-performance) concrete containing fly ash, have chloride ion diffusion coefficients on the order of 0.12 to 0.19 x 10-8 cm2/s (*Li, Peng, Ma, 1999*). Oregon DOT currently specifies the use of such concrete for coastal bridge construction (*Nelson, 2000*). Figure 4.27 shows their use will significantly extend the time

required for chloride levels to build to the corrosion threshold for shear stirrups and square rebar: more than 40 years for the shear stirrups compared to about 10 years for the 1954 original concrete mix. Combined with newer specifications for cover depths for all steel in coastal structures – 3.8 cm (1.5 inches) minimum, 5.1 cm (2 inches) typical, and 7.6 cm (3 inches) for particularly harsh environments – substantial improvements in structure life can be achieved by changes in the concrete mix design and cover depth specification.

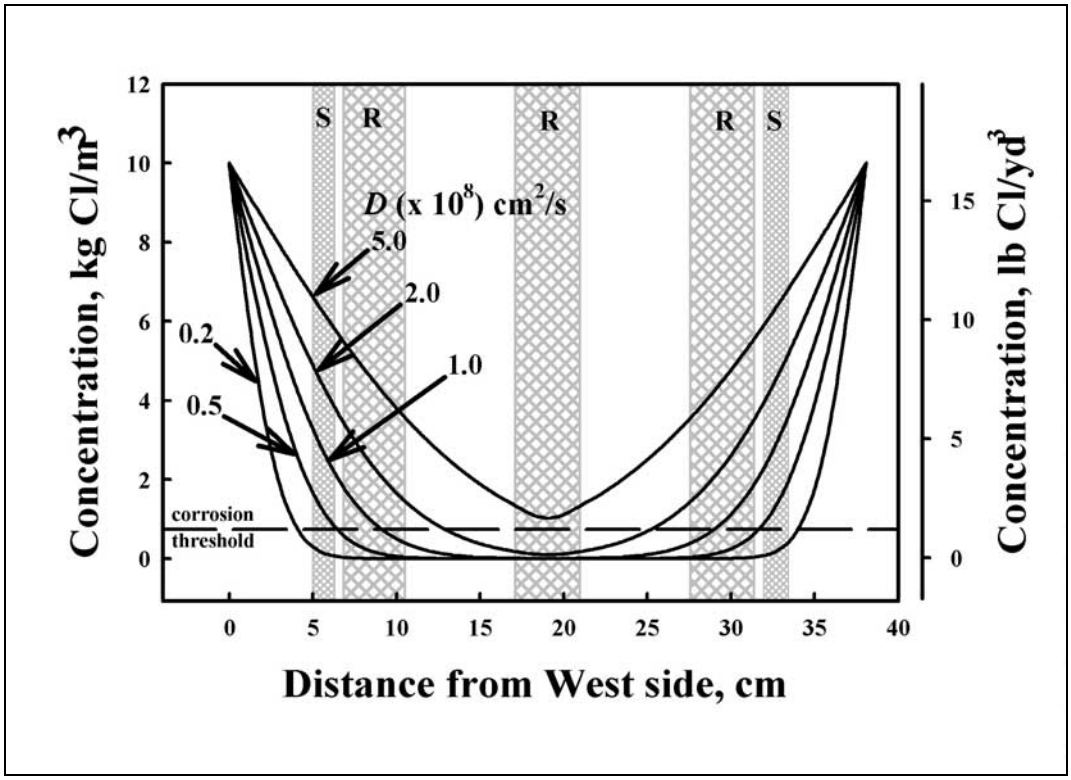

Figure 4.27: Chloride distribution profiles for patch concrete as a function of diffusion coefficient, *D*. Basis: t = 40 years; C_o = 10 kg Cl/m^3. West is the ocean facing side of the beam.

The effect of severity of the environment on the chloride ion profile is shown in Figure 4.28. Higher salt deposition on the structure leads to higher concentration gradients. This shortens the time to reach the corrosion threshold and increases the concentration gradient that affects macrocell corrosion when rebar are electrically continuous. An understanding of the severity of the structure microclimate is important in specifying the materials of construction. As noted in Section 2.1, there are three methods that seem reasonable for use in quantifying the corrosivity of a site. These are measurement of atmospheric corrosion rates on mild steel coupons, measurement of salt deposition rates, or determination of the surface chloride concentration from chloride ion profile analysis. Each of these methods would require some work to convert it into a meaningful index for rebar corrosivity. Chloride profiling is the method that measures parameters that most directly affect the threat of corrosion to rebar. Furthermore, the surface chloride concentration is determined to a large extent by the salt deposition rate.

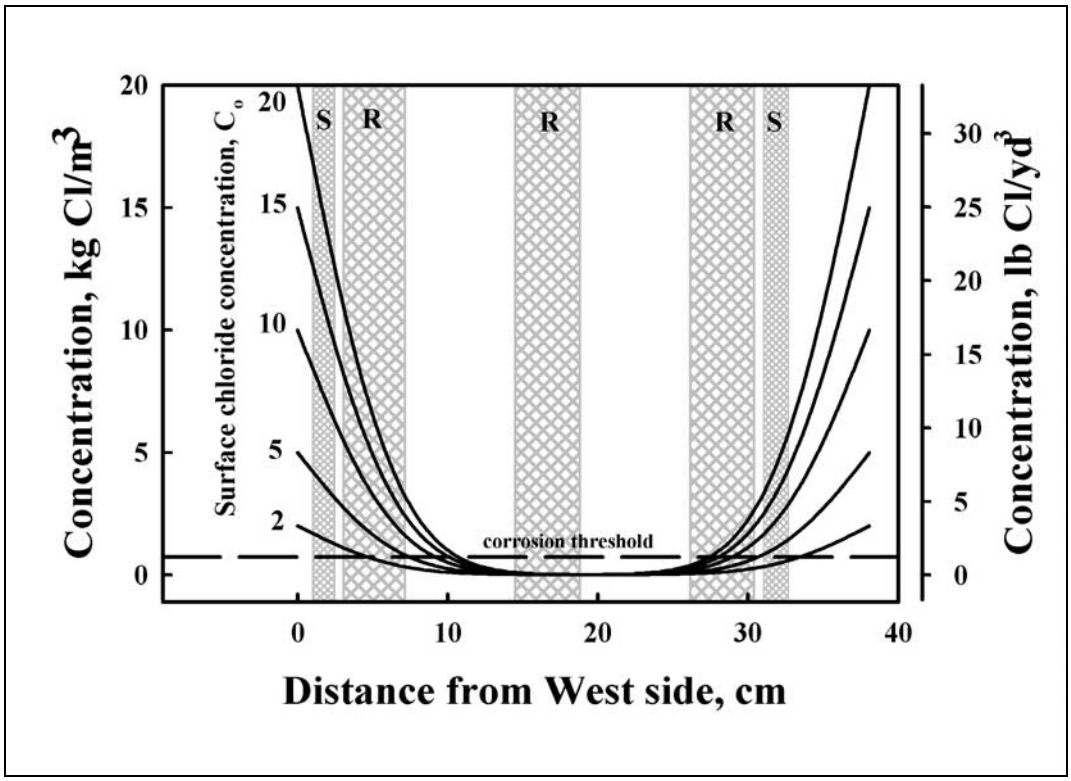

Figure 4.28: Chloride distribution profiles for patch concrete as a function of the surface chloride concentration, C_o . Basis: t = 40 years; $D = 10^{-8}$ cm^2/s. West is the ocean facing side of the beam.

Inspection of Figures 4.22 and 4.23 and the data for surface chloride concentration in Table 4.8 shows the chloride concentration in 40-year-old concrete bridge at one of the harshest sites on the Oregon coast will not yield concrete with a chloride concentration much above 15 kg Cl/m3 (25 lb Cl/yd3). This is a little higher than the corrosion threshold for 304 stainless steel rebar, 11 kg Cl/m3 (19 lb Cl/yd3), and less than the corrosion threshold for 316 stainless steel rebar, 18 kg Cl/m3 (31 lb Cl/yd3) (*McDonald, Pfeifer and Sherman, 1998*). Thus, the chloride ion profile data suggest that the Oregon DOT decision (*Nelson, 2000*) to use 316 stainless or similar stainless steel rebar in all future coastal bridge construction for critical structural elements (deck, beam, and precast girders) will result in a structure that may never reach the corrosion threshold at the depth of the rebar. The specification of microsilica concrete and more exacting standards for cover depth for all steel would seem to assure a low-maintenance structure with a service life far exceeding that of present coastal bridges. This combination would seem to yield the goal (*Nelson, 2000*) of a 120+ year bridge for coastal environments.

4.6 CORROSION RATE AND CONCRETE RESISTIVITY

Corrosion rates, measured with the GECOR6, are shown in tabular form in Appendix E and as a contour plot in Figure 4.29. Two high corrosion rate (>5 µm/y) locations, B3/B4 and D13/E13, were identified on the small part of the east face of Section 1 that was examined. The high corrosion rate location B3/B4, upper right of Figure 4.29, corresponded to a region of low

potentials (< -400 mV vs. Cu/CuSO4) in Figure 4.11. The other high corrosion rate location D13/E13, lower left of Figure 4.29, corresponded to a region of some delamination and low potentials, Figures 4.7 and 4.11.

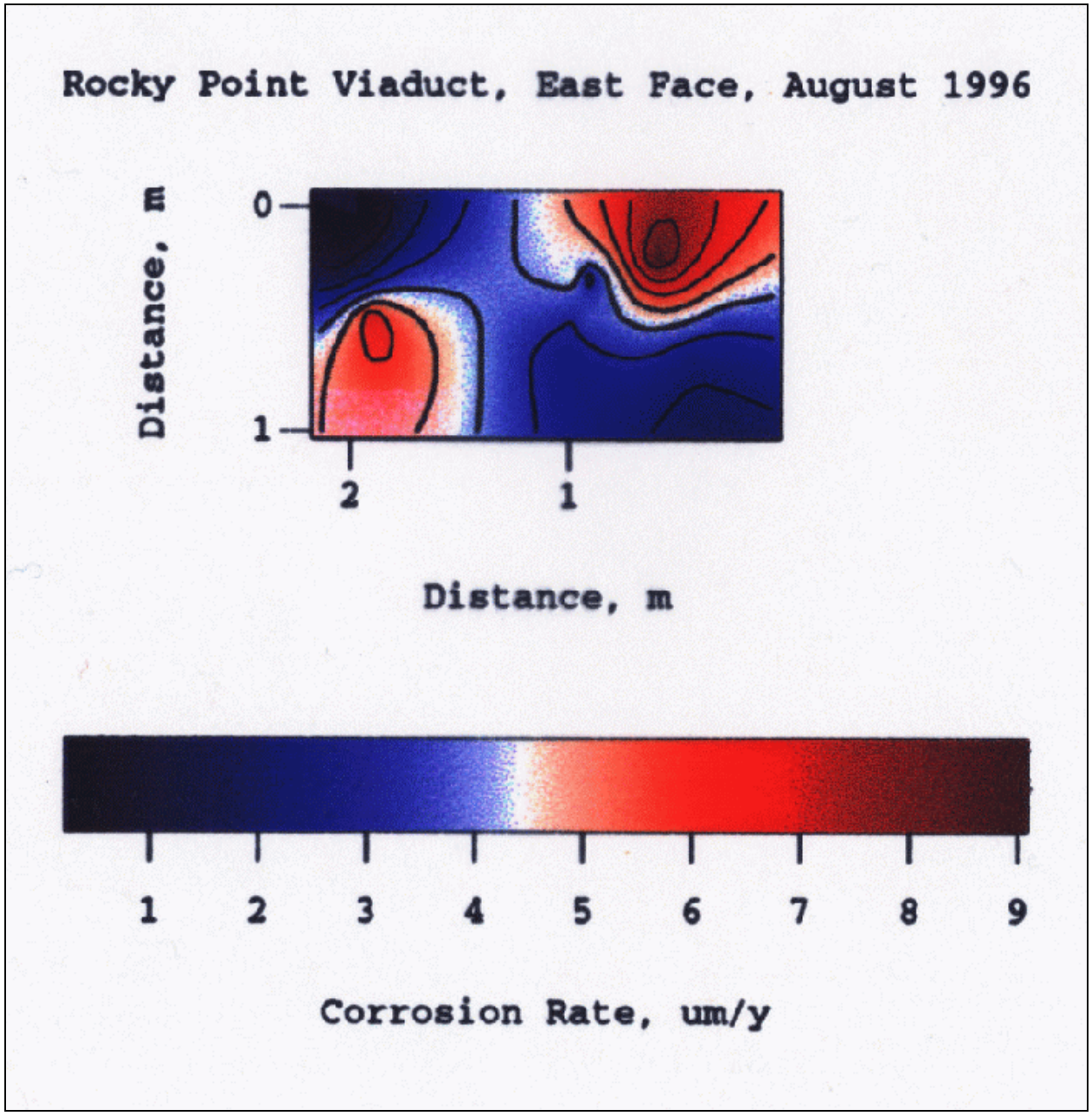

Figure 4.29: Contour map of corrosion rate for Section 1 (east face).

Duplicate corrosion rate measurements (made immediately after the first without moving the sensors) showed a wide variation in value. The standard deviation, *s*, of the corrosion rate was determined from:

$$s = \sqrt{\frac{\sum_{j=1}^{N}\sum_{i=1}^{2}\left(a_i - \overline{a}_j\right)^2}{2N-1}} \qquad \textbf{(4-3)}$$

where:
N is the number of locations where duplicate measurements were made; and
$\overline{a_j}$ is the average of the two measurements (a_i with i=1 and 2) at location j.

Table 4.9 summarizes the results. The standard deviation increased with increasing I_{corr}. The standard deviation was about 20% of I_{corr} on average.

Table 4.9: Standard deviations of Icorr measurements.

Range of I_{corr} $\mu A/cm^2$	***N***	***s*** **$\mu A/cm^2$**
0.02 to 0.10	19	0.016
0.10 to 0.20	5	0.013
0.20 to 0.30	5	0.033
0.30 to 0.40	4	0.046
0.40 to 0.90	3	0.090
0.02 to 0.90	36	0.033

The GECOR6 measuring instrument was unstable, with most measurement attempts terminated by the instrument without result. Measurements were made on four different days. Only results from the day (October 25) when the unit was the most stable were used to generate the contour map of corrosion rates shown in Figure 4.29.

The algorithm for computing concrete resistivity using GECOR6 does not agree with the physics of typical resistivity measurements. Furthermore, cover depth was not included in the algorithm although it is a necessary parameter in such computations. Hence, concrete resistivity measurements by GECOR6 could not be interpreted in terms of a known and physically significant model, and there was no value in making such measurements with this instrument.

4.7 CHLORIDE MIGRATION

4.7.1 System Operating Characteristics

The operating voltages for the three slices are shown in Figure 4.30, and current densities are given in Table 3.2. After an initial break-in period where slices 48-49 and 52-53 equilibrated with the enclosure humidity, the circuit resistances were below 500 Ωm^2 for the first 200 days of the test period. Beyond 200 days, the circuit resistance of slices 48-49 and 52-53 increased with further aging to values still well below 1000 Ωm^2. The circuit resistance for slice 50-51 remained below 500 Ωm^2 for the entire test period. These changes in the operating performance of the ICCP system on the beam slices are consistent with trends observed for electrochemically

aged laboratory and bridge anodes in ICCP systems. However, the actual increase in circuit resistance was substantially less.

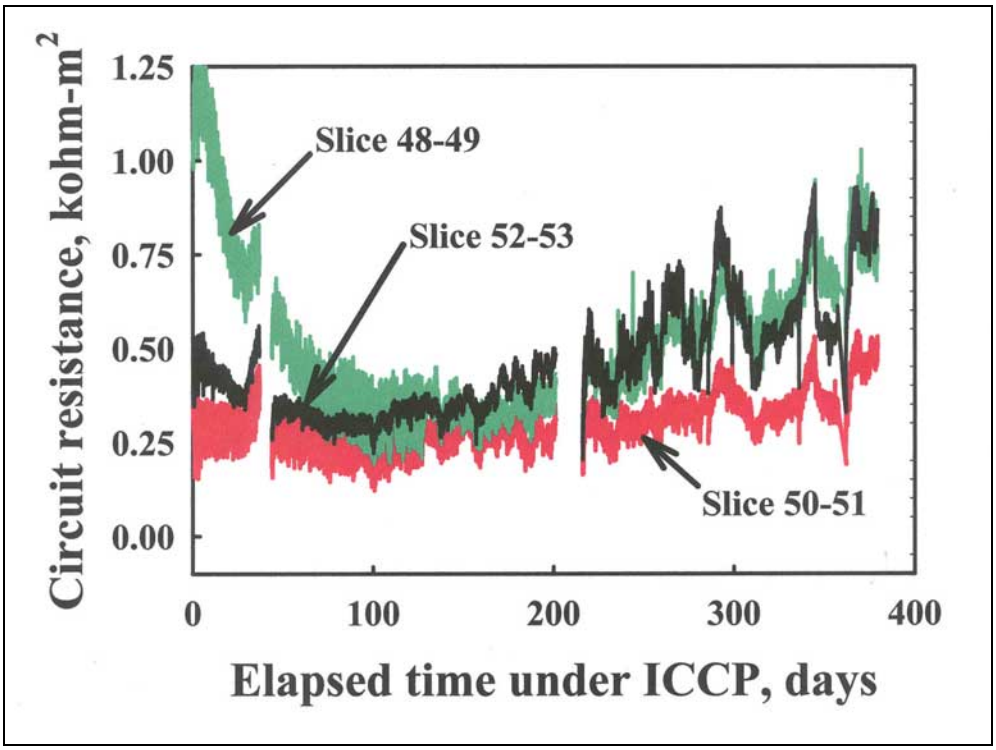

Figure 4.30: Voltage of beam slices as a function of time for ICCP in chloride migration experiment. Anode current density, 20 mA/m^2 (2 mA/ft^2); cathode current density, 33 mA/m^2 (3 mA/ft^2).

4.7.2 Chloride Ion Migration

Figures 4.31 and 4.32 show the Cl profiles for original and patch concrete, respectively, from beam slices after 0.5 years ICCP operation. The profile for original concrete slice 53E may contain contributions from patch concrete, which would account for the high chloride values at the outer edges. Figure 3.3 shows why this is possible with patch concrete extending far down the sides of the beam. By the same token, the profile for patch concrete slice 53B may contain contributions from the original concrete. The profiles after 1.0 years ICCP operation are shown in Figures 4.33 and 4.34 for original and patch concrete, respectively.

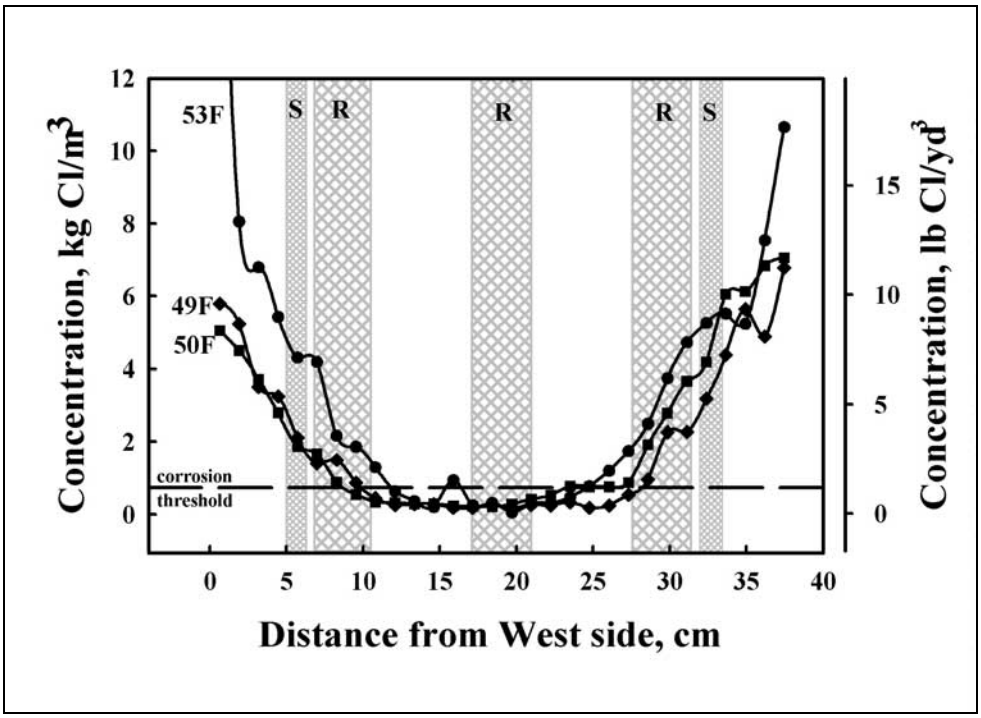

Figure 4.31: Chloride profiles for original concrete showing chloride migration after 0.5 years ICCP. West is the ocean facing side of the beam.

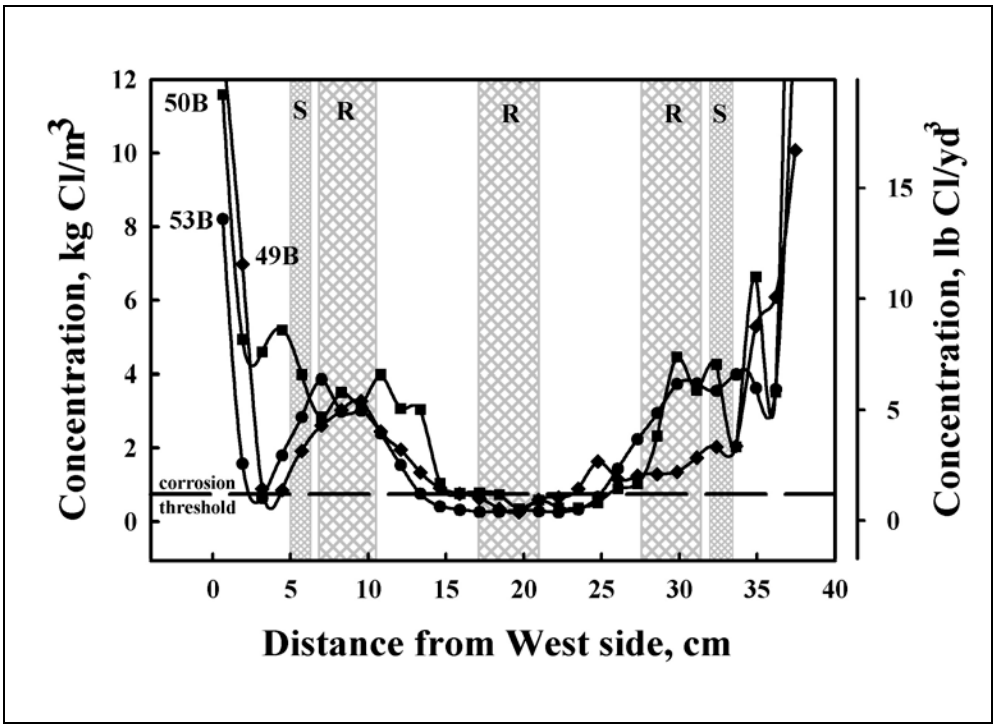

Figure 4.32: Chloride profiles for patch concrete showing chloride migration after 0.5 years ICCP. West is the ocean facing side of the beam.

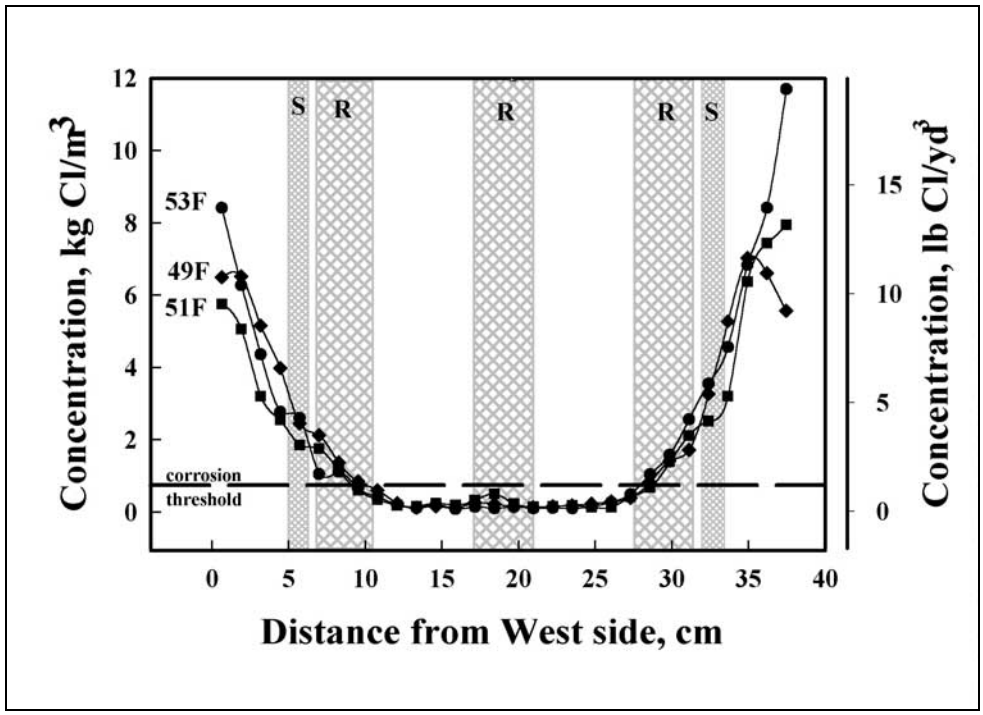

Figure 4.33: Chloride profiles for original concrete showing chloride migration after 1.0 years ICCP. West is the ocean facing side of the beam.

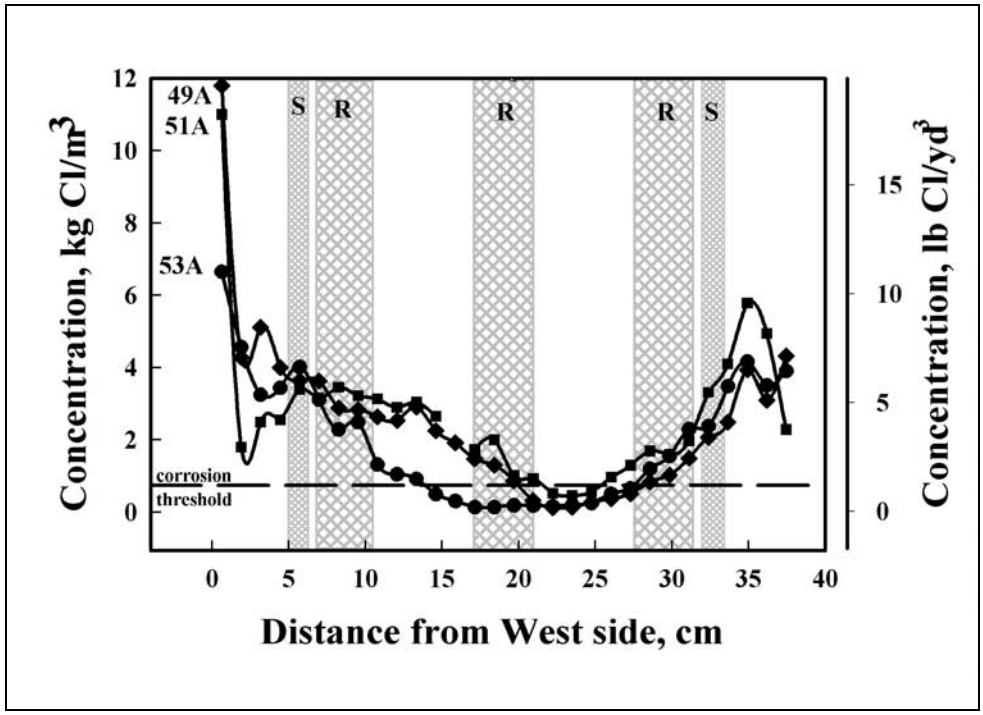

Figure 4.34: Chloride profiles for patch concrete showing chloride migration after 1.0 years ICCP. West is the ocean facing side of the beam.

Individual curves have been averaged in APPENDIX F.3 for "as-received" or 0.0 year, 0.5 year and 1.0 year ICCP. These data are summarized in Figure 4.35 for original concrete and Figure 4.36 for patch concrete as a function of years ICCP. The profiles for 0.5 and 1.0 years ICCP in the patch concrete were taken at different locations with respect to the beam geometry. This is the reason the 1.0 year profile is higher than the 0.5 year profile in the region where chloride is being extracted.

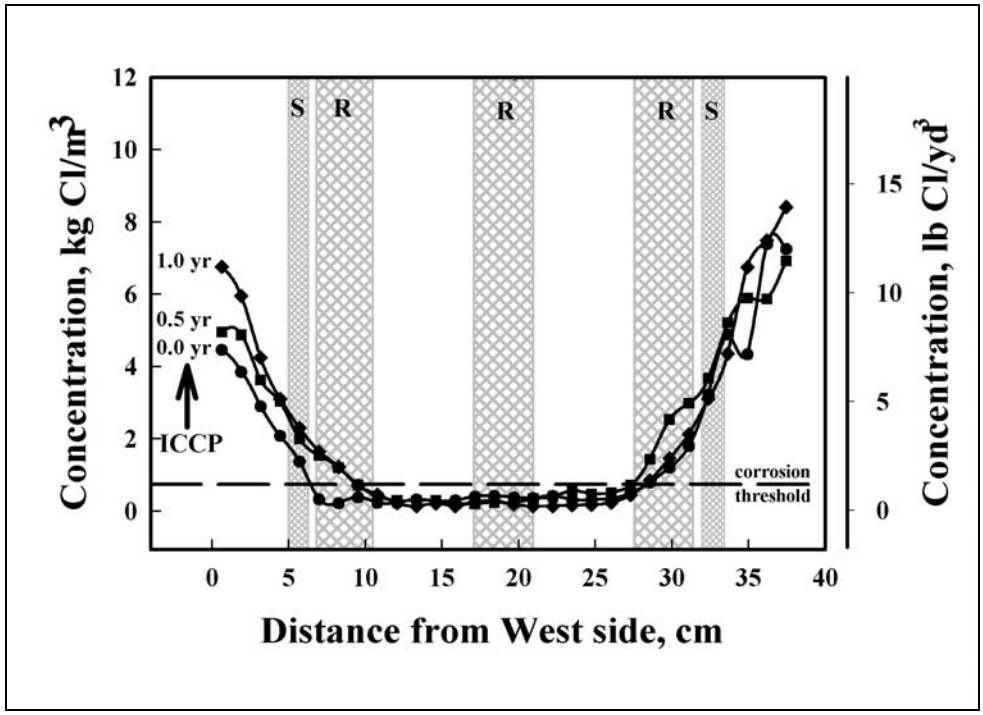

Figure 4.35: Chloride profiles for original concrete showing chloride migration after 0.0, 0.5 and1.0 years ICCP. West is the ocean facing side of the beam.

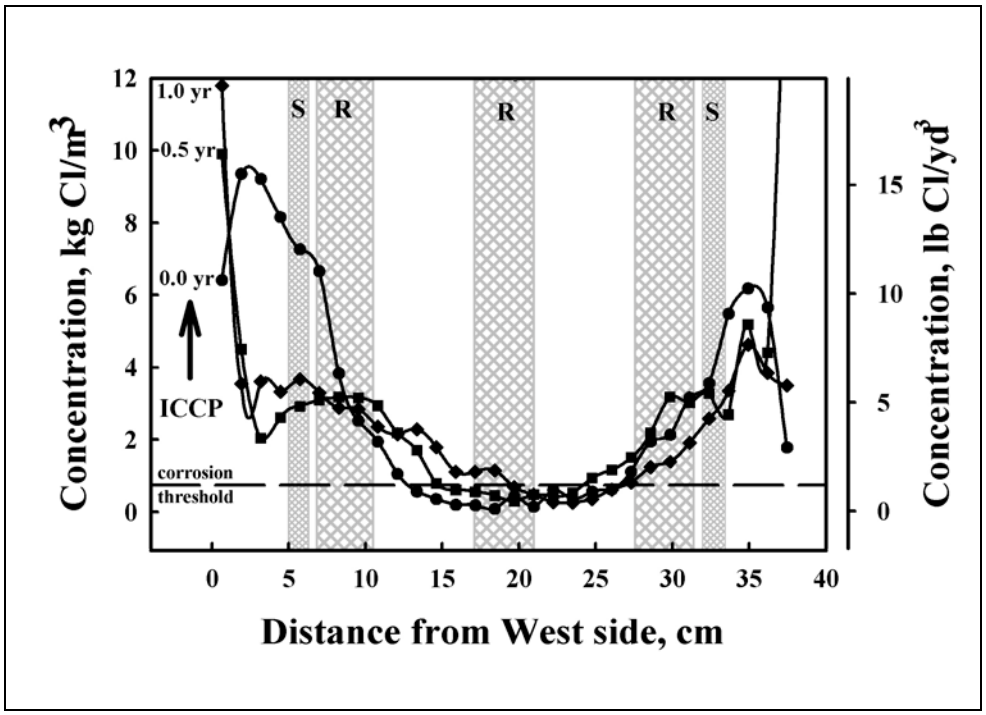

Figure 4.36: Chloride profiles for patch concrete showing chloride migration after 0.0, 0.5 and 1.0 years ICCP. West is the ocean facing side of the beam.

Comparison of the average Cl profiles for original concrete after ICCP operation show them to be similar to the profile for the "as-received" beam, Figure 4.35. This was true because there was no rebar in the original concrete except for the occasional shear stirrup and hence hardly any charge to be carried by the chloride ions. Recall that a coal-tar epoxy coating separated and insulated the patch concrete from the original concrete. The large mass of rebar in the patch and the small amount in the original concrete formed essentially a parallel circuit with the zinc anode. Most of the current went to the rebar in the patch concrete. Consequently, the original concrete chloride profiles were essentially unaltered by ICCP.

In contrast, comparison of the average Cl profiles for the patch concrete after ICCP operation show them to be very different from the profile for the "as-received" beam, Figure 4.36. Surface concentrations of Cl were high relative to the "as-received" beam, well in excess of 12 kg Cl/m3 (20 lb Cl/yd3) on both the east and west faces. Furthermore, in the space between the outer square rebar and beam surface, Cl had migrated from the beam interior outwards to the beam surface, concentrating in the near surface region. This migration was more pronounced on the west side of the beam compared to the east side of the beam, but occurred on both sides. Visual inspection showed large amounts of salt accumulated on the anode surface after 0.5 and 1.0 year of ICCP.

Comparing the 0.5 year profile with the "as-received" profile shows there was a net loss of chloride from the beam. The difference between the two curves was integrated from the beam centerline to the outer surface to compute the amount of chloride extracted. The value was 0.34

kg Cl/m2 through the west vertical face and 0.04 kg Cl/m2 through the east face. Thus, ICCP not only reduced corrosion by maintaining the rebar at a potential where the corrosion reaction is retarded to an acceptable level, but ICCP gradually altered the rebar environment by extracting Cl from the vicinity of the rebar. In this way ICCP yields three benefits: (1) it prevents further corrosion of steel reinforcing bar; (2) it reduces the chloride concentration in concrete surrounding the reinforcing bar; and (3) it restores alkalinity at the rebar-concrete interface, Equation 3.3.

4.7.3 Finite Element Analysis of Chloride Ion Migration

Initial conditions for the finite element analysis were from fitting the "as-received" Cl profile for patch concrete on the west side of the beam, Figure 4.34. The equation used to fit the data was the one-dimensional solution to Fick's second law for chloride diffusion into a broad concrete plate with constant surface chloride composition, Equation 4.2. The value C_o was 15.0 kg Cl/m^3 and the value of D was 3.2×10^{-8} cm^2/s, Table 4.7.

Under the influence of a potential gradient, where the surface is positively charged and the interior is negatively charged, the negatively charged Cl ions will migrate to the surface. Thus, the flux, J, of Cl ions across any plane parallel to the surface is the algebraic sum of migration under the influence of the concentration gradient and migration in the opposite direction under the influence of the potential gradient:

$$J = -D\frac{dC}{dx} + CFu = -D\frac{dC}{dx} + Cv \qquad \textbf{(4-4)}$$

where the velocity, v, of Cl ions due to the potential gradient is equal to the product of the driving force, F, and the velocity at a unit force, u. An equation analogous to Fick's second law of diffusion results from this application of an external force, i.e., the potential gradient (*Jost, 1960*):

$$\frac{dC}{dt} = D\frac{d^2C}{dx^2} - v\frac{dC}{dx} \qquad \textbf{(4-5)}$$

It is usual to use potential as the driving force. However, the potential across the concrete was not constant with respect to time and position. Since current density and potential are related and the current density was kept constant, current density was used instead. So the velocity v was assumed to be proportional to the current density, where k is the proportionality constant:

$$v\left(cm/s\right) = k\left(cm^3/C\right)\cdot i\left(A/cm^2\right) \qquad \textbf{(4-6)}$$

To model the rebar position and the expected low current flow behind the rebar, the value for v was assumed to be a constant between the surface of the concrete and the shear stirrup, 0 to 4.97 cm in depth, to be 0 at depths beyond the innermost square rebar, >10.56 cm in depth, and to vary linearly between the shear stirrup and innermost square rebar, 4.97 to 10.56 cm in depth.

The finite element analysis was one dimensional with thin sections of thickness, Δx, into the concrete from the surface (indexed by j) and relatively small time increments of time, Δt, (indexed by k). The following equation was used:

$$C_j^{k+1} = C_j^k + \frac{D\Delta t}{\Delta x^2}\left[C_{j+1}^k - 2C_j^k + C_{j-1}^k\right] - \frac{v\Delta t}{\Delta x}\left[C_{j+1}^k - C_j^k\right] \quad \textbf{(4-7)}$$

The boundary conditions at the surface and "infinitely" into the concrete (i.e., 20 cm) were $C_o = C_{0+\Delta x}$ and $C_{20cm} = C_{20cm-\Delta x}$. The values of Δx and Δt were 0.1 cm and 31536 sec (i.e., 0.001 year), respectively. For stability (without considering the velocity term), these values were chosen such that $D\Delta t/\Delta x^2$ was less than 0.5 (*Pearson, 1986*). The value of $D\Delta t/\Delta x^2$ was equal to 0.1 for the chosen values. The finite element analysis was stepped forward for 1000 time increments, equivalent to ICCP for one year.

The calculated chloride profiles at 0.5 and 1 year are shown in Figure 4.37 with the measured chloride ion profiles after 0.5 and 1 years ICCP. A value for v of -3.96×10^{-7} cm/s minimized the variance between the measured and calculated chloride profiles. For an anode current density of 20 mA/m^2 (2×10^{-6} A/cm^2), the proportionality constant k was 0.198 cm^3/C. The calculated profiles for 0.0, 0.5 and 1.0 years ICCP are similar to the measured profiles. They show that salt is extracted from the region between the rebar and the zinc anode. Furthermore, they demonstrate that the driving force associated with the potential gradient dominates that due to the concentration gradient. Some salt extraction occurred in the region surrounding the shear stirrup and the outer square rebar. There was no extraction of chloride from the region between the inner and outer square rebar.

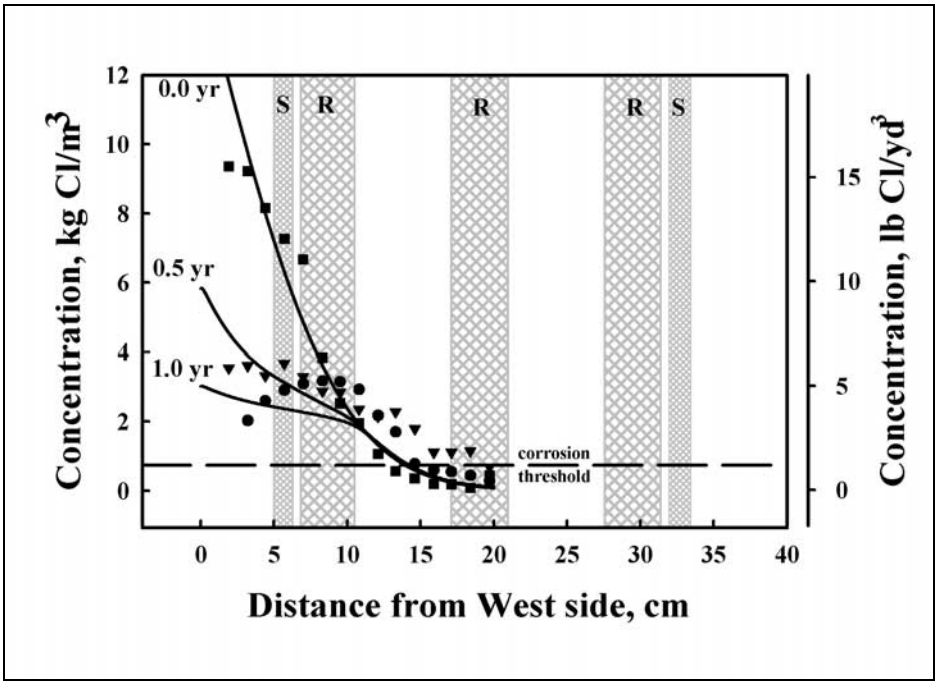

Figure 4.37: Chloride ion migration in concrete under potential and concentration gradients modeled using finite element analysis; comparison between experiment and theory.

The proportionality constant, *k*, was used with different current densities to generate a series of concentration curves for ICCP from 0 to 2.0 years, Figure 4.38. This figure shows that the amount of Cl extraction was close to the maximum possible after only 1.0 years ICCP, equivalent to 15 years at Oregon DOT bridge CP conditions. Chloride extraction could only be increased further by adding a chloride sink to the concrete surface to remove the accumulated salt, for example, by regular washing of the anode surface.

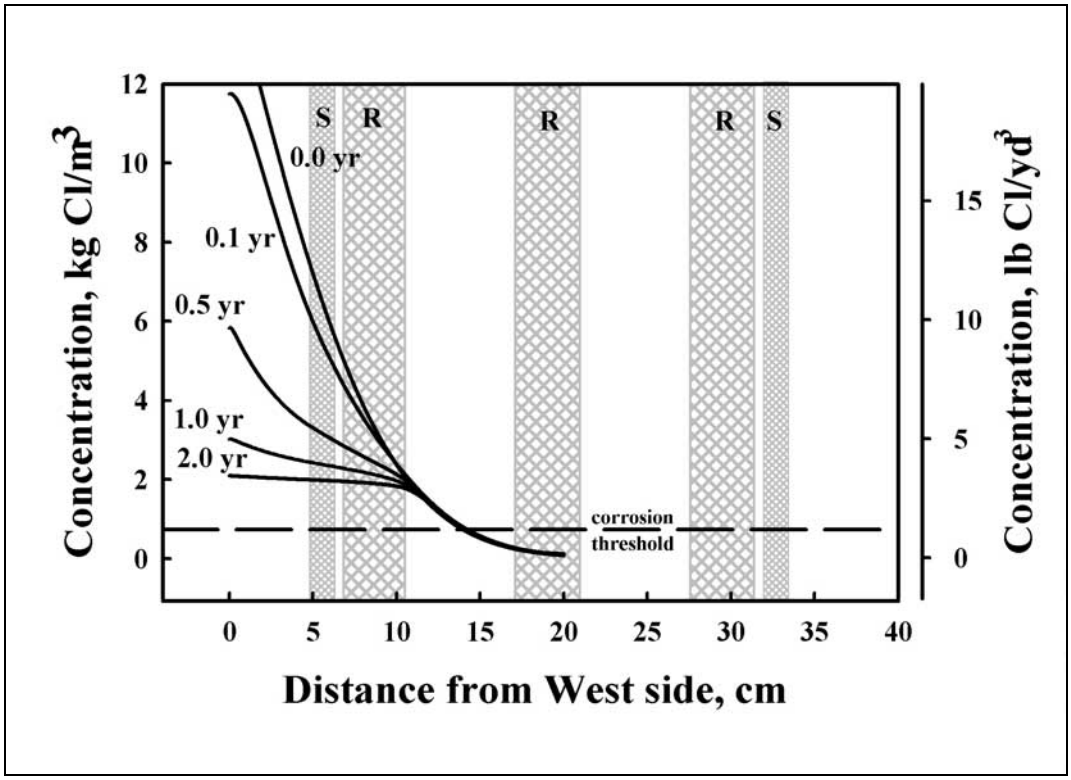

Figure 4.38: Chloride ion migration in concrete under potential concentration gradients generated from finite element analysis for 0 to 2 years ICCP at a current density 10 times higher than ODOT uses on coastal bridges.

5.0 CONCLUSIONS

Chloride ion distribution profiles suggest that severe environment and insufficient cover over shear stirrups were responsible for the early corrosion damage of the Rocky Point Viaduct. Visual inspection and half-cell potential surveys of Beam A1 support this finding. Evidence suggests that the 1969 repair delayed further corrosion damage to the Viaduct by no more than 8 to 9 years. Efforts to prevent further corrosion damage in 1969 were ineffective and did not significantly delay rebar corrosion and corrosion-related deterioration of the Viaduct.

5.1 BRIDGE FAILURE MECHANISM

The harsh environment at the site was an important factor in the premature failure of the Viaduct. This led to salt penetration of the concrete and diffusion of chloride ions to the depth of the rebar. The shear stirrups had inadequate concrete cover for the severity of the Viaduct site environment. Concrete cover was even less on the bottom of the beam where salts can concentrate leading to even earlier initiation of rebar corrosion. Concrete cracking occurs within 3 to 5 years after corrosion initiation. Time-to-cracking estimates from chloride profiles for original concrete, and bridge maintenance observations of cracking, are in good agreement. These factors support the theory that early corrosion initiation on the shear stirrups was critical in causing cracking and corrosion damage that subsequently required the 1969 repair and patching of the Viaduct.

Chloride ion diffusion through the patch concrete was more rapid than through the original concrete on the west side of the beam; it was similar on the east side of the beam. The higher chloride ion diffusion rate through the patch concrete on the west side was due both to a higher concentration gradient resulting from greater surface chloride concentration and to the higher diffusion coefficient. Patch concrete porosity combined with environmental conditions on the west face led to conditions that concentrated salt on the beam face.

Chloride contamination of the concrete used to construct the Rocky Point Viaduct was a lesser factor in the early initiation of shear stirrup corrosion and the appearance of corrosion damage on the beams and piers. Evidence suggests the chloride originated in the use of unwashed beach sand in the preparation of the concrete mix.

5.2 BRIDGE CONSTRUCTION PRACTICES

Shallow concrete cover over the shear stirrups was a primary cause of early corrosion initiation and subsequent damage to the Rocky Point Viaduct. Cover depth was particularly shallow on the bottom and edges of the beam where salts can concentrate as the result of precipitation draining from the beam face and then evaporating.

Application of coal-tar epoxy and inorganic zinc coatings on the rebar during the 1969 repair failed to halt corrosion of the rebar in subsequent years. Application of a linseed oil coating on the concrete failed to prevent further Cl penetration of the concrete. The 1969 patch concrete delayed continued corrosion-related damage to the Viaduct by only 8 to 9 years. The 1969 repair and corrective efforts were ineffective for reasons related to the severity of the environment and properties of the patch concrete.

Impressed current cathodic protection over a period equivalent to 15 years service at Oregon DOT coastal bridge conditions resulted in significant reduction of chloride ion concentration in the concrete between the rebar and the zinc anode on the beam surface. Salt was extracted from the concrete by transport from the beam interior to the zinc anode. Salt extraction resulted in a lessening of corrosive conditions in the vicinity of the rebar. ICCP yields three benefits in preventing further corrosion of rebar. It shifts the rebar to a state of diminished corrosion, i.e., a protected state. It gradually reduces the aggressiveness of the concrete environment surrounding the rebar by reducing chloride concentration. It increases alkalinity at the rebar surface so that the rebar may eventually return to a naturally passive state.

Finite element analysis of chloride ion profiles under the combined influences of diffusion and concentration gradients show that salt will be extracted by ICCP. The effect of potential gradient effects dominated that of the concentration gradient. After the equivalent of 15 years the amount of salt extracted reached a maximum. Without the benefit of a chloride sink at the anode surface to remove accumulated salt, further extraction of salt would not occur.

Chloride profiles on existing coastal bridges support the Oregon DOT decision to use stainless steel rebar in coastal bridge construction for deck, beams and prestressed girders and to use microsilica concrete containing flyash. Surface chloride concentrations for the Rocky Point Viaduct were below the corrosion threshold for 316 stainless steel. Diffusion rates in microsilica concrete are 1/5 to 1/10 those observed in the Rocky Point Viaduct. It is unlikely that rebar under these conditions on the Oregon coast will experience chloride ion concentrations at a level that would initiate corrosion. Furthermore, the corrosion rate of stainless steel in chloride-contaminated concrete is a factor of 700 less than that of black iron bar. Therefore, the time from corrosion initiation to concrete cracking would be very long should corrosion initiate.

5.3 BRIDGE EVALUATION METHODS AND MONITORING

Powder sampling of the chloride-contaminated bridge concrete to produce a chloride ion distribution profile is a powerful method for evaluating bridge condition and predicting future corrosion-related performance. This method provided the best evidence for explaining the early corrosion failure of the Viaduct. This report provides some guidelines for effective chloride profiling of concrete structures. Chloride profiling provides a means for characterizing the corrosivity of the environment and the durability of the concrete. It provides an effective method for anticipating future corrosion-related damage and diagnosing present damage.

Porosity and permeability data were qualitatively useful in understanding factors that influenced chloride migration in original and patch concrete.

Petrographic analysis established the nature and extent of chemical reactions involving aggregate and cement paste and provided the basis for including and eliminating the contributions of specific reaction mechanisms to the concrete deterioration process. The original concrete included a high amount of cryptocrystalline silica, sources of sodium in plagioclase feldspar and sea salt, and a source of sulfur in pyrite, constituents known to contribute to the formation of ASR, gypsum and ettringite. However, no sodium-rich gel products or reaction rims were found, indicating that neither ASR or ACR reactions had occurred in either the original concrete or in the patch concrete. No sulfate minerals indicative of gypsum or ettringite formation were detected in the original concrete samples. Petrographic analysis established that the premature deterioration of the Rocky Point Viaduct was not due to the presence of any of these minerals.

The half-cell potential survey was a useful measurement technique for understanding the corrosion failure of the Viaduct. It provided evidence suggesting early corrosion of the shear stirrups was significant. Timely application of potential surveys can provide clues that warn of corrosion damage to the structure. Other techniques (visual and delamination surveys) are of limited value for anticipating corrosion damage.

While apparently not a significant factor contributing to corrosion damage of the Rocky Point Viaduct, microbial deterioration of the concrete may contribute in a small way to changes that occur in the mechanical properties of the concrete. Bacteria that lead to this deterioration are the sulfur oxidizing bacteria *T. thiooxidans*. Populations of these bacteria were only found on the west (ocean-facing) side of the beam where the compressive strength of the original concrete was lower than on the east (landward) side.

The GECOR6 instrument did not produce useful data on either corrosion rates of rebar or concrete resistivity.

6.0 RECOMMENDATIONS

6.1 BRIDGE CONSTRUCTION PRACTICES

- Effective cover depth is a significant factor leading to a structure that resists the effects of corrosion. Bridge design must consider not only the quality of concrete used and the corrosion threshold of the rebar chosen, but also the aggressiveness of the site environment including meteorological conditions and the effects of washing and sheltering. Present Oregon DOT mix design and concrete cover specifications yield a structure that is significantly more resistant to harsh coastal environments than in the past.

- Concrete cover must be determined based on the steel nearest to the surface of the concrete. In the case of the Rocky Point Viaduct this was the shear stirrups with cover in some cases of 2.8 cm (1.1 inches). Compliance with concrete cover specifications is particularly important for the underside and edges of beams, decks and girders.

6.2 BRIDGE EVALUATION METHODS

- Chloride powder sampling at 1.3 cm (0.5 inch) increments to establish a chloride profile that can be used to determine an effective diffusion coefficient, D, and a characteristic surface chloride concentration, C_o, is one of the more powerful techniques Oregon DOT has for assessing the condition of bridges on the Oregon coast. Sampling to a total depth of no more than 15 cm (6 inches) in 1.3 cm (0.5 inch) increments would be adequate to define D and C_o for bridges on the Oregon coast. Vertical profiling from the bottom of a structure may be the preferred strategy where the bottom and edges of beams and girders are exposed to particularly high chloride ion concentrations. D and C_o values obtained from the fit of the data can be used to assess environmental conditions, to look back in time to understand performance problems related to corrosion damage, and to look forward in time to anticipate maintenance and repair needs. Powder sampling may not be necessary except on a long term basis (10-15 years) to check predictions once good values of D and C_o are measured.

- Half-cell potential mapping, concrete void fraction measurements, and concrete petrography are other methods that are particularly useful for characterizing the condition of coastal bridges.

6.3 BRIDGE MONITORING

- While Oregon DOT controls the quality of concrete specified and properties of rebar chosen, it does not control the inherent aggressiveness of the bridge site environment. It would be useful to include an assessment of site environmental conditions as an input to bridge design to assure a structure that will achieve the intended design life. Such an assessment recognizes that a wide range of microclimates exist on the Oregon coast. This could be done either through measuring atmospheric corrosion rates for mild steel, measurement of salt deposition rates, or determining chloride profiles to yield an estimate of the surface chloride concentration, C_o, from Fick's law. The latter method would be the most useful for Oregon DOT and one that Oregon DOT has expertise in performing.

- Measurements should be made on coastal bridges to determine if chloride migration towards the anode is occurring in field structures with thermal-sprayed anode ICCP systems. This would be done by measuring the chloride profile at the location of the rebar in bridge elements that have the greatest electrochemical age. Candidate bridges would be the Cape Creek Bridge and the Yaquina Bay Bridge. Chloride profiles on bridge elements well away from rebar would not be significantly affected by ICCP and could serve as reference profiles for evaluating changes due solely to ICCP.

- Complete chloride profiles of sound concrete should be measured immediately before installing bridge cathodic protection systems to provide a reference for evaluating future performance of the system.

7.0 REFERENCES

AASHTO, "Compressive Strength of Cylindrical Concrete Specimens," T 22-92, in *Standard Specifications for Transportation Materials and Methods of Sampling and Testing*, 17th Ed., Part II, American Association of State Highway and Transportation Officials, Washington, D.C., 1995a.

AASHTO, "Maximum Specific Gravity of Bituminous Paving Mixtures," T 209-94, in *Standard Specifications for Transportation Materials and Methods of Sampling and Testing*, Part II – Tests, American Association of State Highway and Transportation Officials, Washington, D.C., pp. 416-418, 1995.

AASHTO, "Sampling and Testing for Chloride Ion in Concrete and Concrete Raw Materials," T 260-94, in *Standard Specifications for Transportation Materials and Methods of Sampling and Testing*, 17th Ed., Part II, American Association of State Highway and Transportation Officials, Washington, D.C., 1995b.

Allan, M. L., "Probability of Corrosion Induced Cracking in Reinforced Concrete," *Cement and Concrete Research*, Vol. 25, No. 6, pp. 1179-1190, 1995.

Appostolos, J. A., D. M. Parks, and R. A. Carello, "Cathodic Protection of Reinforced Concrete Using Metallized Zinc," *Materials Performance*, Vol. 26, No. 12, pp. 22-28, 1987.

ASTM, "Practice for Measuring Delaminations in Concrete Bridge by Sounding," D 4580-86, V. 4.03, *Road and Paving Materials; Pavement Management Technologies*, American Society for Testing and Materials, Philadelphia PA, 1994a.

ASTM, "Standard Test Method for Half-Cell Potentials of Uncoated Reinforcing Steel in Concrete," C 876-91, V. 4.02, *Concrete and Aggregates*, American Society for Testing and Materials, Philadelphia PA, 1994b.

ASTM, "Standard Test Method for Specific Gravity, Absorption, and Voids in Hardened Concrete," C 642-90, V. 4.02, *Concrete and Aggregates*, American Society for Testing and Materials, Philadelphia PA, 1994c.

Bentz, Dale P., "Database of Values for Concrete Chloride Ion Diffusivity," NIST Website – http://ciks.cbt.nist.gov/bentz/clvaldat.html (other useful pages are advipen.html, clpencon.html, binding.html, and reaction.html), Construction and Building Technology, National Institutes of Standards and Technology, February 2000.

Bullard, S. J., S. D. Cramer, B. S. Covino, Jr., G. R. Holcomb, G. E. McGill, and R. Reis, "Thermal-Sprayed Anodes for Cathodic Protection of Reinforced Concrete Bridges," in

Concrete Under Severe Conditions 2, O. E. Gjørv, K. Sakai, N. Banthia, Eds., E & FN Spon, London, pp. 959-968, 1998.

Burke, P., "Status of the Nation's Bridges," *Materials Performance,* V. 33, No. 6, pp. 48, 1994.

Covino, Jr., B. S., S. J. Bullard, G. R. Holcomb, J. H. Russell, S. D. Cramer, J. E. Bennett, and H. M. Laylor, "Chemically Modified Thermal-spray Zinc Anodes for Galvanic Cathodic Protection," *Materials Performance,* Vol. 38, No. 12, pp. 28-32, 1999.

Covino, Jr., B. S., S. J. Bullard, G. R. Holcomb, J. H. Russell, S. D. Cramer, G. E. McGill, and C. B. Cryer, "Bond Strength of Electrochemically Aged Arc-Sprayed Zinc Coatings on Concrete," *Corrosion,* Vol. 53, No. 5, pp. 399-411, 1997.

Covino, Jr., B. S., S. D. Cramer, S. J. Bullard, G. R. Holcomb, G. E. McGill, and C. B. Cryer, "Factors Affecting Thermal-Sprayed Zinc Anodes on Concrete," paper no. 173, *Proc. 13th International Corrosion Congress,* Australasian Corrosion Association, Clayton, Vic, Australia, 7 pp., 1996.

Covino, Jr., B. S., S. D. Cramer, G. R. Holcomb, S. J. Bullard, and H. M. Laylor, "Postmortem of a Failed Bridge," *Concrete International,* pp. 39-45, February 1999.

Cramer, S. D., personal communication, data from Oregon coast atmospheric corrosion study conducted 1992-1996 by the Albany Research Center, U. S. Department of Energy, Albany OR, April 2000.

FHWA, *Corrosion Detection in Reinforce Concrete Bridge Structures*, Demonstration Project No. 84, Federal Highway Administration, U. S. Department of Transportation, Washington D.C., March 1992.

FHWA-SHRP, *Showcase Workshop on Concrete Durability*, FHWA-SA-96-025, U. S. Department of Transportation, Washington D.C., October 1995.

Foran, M. R., Gibbons, E. V., and Wellington, J.R., "The Measurement of Atmospheric Sulphur Dioxide and Chlorides," *Chemistry in Canada*, Vol. 10, No. 5, pp. 33-41, May 1958.

ISO, *Corrosion of Metals and Alloys: Corrosivity of Atmospheres -- Measurement of Pollution,* ISO 9225: 1992(E), International Organization for Standardization, Geneva, 10 pp., 1992.

Johnson, B. and F. Nelson, "Project Selection Method Integrating BMS Data and Non-Deterioration Based Needs," presented at the International Bridge Management Conference, Transportation Research Board, Denver CO, April 1999.

Jost, W., *Diffusion in Solids, Liquids, Gases,* Academic Press, New York, NY, p. 47, 1960.

Kubaschewski, O. and B. E. Hopkins, *Oxidation of Metals and Alloys*, Butterworths, p. 5-14 and 24, 1962.

Li, Z., Peng, J. and Ma, B., "Investigation of Chloride Diffusion for High-Performance Concrete Containing Fly Ash, Microsilica and Chemical Admixtures," *ACI Materials Journal*, pp. 391-396, May-June 1999.

Liu, Y., and Weyers, R. E., "Modeling the Time-to-Corrosion Cracking in Chloride Contaminated Reinforced Concrete Structures," *American Concrete Institute Materials Journal*, pp. 675-681, November-December 1998.

McDonald, D. B., D. W. Pfeifer, and M. R. Sherman, *Corrosion Evaluation of Epoxy-Coated , Metallic-Clad and Solid Metallic Reinforcing Bars in Concrete*, FHWA-RD-98-153, Federal Highway Administration, U.S. Department of Transportation, Washington, D.C., 127 pp., December 1998.

Mudd, C. J., G. L. Mussinelli, M. Tettamanti, and P. Pediferri, "Cathodic Protection of Steel in Concrete," *Materials Performance*, Vol. 27, No. 9, pp. 18-23, 1988.

Nelson, F. J., Personal communication, Bridge Section, Oregon Department of Transportation, Salem OR, May 2000.

Pearson, C. E., *Numerical Methods in Engineering and Science*, Van Nostrand Reinhold, New York, NY, p. 170, 1986.

Rogers, F., "Benefits and Technology Developed to Arc Spray 3/16"(4.8 mm) Diameter Wires Used for Corrosion Protection of Steel," in *Thermal Spray: Surface Engineering via Applied Research*, Proc. First International Thermal Spray Conference 2000 (Montreal Canada), C. Berndt, Ed., ASM International, Materials Park OH, pp. 691-695, May 2000.

Sagues, A. A., *Corrosion of Epoxy Coated Rebar in Florida Bridges*, Final Report to Florida Department of Transportation, WPI No. 0510603, University of South Florida, Tampa Fl, 1994.

Shewmon, P. G., *Diffusion in Solids*, McGraw-Hill, New York, NY, p. 12, 1963.

Thomas, M., "Chloride Thresholds in Marine Concrete," *Cement and Concrete Research*, V. 26, No. 4, pp. 513-519, 1996.

Tratnall, R. E. and D. H. Pope, "Identification of MIC", in *Microbiologically Influenced Corrosion*, G. Kobrin, Ed., NACE International, Houston TX, pp. 65-77, 1993.

West, R. E., and S. W. Hime, "Chloride Profiles in Salty Concrete," *Materials Performance*, V. 24, No. 7, 1985, pp. 29-36.

Whiting, D. and P. D. Cady, "Method for Field Measurement of Concrete Permeability," Vol. 7 in *Condition Evaluation of Concrete Bridges Relative to Reinforcement Corrosion*, SHRP-S-329, Strategic Highway Research Program, National Research Council, Washington, D.C., 87 pp., 1993.